SKID RESISTANCE AND HYDROPLANING ANALYSIS OF RIB TRUCK TIRES

CAO CHANGYONG

DEPARTMENT OF CIVIL AND ENVIRONMENTAL ENGINEERING

NATIONAL UNIVERSITY OF SINGAPORE

December 2010

SKID RESISTANCE AND HYDROPLANING ANALYSIS OF RIB TRUCK TIRES

CAO CHANGYONG
HT080201R

A THESIS SUBMITTED

FOR THE DEGREE OF MASTER OF ENGINEERING

DEPARTMENT OF CIVIL AND ENVIRONMENTAL

ENGINEERING

NATIONAL UNIVERSITY OF SINGAPORE

December 2010

ACKNOWLEDGEMENTS

I would like to take this opportunity to express my deepest appreciation and gratitude to all the people who have contributed to this thesis. To begin with, I am greatly indebted to my supervisor, Prof. Fwa Tien Fang, for his constant guidance, help and encouragement throughout the research. He encouraged me to develop independent thinking and research skills. His breadth of intellectual inquisition continually stimulated my analytical thinking skills. His constant attention to the development of the FSI models and the text of this thesis was invaluable. All of these are essential to complete this research study.

I am also grateful to Dr. Ong G.P. who has given me suggestions and comments during this process. Many thanks are also given to the technical staff from the Highway and Transportation Engineering Laboratory. I would like to acknowledge all my colleagues at Highway Lab, Mr. Wang Xinchang, Mr. Qu Xiaobo, Mr. H.R, Pasindu, Mr. Yang Jiasheng, Mr. Kumar Anupam, Mr. B.H. Setadji and Mr. J. Farhan, for their discussion, help and kindness. In addition, I would like to thank my friends - both at and outside of NUS for pleasant moments spent together over the past years. Special thanks are also given to the Department of Civil and Environmental Engineering and the National University of Singapore for providing the research scholarship and tutorship during the course of research.

Last but not least, I would like to express my heartfelt thanks and gratitude to my wife Fang Yuhui, my parents and parents-in-law for their tremendous care, utmost support and constant encouragement during my study in the past several years.

Thanks also to my brother for his care and encouragement. They deserve more thanks than I can ever give.

TABLE OF CONTENTS

CHAPTER 3 BASIC THEORY FOR FSI SIMULATION

CHAPTER 4 HYDOPLANING ANALYSIS OF WIDE-BASE TRUCK TIRE

CHAPTER 5 SKID RESISTANCE ANALYSIS OF RIB TRUCK TIRES

ABSTRACT

Traffic crashes and the associated injuries and fatalities remain a significant problem for transportation professionals. The relationship between skid resistance and roadway safety has long been recognized by transportation agencies and concern has grown with the number of accidents occurring in wet pavement conditions. It is well documented that a pavement with high skid resistance properties can be a significant factor in reducing the likelihood of a crash. Inadequate skid resistance can lead to higher incidences of skid-related crashes.

Considering its importance, research on pavement skid resistance had started since 1920s and most of them mainly focused on two aspects: to measure and predict wet pavement skid resistance accurately, and to develop strategies to increase skid resistance of wet pavements. Compared with the large amount of experiments and measurements on skid resistance, however, understanding in skid resistance mechanism has not improved much over the past century because it is hampered by the lack of development in the theoretical, analytical or numerical models that can explain and analyze skid resistance. This results in the reliance of empirical relationships in skid resistance prediction. It is noted that it is still not possible to predict the traction performance of a tire-road system based on the various tire and surface variables. Indeed, there is, as yet, no agreement as to how to quantify many of these variables in a meaningful way. It is clear that there is a great deal of definitive work yet to be done in this field.

The main objective of this research is to simulate the skid resistance and hydroplaning phenomenon of rib truck tires and explore the effect of different

affecting factors on them, which has the potential to shed some new light on this problem. The scope of this research mainly consists of the following three parts: to develop a Fluid Structure Interaction numerical model suitable for hydroplaning and skid resistance of rib truck tires; to evaluate the hydroplaning performance of wide-base truck tires under different operation conditions; and to simulate and predict skid resistance of rib truck tires under different operation conditions.

In this research, an effective three dimensional FSI numerical model, considering the interactions among tire, water and pavement, was developed to analyze the hydroplaning phenomenon of wide-base truck tires. The verification of the FSI model using the experimental data indicated that the proposed models can be used to simulate truck hydroplaning phenomenon and to predict truck hydroplaning speeds satisfactorily. Several cases were simulated and discussed, which involved different wheel loads, tire inflation pressures and water film thickness on pavement surface.

The extended FSI simulation model involving friction contact was employed to simulate the skid resistance of rib truck tire in this research. The proposed model was also verified against the measurements of skid resistance from rib truck tires. The effects of tread depth, tire groove width, position and number of tire grooves, water depth, inflation pressure, wheel load and sliding speed on skid resistance were then studied. It had given a better insight than experiments which could not supply information of detailed velocity and hydrodynamic pressure distribution to researcher. The findings and conclusions from this research are summarized in the last chapter. Finally, the recommendation and outlook for future research are also given.

LIST OF FIGURES

LIST OF TABLES

CHAPTER 1 INTRODUCTION

1.1 Background

Motor vehicle crashes are the sixth leading cause of death and the leading cause of injuries in the United States. It is reported that in 2008 more than 37,000 people were killed and nearly 2.35 million were injured in crashes on the nation's roadways of USA (NHTSA, 2009). The consequences of traffic crashes are felt not only by those directly involved but also by family members, friends, and coworkers who must deal with a devastating loss or find resources to cope with disabling injuries. The costs to society such as lost productivity, property damage, medical costs, emergency services, and travel delays are also tremendous. In 2004, the American Association of State Highway Officials (AASHTO) estimated traffic crashes in the United States accounted for over $230 billion in economic losses every year (AASHTO, 2004). Recent European crash statistics are comparable to those in the United States. The World Health Organization (WHO) reports that motor vehicle crashes worldwide kill 1.2 million and injure 50 million people annually. The worldwide economic loss is estimated at $518 billion each year (WHO, 2004).

For these reasons improving safety is one of the primary goals of transportation officials. Through numerous investigations, the relationship between surface friction and roadway safety has been recognized by transportation agencies and concern has grown with the number of accidents occurring in wet pavement conditions. NTSB and FHWA reports indicated that 13.5% of fatal crashes and 18.8% of all crashes occur when pavements are wet (Dahir and Gramling 1990). It is well

documented that a pavement with high skid resistance properties can be a significant factor in reducing the likelihood of a crash. Inadequate skid resistance can lead to higher incidences of skid-related crashes. Hosking (1987) reported that an improvement in the average skid resistance level of 10% could result in a 13% reduction in wet skid rates. These studies show the importance of adequate frictional characteristics between the tire and pavement surface and its associated reduction in the risk of hydroplaning occurrences.

Pavement skid resistance is related to properties of both the vehicle tire and the pavement surface, and can be affected by volume and composition of the traffic load, available tire tread depth and pattern, pavement temperature, the presence of water (rain), and other pavement surface conditions. It has been involved in design guidelines of highways and runways. For example, the geometric design of highway curves requires information on the coefficient of side friction for the determination of the minimum curve radius in order to prevent vehicle from skidding out of the curve (AASHTO, 2004). Cross slopes have to be designed to provide adequate surface drainage and this is considered a key measure to reduce hydroplaning occurrence (AASHTO, 2004; Wolshon, 2004). The design stopping distances are determined based on assessments of the available pavement skid resistance, while speed limits on highways have to take into consideration operational safety, i.e. skidding and hydroplaning (Lamm et al., 1999).

Considering its importance, research on pavement skid resistance started since 1920s and most of them mainly focused on two aspects, i.e. to measure and predict pavement dry and wet skid resistance accurately, and to develop the strategies to increase skid resistance of wet pavements. Several devices, from the simplest locked

wheel method to the more sophisticated trailers capable of measuring braking force over the entire range of wheel slip, have been invented to measure skid resistance of road pavements or runways. Investigators (Close, 1968; Bergman, 1971; Fancher, 1970; Giles, 1956; Henry, 2000) employed these measured filed data to regress empirical models to describe the relationship between skid resistances and affecting factors. Many researchers also investigated the effects of different factors, such as tire parameters, inflation pressure, wheel load, water film thickness, pavement grooves and so forth, on skid resistance and hydroplaning speed (Henry and Meyer 1983; Henry, 1986; Meyer, 1991; Kulakowski and Meyer, 1989; Ong and Fwa, 2007, 2008).

However, the understanding of skid resistance mechanisms have not improved much over the past century despite the improvements in the measurement techniques because it is hampered by the lack of development in the theoretical, analytical or numerical models that can easily explain and analyze skid resistance. This results in the reliance of empirical relationships in skid resistance prediction. It is still not possible to predict the traction performance of a tire-road system based on the many tire and surface variables. Indeed, there is, as yet, no agreement as to how to quantify many of these variables in a meaningful way. It is clear that there is a great deal of definitive work yet to be done in this field.

Up to date, modern theories still cannot grasp the complex mechanism due to their dependence on empirical constants obtained from experiment. The contact area and adhesion mechanism between the moving rubber tire and pavement is hard to obtain. The lubrication theories and rubber constitutive modeling result in non-linear partial differential equations where the solutions could not be obtained analytically. However, with the development of computing power, researchers can employ the

numerical model to simulate the complex phenomenon. It is feasible to establish a more complex finite element model considering tire-fluid-pavement interactions so as to gain a better understanding of the skid resistance and hydroplaning and to offer new perspectives to the skid resistance problem.

1.2 Objective of Study

The objective of this research is to investigate the skid resistance and hydroplaning performance of rib truck tires including wide-base truck tire by using a 3D Fluid-Structure-Interaction (FSI) model. The different parameters in the model, including water depth, tire inflation pressure, wheel load, sliding speed, and depth, width and spacing of tire tread grooves, are studied in order to give a better understanding of skid resistance and hydroplaning of truck tires. The details of the objective are summarized as follows:

- To develop a robust FSI simulation model with rib truck tires based on the smooth tire-fluid-pavement model developed earlier (Fwa and Ong, 2008).
- To verify the established FSI model against experimental data in literatures.
- To examine the difference of hydroplaning performance between traditional dual truck tires and wide-based truck tires and investigate the effect of tire inflation pressure, wheel load, water film thickness on hydroplaning risk of wide-base truck tires.
- To utilize the proposed model to investigate the effect of depth, width and spacing of tire tread grooves, wheel load, sliding speed, and inflation pressure of rib truck tires on skid resistance.

1.3 Organization of Thesis

In Chapter 1 the background of the research and the necessity and feasibility of the research are introduced. The research objectives are also listed out. Then in Chapter 2, a comprehensive literature review on skid resistance and hydroplaning of pneumatic tires is presented. The basic concepts and mechanism are introduced. Previous researches, both empirical and analytical, are reviewed and discussed in detail. Some important findings from previous researches are given out for reference. Next, in Chapter 3 the basic theory used and concerned in this research is presented.

Chapter 4 depicts the hydroplaning performance of wide-base truck tires. One effective and efficient FSI simulation model considering the tire-water interaction is proposed with the help of ADINA software package. The analysis and discussion of hydroplaning of wide-base truck tire are given. The effects of water-film thickness, tire inflation pressure, wheel load and sliding speed on hydroplaning speed is discussed based on the simulation results from the FSI simulation model.

Chapter 5 addresses the skid resistance of rib truck tires by the extended FSI model based on the one used in Chapter 4. The effect of tread depth, groove width, groove position and inflation pressure of rib truck tires, water film thickness on pavement, wheel load and sliding speed on skid resistance are investigated in detail. The variation of contact patch and the pressure and velocity distribution in water are also discussed.

Finally, the summary of present research and recommendations for future research are presented in Chapter 6.

CHAPTER 2 LITERATURE REVIEW

2.1 Introduction

A comprehensive literature review on major aspects of skid resistance and hydroplaning is presented in this chapter. The first part of the chapter is focused on the skid resistance which includes the definition and mechanism of skid resistance, the major affecting factors for skid resistance, the measurement techniques of skid resistance in laboratory and field, and the major advancements on skid resistance research. The second part of the chapter is concentrated on the hydroplaning problem, including the types and manifestations of hydroplaning, three-zone model of hydroplaning, experimental and analytical studies for hydroplaning, and predictive equations for hydroplaning speeds. Finally, a special review on skid resistance and hydroplaning of truck tires are carried out.

2.2 Skid Resistance

Skid resistance is the opposing force developed at the tire-pavement contact area. In other words, skid resistance is the force that resists the tire sliding on pavement surfaces. It is a measure of the ability of pavement to resist the skidding of a tire and an essential component of traffic safety to maintain vehicle control and reduce the stopping distance in emergency braking situations. The terms *skid resistance*, *pavement friction*, and *skid friction* are used interchangeably in literatures and will be used in the same manner in this thesis.

Skidding occurs when the frictional demand exceeds the available friction force at the interface between a tire and pavement (Kennedy et al. 1990). Numerous factors can influence the magnitude of the skid resistance generated between the tire and pavement surface. These factors include characteristics of pavement surface (microtexture and macrotexture), tread depth and patterns, groove width, construction material and inflation pressure of tires, presence of contaminant, vehicle speed and so forth.

2.2.1 Mechanism of Skid resistance

Skid resistance developed between tire and pavement surface has two major components: adhesion and hysteresis. The two components are respectively related to the two key properties of pavement surfaces, i.e. microtexture and macrotexture, as presented in Figure 2.1. In the dry case the mechanism of molecular-kinetic bonding is most widespread due to the maximum interfacial area. However, upon wetting, the interfacial film of fluid is spread uniformly and this effectively suppresses the electrical roughness of the surface, thereby reducing the adhesion component to a very low value (Moore, 1972). If the road surface has a high macrotexture, the voids in the asperities can act as reservoirs for the fluid and the pressure distribution at each asperity summit promotes local drainage. Thus, some adhesion under wet condition for a pavement with good macrotexture will still exist to provide friction.

Adhesion

The adhesion component of skid resistance indicates the shear force which develops at the tire-pavement interface as the tire conforms to the shape of the contact area (Choubane et al. 2003). It is due to the actual contact between the rubber tire and the

pavement and results from the shearing of molecular bonds formed when the tread rubber is pressed into close contact with pavement surface particles (Panagouli and Kokkalis, 1998).

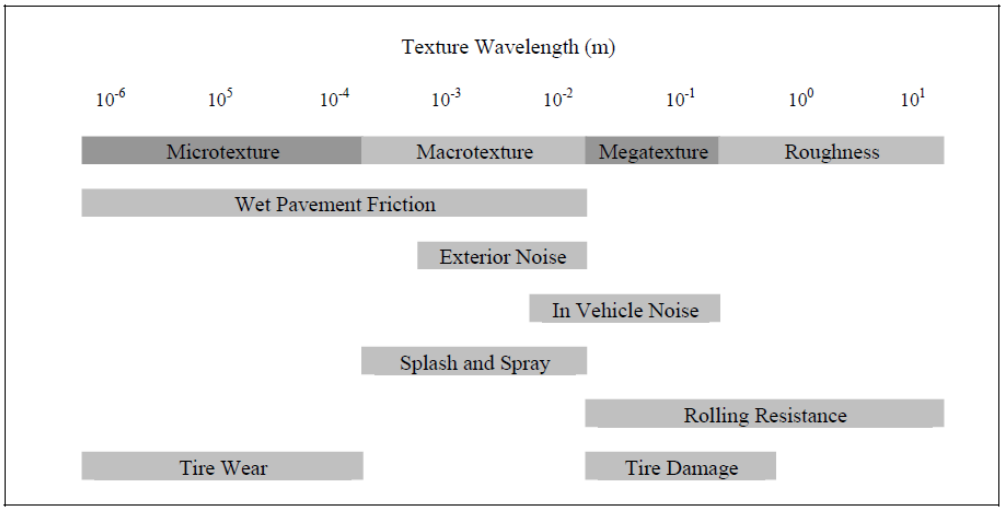

Figure 2.1 Texture wavelength influence on surface characteristics (PIARC, 1987)

It has been noted that the adhesion component is reduced when particles or water film are present at the contact surface (Roberts, 1992; Person, 1998) and will disappear if the surface is completely covered by a lubricant. It is believed that the adhesion component of skid resistance is governed by the microtexture of pavements (Priyantha and Gary, 1995). On wet pavements, the intimate contact remains by breaking through the thin water film even after the bulk of water has been displaced. However, the manner in which microtexture is effective is complex because it affects the molecular and electric interaction between the contacting surfaces (Kummer, 1966). The adhesion component is dependent of vehicle speed and is dominant at low speeds (Moore, 1972). In the low speed range, the microtexture ensures physical penetration of the interface squeeze-film so that good adhesion is obtained.

Hysteresis

The hysteresis component of skid resistance is related to the energy storage and dissipation as the tire rubber is deformed when passing across the asperities of a rough surface pavement. The hysteresis component typically becomes dominant after the tire begins to skid. At that moment, the adhesion component, which is dominant prior to a skidding condition, begins to decrease and the hysteresis component undergoes a corresponding increase (Choubane et al. 2003).

The hysteresis contribution usually is fairly independent of speed in the range in which highway tires are likely to slide. Thus it gains in importance at higher speeds when adhesion component decreases (Moore, 1969). Although both microtexture and macrotexture have effect on the hysteresis friction, it is believed that the magnitude is mainly controlled by the macrotexture of pavement surface (Priyantha and Gary, 1995).

2.2.2 Affecting factors of Skid Resistance

Pavement skid resistance can be affected by many factors, which can be broadly classified into five categories:

(a) Pavement surface characteristics and drainage: pavement surface texture, aggregates polishing, bleeding, rutting and drainage design;

(b) Environmental condition: pavement surface temperature, climate change, rainfall flushing;

(c) Vehicle factors: inflation pressure, tire temperature, tire treads pattern and tread depth, wheel load and vehicle speed;

(d) Contaminants: presence of water, water film thickness, presence of rubber or oil or ice;

(e) Other factors: such as pavement markings.

The five categories as stated above constitute the major components of the tire-fluid-pavement interaction in a very general sense. A thorough investigation of the interactions among these components would give researchers a better understanding for the development of skid resistance and the occurrence of hydroplaning. These factors will respectively be described in the following sections.

2.2.2.1 Pavement Factors

Affecting factors involving pavement are surface characteristics and drainage. The most common surface characteristics that affect skid resistance are pavement surface texture, aggregates polishing, bleeding and rutting.

Surface Texture

Microtexture and macrotexture are the two levels of pavement texture which affect the friction between the pavement and tire, as depicted in Figure 2.2. Microtexture refers to irregularities in the surfaces of the stone particles (fine-scale texture) that affect adhesion. It has the function of preventing the formation of a thin, viscous, lubrication film of water between the tire and road. A harsh microtexture provides a high level of friction, but a surface having a smooth, polished microtexture will give poor friction even at low speeds (Leland and Taylor, 1965). Microtexture and adhesion contribute to skid resistance at all speeds especially at speeds less than 30 mph (48km/h).

Macrotexture refers to the larger irregularities in the road surface (coarse-scale texture) that affect hysteresis. Macrotexture has the primary function of providing drainage channels for water trapped between the tire and road. Surfaces having rough macrotexture show a less rapid decrease of friction with increasing speed than do surfaces having smooth macrotexture (Sabey, 1966), as shown in Figure 2.3. Macrotexture and hysteresis are less critical at low speeds; however, as speeds increase a coarse macrotexture is very desirable for wet weather travel.

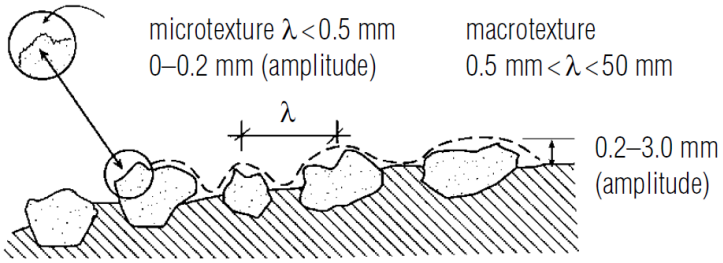

Figure 2.2 Comparison between microtexture and macrotexture (Flintsch et al., 2003)

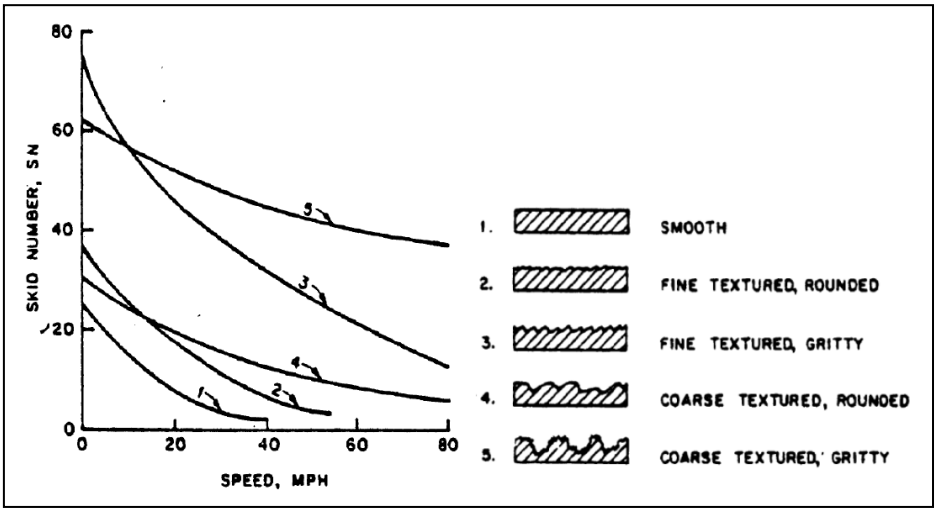

Figure 2.3 Skid resistances of pavements with different surface characteristics (Sabey, 1966)

The other two surface texture properties, megatexture and roughness, are less

significant than micro- and macro-texture in the generation of skid resistance. However, they are key components in the overall quality of the pavement surface.

Aggregate Polishing

As described in the former section, surface texture is an important affecting factor of skid resistance. It has been noticed that microtexture depends largely on the mineral composition and roughness of the aggregates while initial macrotexture depends on the specific type of mix, the aggregate gradation, and the stability of the mix (Jayawickrama, et al., 1996). Polishing directly affects the microtexture of pavement. Thus skid resistance diminishes at all speeds as a result of polishing (Gandhi et al. 1991). When surface aggregates become smooth, the friction between the pavement and tires is considerably reduced during wet weather, and the pavement may become dangerously slippery.

Bleeding

Bleeding occurs on bituminous pavements when the asphalt binder fills the air voids of the mix and expands to form a thin film on the pavement surface. It occurs at high temperatures and is not reversible in cold weather. Therefore, the film of asphalt accumulates on the pavement surface, obscuring the effectiveness of the skid resistance qualities of the aggregate and resulting in a significant loss of skid resistance when the pavement becomes wet.

Rutting

Rutting is most noticeable to the driver after rainfall when the ruts remain filled with water while the pavement surface begins to dry. The excess water in the wheel paths

can lead to hydroplaning at lower speeds, as well as increase splash and spray, all of which are potential hazards to drivers.

Drainage System

A good drainage system with appropriate cross slopes is also necessary in order to provide rapid removal of water from the pavement surface, thereby reducing the risk of hydroplaning.

2.2.2.2 Environmental Conditions

Environmental conditions have both long- and short-term effects on the skid resistance of a pavement. Seasonal variation of skid resistance is an example of the long-term effects of climate condition. It is found that skid resistance is higher in the winter and spring than in the summer and fall (Figure 2.4).

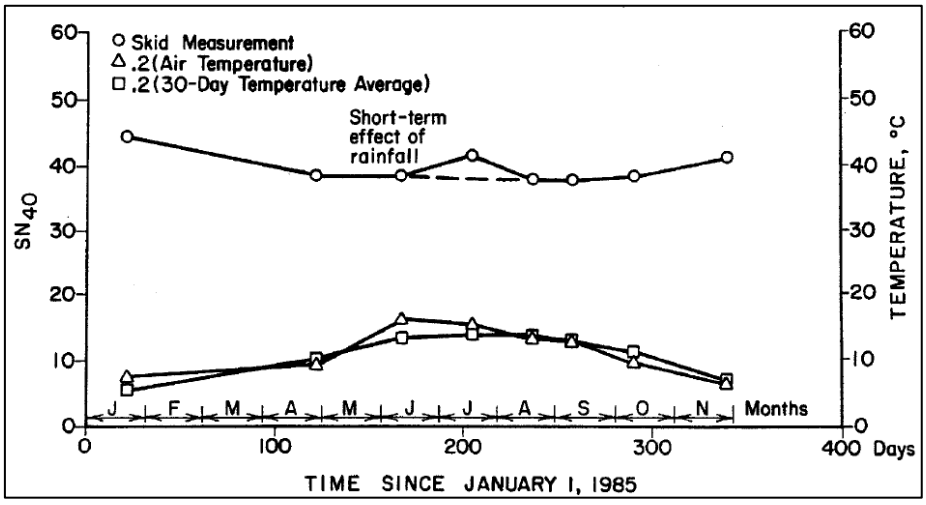

Figure 2.4 Long-Term Variations of Skid Resistance in Pennsylvania (after Kulakowski et al., 1990)

The magnitude of these variations has been reported as high as 30 SN, however, variations of 5 to 15 SN are more common (Jayawickrama and Thomas

1998). In UK, side force coefficient values have been shown to vary by more than 25 percent across the seasons (Gargett 1990).

Short-term fluctuations in friction coefficient were found to be superimposed on the long term trends in the summer data (Saito and Henry, 1983; Kulakowski et al., 1990). The friction coefficients were highly variable, by up to 20 SN (Figure 2.5). Saito and Henry (1983) noted the skid resistance values were lowest at the end of a long dry period and highest just after a rainstorm. This was believed to be due to the accumulation of dust, engine products (e.g., carbon), and other debris filling in the pavement microtexture, effectively causing "lower texture" pavement in the dry periods.

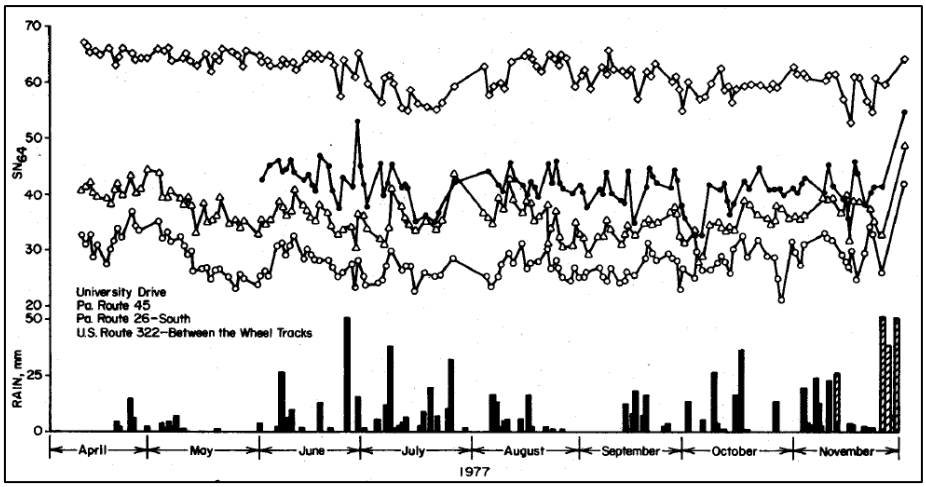

Figure 2.5 Short-Term Variations on Highways in Pennsylvania (after Saito and Henry, 1983)

2.2.2.3 Vehicle Factors

Vehicle factors affecting skid resistance include tire inflation pressure, tire temperature, tread pattern, tread depth, wheel load, and vehicle speed. These factors contribute to the level of strength in the interaction generated between the tire and the

pavement. In general, friction decreases with speed increasing, while increases as tire pressure and wheel loads increasing, particularly on wet pavements. It is reported that both peak and locked wheel braking force coefficients decrease with increasing speed on the wet pavements. However, the locked wheel value usually decreases more rapidly than does the peak value. The combination of high speeds and wet pavements can lead to hydroplaning. The decreasing trends of wet pavement high-speed skid resistance can be seen in Figures 2.6.

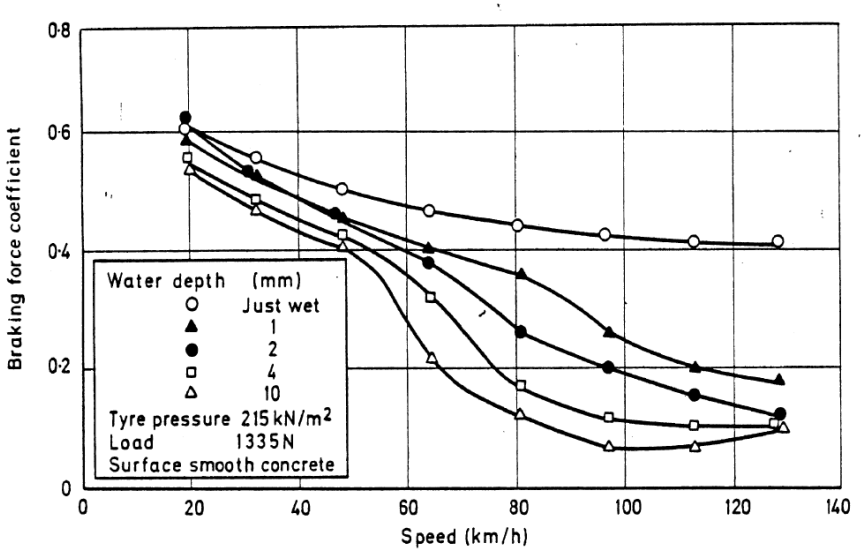

Figure 2.6 Effect of speed on wet pavement skid friction (McLean and Foley, 1998)

Tire treads are another important factor. After the tread is worn away, tires develop more friction on dry pavements because more rubber comes into contact with the pavement. However, when the pavement becomes wet, the friction diminishes with tread wear as shown in Figure 2.7 because the tire cannot expel water from the contact area through the treads. In addition, the types of tires also have significant influence on skid resistance. Truck tires generally have remarkably lower skid

resistance compared with car tires as shown in Figure 2.8 (Dijks, 1976; Williams and Meades, 1975).

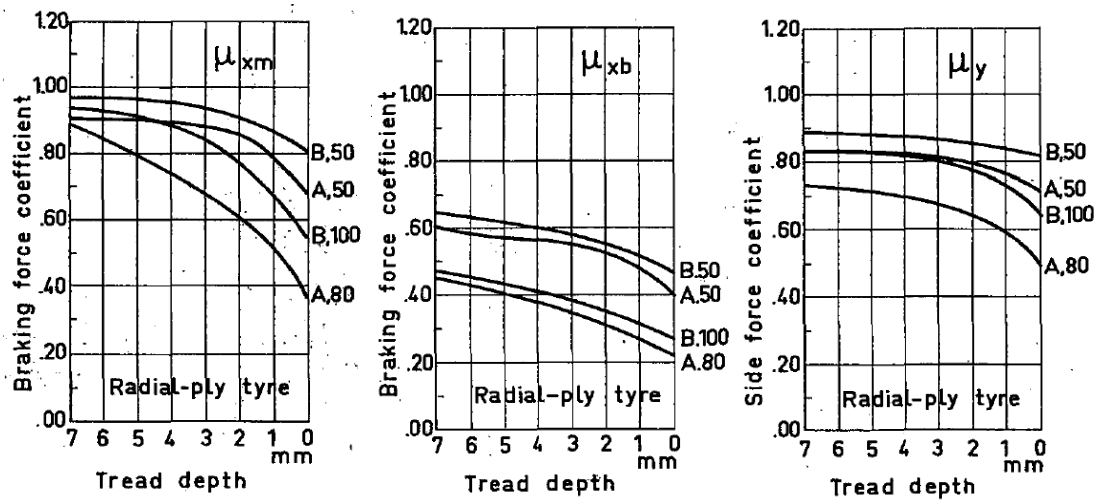

Note: $\mu_{xm} = (F_x / F_z)_{\max}$ is the maximum value of the braking force coefficient before locking; $\mu_{xb} = F_x / F_z$ is the average braking force coefficient when the wheel is locked, and $\mu_y = F_y / F_z$ is the average side force coefficient at a slip angle, where F_x is braking force, F_y is side force and F_z is the vertical load. 50, 80, and 100 are three test speeds.

Figure 2.7 Skid resistance decreases with the tread depth for car tires (Dijks, 1976)

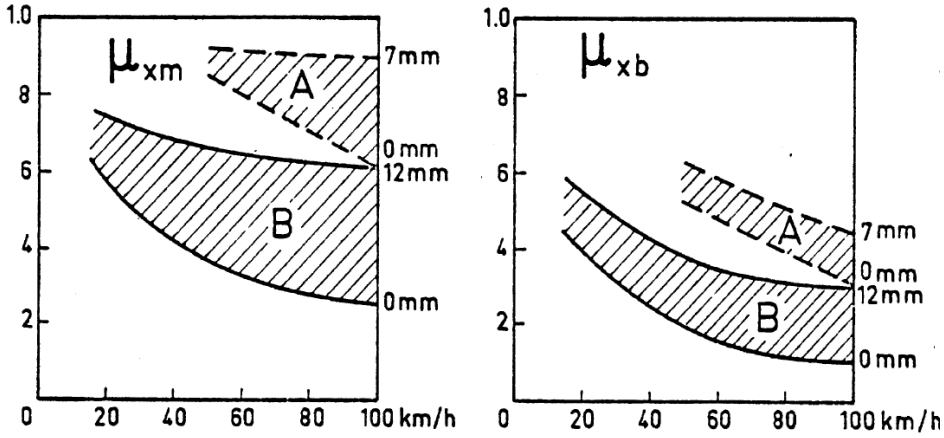

Note: Refer to Figure 2.7 for definition of symbols.

Figure 2.8 Comparison of skid resistance (A: car tires; B: truck tires) (Dijks, 1976)

2.2.2.4 Contaminants

Rubber, oil, and water are some of the more common contaminants that are found on roadways. When contamination, such as a thin film of oil or water, is present, the tire-pavement interface will be lubricated, thus reducing tire-pavement friction significantly (Irick, 1972). It has been noticed that even a very small amount of water can cause a large decrease in friction coefficient, especially on surfaces having a polished microtexture (Leland and Yager, 1968). As shown in Figure 2.9, an increase in water depth causes a decrease of wet friction. The effect is greatest at high speed on smooth surfaces.

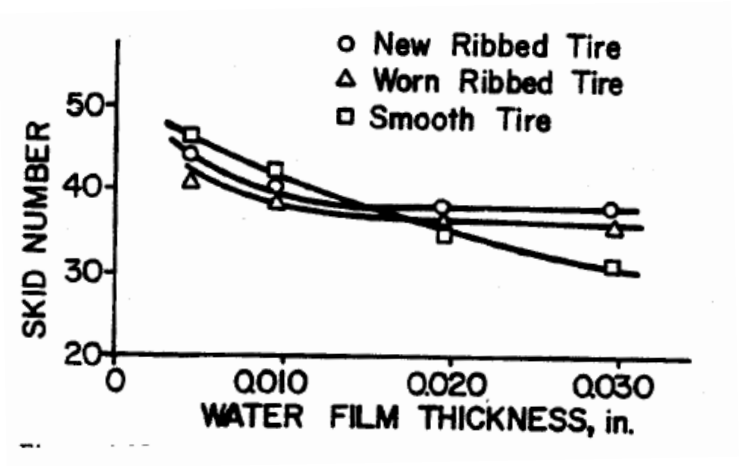

Figure 2.9 Effect of Water Film Depth (Meyer et al, 1974)

Most of the decrease occurs in the first 3-4 mm of water depth. At greater depths, for most tires, the tread grooves become flooded and no further effect of increasing depth was seen (Staughton and Willians, 1970). In deep water (more than 3-4 mm), tread pattern and surface texture have a large effect only at speeds below the hydroplaning speed; but in shallow water tread pattern and surface texture continue to have an effect at higher speeds.

2.2.2.5 Other factors

Large pavement markings, such as STOP bars, large arrows, school zone marking, box junctions, and other large marking are detrimental to the skid resistance provision particularly in the approach of roundabouts or intersections, where braking usually occurs. Therefore, the selection of appropriate pavement marking material can also be important when considering pavement skid resistance.

2.2.3 Measurement of Skid Resistance

2.2.3.1 Laboratory Measurement of Pavement Friction

Two major devices, British Pendulum Tester and Dynamic Friction Tester, are used for the measurement of pavement friction characteristics in laboratory. Both of the devices can also be used to measure frictional properties in the field. They offer the advantage of being highly portable and easy to handle.

British Pendulum Tester (BPT)

The procedure for measuring frictional properties using BPT (Figure 2.10) is specified in ASTM E303. The BPT operates by releasing a pendulum from a fixed height above the pavement surface. The pendulum has a rubber slider attached to the end. As the slider moves across the pavement surface, the frictional force reduces the kinetic energy of the pendulum. The magnitude of the frictional force of the pavement can be measured from the difference in the height of the pendulum before and after the slider crosses the pavement (Henry 2000).

The slip speed for BPT is very low (6 mph or 10 km/h) and as a result British Pendulum (BPN) is typically used as a surrogate for pavement microtexture. The

disadvantages of BPT are that it only provides a measurement for the friction at very low speeds and that the values of BPN do not correlate well with the frictional properties measured using other devices (Saito et al. 1996).

Figure 2.10 British Pendulum Tester (BPT)

Dynamic Friction Tester (DFT)

DFT was developed as an alternative to BPT, which could measure pavement friction and its speed dependency. The DF tester is specified in ASTM E1911, as shown in Figure 2.11.

Figure 2.11 Dynamic Friction Tester (DFT)

DFT consists of a rotating disc with three attached rubber sliders. Water is applied to the pavement surface as the disc begins to rotate without contact between the sliders and the pavement surface. Once the target speed, typically 90 km/h, is reached, the water supply is stopped and the disc is lowered to the pavement surface and a vertical load is applied. As the disc rotates, a frictional force develops between the pads and pavement surface. The coefficient of friction is then computed based on the frictional force and the vertical load applied to the disc. The coefficient of friction is measured continuously as the speed of the disc's rotation decreases due to the application of the frictional force. This provides a profile of the speed dependency of the pavement friction (Saito et al. 1996).

2.2.3.2 Full-Scale Measurement of Skid Resistance

There are four basic types of full-scale friction measurement devices currently used around the world, which are locked wheel method, side-force method, fixed-slip method, and variable slip method (Henry 2000). All of them utilize one or two full-scale test tires to measure the pavement friction properties under different conditions. These devices have an advantage over the small-scale lab measurement devices in that the friction measurements can be taken at or close to highway speeds.

Locked-Wheel Device

The locked-wheel method, specified in ASTM E274, is the most common method for measuring pavement friction. This method is meant to test the frictional properties of the surface under emergency braking conditions for a vehicle without anti-lock brakes. The locked-wheel approach tests at a slip speed equal to the vehicle speed, while the wheel is locked and unable to rotate. The results of a locked-wheel test

conducted under ASTM specifications are reported as a Skid Number (SN) which is calculated by

$$SN = 100\frac{F}{N} \tag{2.1}$$

where F is the friction force and N is the vertical load on the test tire.

Locked-wheel friction testers (Figure 2.12) usually operate at speeds between 40 and 60 mph (1 mph=1.61 km/h). Once the target test speed has been attained, a film of water is sprayed onto the pavement 10 to 18 inches (1 inch = 2.54 cm) in front of the test tire with a nominal thickness of 0.5 mm. At this point, a vertical load of 1085 ± 15 pounds (1 pound=0.453 kg) is applied to the test wheel and the wheel is locked. The wheel is locked for a period of 1 second and the frictional force is measured and averaged over that period of time.

Figure 2.12 Locked-wheel skid resistance testers

The locked-wheel trailer offers the advantage that the test variables are easy to understand and control. The primary disadvantage of this method is that the friction measurement is not continuous over the test section. In order to avoid undue wear on

the test tire, the tire can only be locked for one-second increments. This means that locations with low friction could be missed in the testing procedure.

Side-Force Device

The side-force device is used to measure the ability of vehicles to maintain control in curves. This method involves maintaining a constant angle, the yaw angle, between the tire and the direction of motion. Water is applied to the pavement at a prescribed rate in front of the test wheel, a vertical load is applied to the test tire, and the force perpendicular to the plane of rotation (the side-force) is measured. The side-force coefficient (SFC) is calculated based on the following equation (Gargett 1990)

$$SFC(v,\alpha) = 100\frac{F_s}{N} \tag{2.2}$$

where v is the velocity of the test tire, α is yaw angle, N is the normal force on the test tire, and F_s is the force perpendicular to plane of rotation.

Figure 2.13 SCRIM in operation

Side-force testers are particularly sensitive to the pavement microtexture but are generally insensitive to changes in the pavement macrotexture. The two most

common side-force measuring devices are the Mu-Meter and the Side-Force Coefficient Road Inventory Machine (SCRIM), as shown in Figure 2.13. The primary advantage offered by side-force measuring devices is the ability for continuous friction measurement throughout a test section. This ensures that areas of low friction are not skipped due to a sampling procedure.

Fixed-Slip Device

Fixed-slip method is meant to measure the friction observed for vehicles with anti-lock brakes. Fixed-slip devices maintain a constant slip, typically between 10 and 20 percent, as a vertical load is applied to the test tire; the frictional force in the direction of motion between the tire and pavement is measured. The percent slip can be calculated by

$$slip\% = 100\left(\frac{v - r\omega}{v}\right) \tag{2.3}$$

where $slip\%$ denotes the ratio of slip speed to test speed (in percent), v denotes the test speed, r is the effective tire rolling radius, and ω is the angular velocity of test tire. The measurements from fixed-slip devices are reported as Brake Slip Number (BSN), which are calculated using

$$BSN(v, slip\%) = \frac{F}{N}100 \tag{2.4}$$

where $BSN(v, slip\%)$ denotes the brake slip number for a given test speed and percent slip, F measured friction force, N is the vertical force on test tire, and v is the test speed.

Fixed-slip devices share an advantage with the side-force measuring devices in that they can be operated continuously without producing undue wear on the test tire. These devices are also more sensitive to microtexture as the slip speed is low. The

Griptester device (Figure 2.14) is a representative of fixed slip devices. The operation of this device is covered by BS 7941-2 specification.

Figure 2.14 Griptester for skid resistance testing

Variable Slip Device

Variable slip device measures the frictional force as the tire is taken through a predetermined set of slip ratios. ASTM Standard E1859 outlines the full procedure for measuring pavement friction using a variable slip technique. The slip friction number (SFN) is a measurement of the longitudinal frictional force divided by the vertical force on the test tire (ASTM E 1859). The SFN is recorded over a range of slip speeds from zero up to the test speed and the results are presented in a graphical format.

2.2.3.3 Measurement of Surface Texture

Because pavement skid resistance is tied to surface macrotexture, some methods seek to measure macrotexture then correlate it with skid resistance as measured by other traditional methods. The simplest surface texture measurement is the sand patch test (ASTM E965). The test is carried out on a dry pavement surface by pouring a known quantity of sand onto the surface and spreading it in a circular pattern with a

straightedge. As the sand is spread, it fills the low spots in the pavement surface. When the sand cannot be spread any further, the diameter of the resulting circle is measured. This diameter can then be correlated to an average texture depth, which can be correlated to skid resistance. A texture depth of about 1.5 mm (0.06 inches) is normally required for heavily trafficked areas.

In addition, laser or advanced image processing equipment has been employed to determine surface macrotexture from a vehicle moving at normal travel speeds. One particular device, the Road Surface Analyzer (ROSAN) developed by FHWA (Figure 2.15) can be used for measuring texture, aggregate segregation, grooves, tinning, joints, and faulting. Some integrated analysis units can use surface texture measuring to estimate skid resistance. One drawback of this method is that skid resistance is not entirely determined by surface macrotexture of pavements. Therefore, correlation between surface macrotexture and skid resistance is often difficult to extrapolate into any general guidance.

Figure 2.15 Prototype ROSAN devices

2.2.4 Previous Researches on Skid Resistance

Skid resistance is one of the most important issues and concerns in pavement engineering for traffic safety. It involves pavement design, construction, maintenance and management. Many researchers in the world, especially in USA and Europe, have done numerous experiments and numerical investigations on this topic. Thus in this section, a brief review on important researches for skid resistance, both experimental and numerical, is carried out for reference.

2.2.4.1 Experimental Studies

Two research focuses during the past century are to identify the affecting factors for skid resistance and to correlate them to skid resistance quantitatively. For the first purpose, several devices from the simplest locked wheel method to the more sophisticated trailers capable of measuring braking force over the entire range of wheel slip were invented to measure skid resistance of pavements or runways. They are widely utilized to investigate the effect of different factors on the skid resistance. Many researchers (Close, 1968; Bergman, 1971; Fancher, 1970; Giles, 1956; Henry, 2000) attempted to get a regression relationship between skid resistance and the affecting factors using measured field data. On the other hand, three methods, average texture depth, mean void width and stereo photographs (Sabey, 1966; Schulze and Beckman, 1962) were utilized to quantify surface texture so as to yield a statistically significant correlation between the surface texture measurement and skid resistance. However, these measures of texture deal only with macrotexture though the microtexture is known to have a strong influence on the skid resistance.

Others useful facilities are also constructed in laboratory and field to investigate the effects of parameters on skid resistance and hydroplaning by simulating the real traveling conditions of vehicle. For example, the Langley Landing Loads Track constructed at NASA, USA was used to study hydroplaning phenomena and wet traction performance of aircraft (Horne and Leland, 1962; Leland and Taylor, 1965; Leland et.al, 1968). A wetted internal drum tire testing machine at the University of Karlsruhe, Germany was employed to study the effects of water depth and tread pattern variations though it is not feasible to simulate real road surface texture (Gengenback, 1968; Bergman et.al, 1971).

Maycock (1967) and Gengenbach (1968) conducted many experimental studies to investigate the effects of width, depth and spacing of tire tread groove on skid resistance. They concluded that width, depth and spacing of the tire tread grooves have tremendous effect on wet skid resistance. Giles and Leland (1956) and Lander and Williams (1968) indicated that tire tread pattern could improve wet traction on surfaces with smooth macrotextures but had little or no effect on rough surfaces with sufficient capability of drainage. They also found that smooth tire was actually somewhat superior on very rough surfaces. However, Staughton (1970) claimed that at high speeds more that 80 mph both coarse surface texture and tread pattern were essential for obtaining good skid resistance. Maycock (1967) also concluded that tread grooves were very important on surface with smooth macrotexture but have little or no effect on coarse textured surfaces. He also discovered that increasing the number of ribs while keeping the ratio of rib width to groove width and the rib area constant can just improves the wet traction up to some extent. For a given rib width, groove depth, water depth and number of ribs, there is an optimum groove width for wet braking friction.

Kelly (1968) reported that transverse or lateral grooves in the shoulder region are more important than those in the center and appear to be highly effective. For a given number of grooves there is an optimum tread width to maximize the braking and cornering traction. He also found that increasing tire load at constant inflation pressure increases BFC, while increasing inflation pressure at constant load cannot improve BFC continually and there is an optimum pressure for maximum traction.

Investigation by Grosch and Maycock (1968) concluded that both peak and locked wheel braking force coefficients decrease with increasing speed on wet surfaces. However, the locked wheel value usually decreases more rapidly than does the peak value. This effect is most marked on smooth surfaces, so that smooth surfaces tend to show a greater difference between peak and locked wheel values.

Staughton and Williams (1970) recognized that: 1) Even a very small amount of water can cause a large decrease in friction coefficient; 2) Wet friction decrease with increasing water depth; and 3) Most of the decrease occurs in the first 3-4 mm of water depth. This finding agrees well with the research by Williams (1966). In deep water (more than 3-4 mm), hydroplaning speed depends primarily upon tire inflation pressure and increases with increasing inflation pressure. Tread pattern, tire construction, tire load and surface texture have only small effect. However, locked wheel BFC is not significantly affected by inflation pressure. At low water depths, locked wheel BFC is strongly affected by tire tread pattern and surface texture, especially at high speed. The research conducted on wet tracks by Gengnebach (1968), however, concluded that increasing inflation pressure at constant tire load improves braking and cornering traction. He found that for a given speed, groove depth and water depth, there is a optimal value for the ratio of groove area to total contact area and this value increases with increasing water depth.

Holmes (1970) studied the breaking and corning performance of tires, which indicated that in pure braking, a curve of braking force coefficient versus wheel slip shows a rapid initial rise to a peak between 7% and 25% slip, followed by a gradual decrease as wheel slip increases toward lockup. The effect of a slip angle on the BFC versus wheel slip curve is to decrease the initial slope, shift the peak to a higher value of slip, and to decrease the maximum available braking force. At large slip angles, maximum braking force is obtained at lockup. Also cornering force obtained at a given slip angle is reduced when a braking force is applied.

In the other aspect, several models have been developed to describe the relationship between Skid Number (SN) and affecting factors such as slip speed, mean texture depth (MTD) (Henry and Meyer 1983; Henry, 1986; Meyer, 1991; Kulakowski and Meyer, 1989). Several attempts have also been made to quantify environment effects during the past several decades. Hill and Henry (1982) developed a mechanistic model to account for both the short-term and long-term seasonal effects. Research conducted in Texas attempted to develop a simple regression model including the average temperature and cumulative rainfall just prior to the measurement, as well as the Julian calendar day. This model showed very good correlation with the measured skid data and could account for both short-term and long-term seasonal variations (Jayawickrama and Thomas 1998).

2.2.4.2 Numerical Studies

Compared with the experimental researches, much less literatures can be found on analytical studies of skid resistance due to the complexity of such a problem and the difficulties in establishing effective mathematical models. Skid resistance simulation can be achieved through numerical modeling if the predictive model can adequately

describe the phenomenon in realistic conditions with taking into account the detailed groove structure of tires, the large deformability of tire and the complex fluid structure interaction between tire-pavement and water, together with all the fluid flow features, such as free surfaces, water film atomization and air entrainment, including turbulence effects. This means that one should handle a two-phase flow with interfaces in a computational domain with deforming boundaries and shows the necessity of constructing a fluid-structure interaction model. However, establishing such a model is not an easy work and will be very time consuming in computation.

During the past three decades, finite element method (FEM) has been widely used both for tire design in tire industries and for pavement stress analysis in civil engineering. The modeling of pavement-vehicle interaction is a major academic research topic. Numerous researchers utilized the simplified tire or just the idealized load to analyze the pavement response under static or dynamic loads (AI-Qadi, et al. 2004). They utilized the complex constitutive material model but ignore the accuracy of applied load and simplified the contact relation between tire and pavement. Tanner (1996), Davis (1997), Johnson et al. (1999) and Han (2003) developed finite element models to simulate dry tire-pavement interaction of rolling and sliding tires on smooth pavement surfaces and the response of tire structure due to tire-pavement interaction. These simulations focused on the design and modeling of the pneumatic tire and the selection of materials for the manufacture of tire.

Recent developments in finite element commercial software package such as ABAQUS, ADINA and MSC allow a relatively detailed analysis of the tire-pavement contact and even can involve the complex Fluid-Structure-Interaction (FSI). Liu et al. (2003) developed a 3D finite element model using ABAQUS to simulate the British Pendulum Test. The essential geometric properties were captured using the beam

elements and a spring element to provide the loading mechanism. The results computed from the FEM model showed a very good agreement with laboratory measured test data. They also used this model to study the pattern of macrotexture of pavements. However, the model could not be used to analyze complex surface textures with non-symmetric patterns because it suffered excessive distortion when tested on these surfaces.

Ong and Fwa (2007, 2008) conducted FEM simulation to investigate the skid resistance performance of the smooth passenger car tire. They also evaluated the effects of different factors on skid resistance: sliding speed, wheel load, water-film thickness and tire inflation pressure. The results showed that tire inflation pressure, truck wheel load, water-film thickness and sliding speed had significant effects on the skid resistance experienced by a smooth truck tire. The simulation results indicated that at very low sliding speeds, the sliding skid resistance was not much affected by the values of tire inflation pressure and water-film thickness, although it is sensitive to the magnitude of wheel load. At higher sliding speeds, as some water would be trapped between the tire and pavement surface, the magnitude of skid resistance becomes sensitive to the values of all four factors. When only one factor is allowed to vary, and all other factors and conditions remain constant, the analysis indicates that skid resistance value varies positively with tire inflation pressure and wheel load, but negatively with water-film thickness and truck sliding speed.

Most recently Ong and Fwa (2010) employed a numerical model to discuss the safe braking distance of vehicles. They tried to give an explanation for the implications of braking distance specifications and their relations with pavement friction management. As an illustration, they examined the relationship between the AASHTO stopping distance requirements and the skid resistance threshold level

adopted by several state pavement management authorities. The results of their analysis indicated that it is necessary to maintain consistency between geometric design stopping distance requirements and pavement friction management to achieve safe vehicular operations.

2.3 Hydroplaning

Hydroplaning or aquaplaning, as shown in Figure 2.16, is a phenomenon that occurs when a layer of water builds between the rubber tires of vehicle or aircraft and the surface of road, leading to the loss of traction and thus preventing the vehicle or aircraft from responding to control inputs such as steering, braking or accelerating (Horne et.al, 1963). It was first noticed and demonstrated experimentally during a tire treadmill study in 1957.

Figure 2.16 Phenomenon and test of hydroplaning (Ludema, 1975)

When only a portion of the contact region is separated by water, shear force capability is substantially reduced but not totally lost and the tire is said to be partially

hydroplaning; when the water film pervades the entire contact region, the tire shear force capability is reduced to such a low level that directional control of the vehicle becomes impossible and the tire is said to be totally hydroplaning (Martin, 1966). At such extreme conditions, hydroplaning should be studied carefully and should be avoided in practice; otherwise, it will lead to a high risk of traffic accidents.

2.3.1 Types of Hydroplaning

Hydroplaning can be divided into three categories for pneumatic-tired vehicles: dynamic hydroplaning, viscous hydroplaning and reverted rubber hydroplaning (Horne et al., 1968).

2.3.1.1 Dynamic Hydroplaning

Dynamic hydroplaning results from uplift forces acting on a moving tire from the tire-fluid interaction. Partial dynamic hydroplaning may occur at ordinary speeds, but the uplift forces are not large enough to develop full dynamic hydroplaning without substantial vehicle speed and a significant water-film thickness. Typically, full dynamic hydroplaning occurs on thick water films when the water depth exceeds 2.5mm (Yager et al., 1970). In such a hydroplaning condition, squeeze film zone prevails and transition and traction zones completely disappear. The majority of the friction loss associated with dynamic hydroplaning occurs at high speeds.

2.3.1.2 Viscous hydroplaning

This is a mechanism contributing to friction loss on damp or wet runways, typically at low speeds, under the following conditions: a) Thin water films less than 0.25mm thick (Leland, Yager, and Joyner, 1968); and b) Smooth pavements–the texture

existing on pavement surface is insufficient to break up and dissipate the thin viscous film (Horne et al., 1968). Fluid pressures produced by viscous hydroplaning develop quickly as the ground speed is increased from a low value. They then tend to “level off” as the speed is increased towards the full hydroplaning speed as shown in Figure 2.17. Thus the majority of the friction loss associated with viscous hydroplane-ing occurs at low speeds.

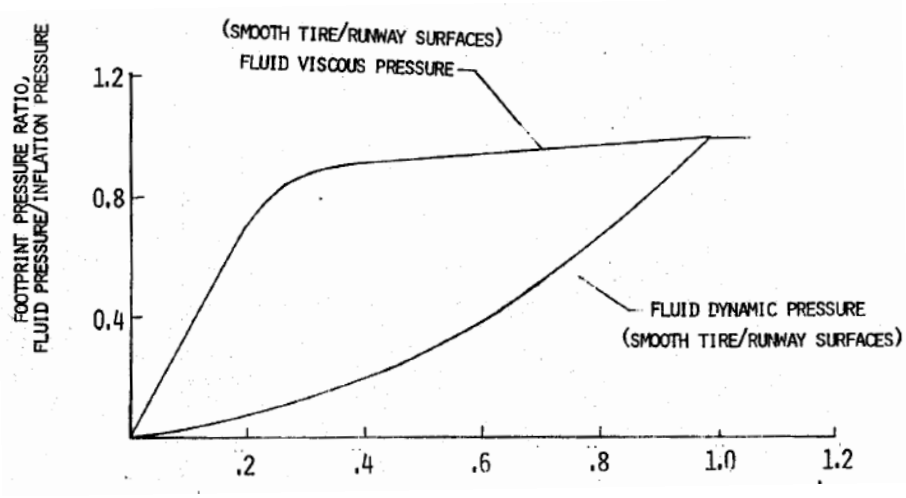

Figure 2.17 Fluid pressures in tire contact zone with ground speed (Horne, 1974)

2.3.1.3 Reverted rubber hydroplaning

This occurs when the tire fails to spin up, which results in a non-rotating tire sliding on the pavement surface. High temperatures are produced which can generate steam in the tire footprint, causing vulcanization of the rubber (Comfort, 2001). The factors contributing to the occurrence of reverted rubber hydroplaning can be summarized as follows: a) Poor pavement texture, b) High speed, c) Wet or flooded pavement and d) Deficient brake system.

2.3.2 Manifestations of Hydroplaning

Eight manifestations of tire hydroplaning had been experimentally observed. These manifestations are: detachment of tire footprint, hydrodynamic ground pressure, spin-down of wheel, suppression of tire bow wave, scouring action of escaping fluid in tire-ground footprint region, peaking of fluid displacement drag, loss in braking traction, and loss of tire directional stability (Horne and Dreher, 1963).

Detachment of tire footprint

It was observed that as ground speed increased, a wedge of fluid progressively penetrates the tire-ground contact region and a hydrodynamic pressure is developed between the tire and the ground. The resulting hydrodynamic lift tends to detach the tire footprint from the runway surface. It is also observed that as ground speed increases the dry contact patch developed between the rolling tire and the ground is progressively reduced and then entirely eliminated when total hydroplaning is achieved.

Variation of Hydrodynamic ground pressure

As ground speed increases, fluid inertia effects would tend to retard fluid escape in the tire-ground contact region and the fluid wedge formed would tend to detach the tire from the ground. At some high ground speed the hydrodynamic lift developed under the tire equals the partial weight of the vehicle acting on the tire and any further increase in ground speed beyond this critical speed must force the tire to lift completely off the runway surface. The tire is termed to be partially hydroplaning at ground speeds below hydroplaning speed and totally hydroplaning at ground speeds in excess of the tire hydroplaning speed.

Spin-down of unbraked-wheel

Unbraked-wheel spin-down arises from two hydrodynamic lift effects which combine to produce a total wheel spin-down moment in excess of the wheel spin-up moment due to all tire drag sources. The two effects are: (a) as ground speed increases, the hydrodynamic lift progressively detaches the tire footprint from the pavement surface and makes the tire ground frictional spin-up moment tend toward zero values, and (b) the center of pressure of the hydrodynamic pressure and resulting lift developed between the tire footprint and ground surface shifts increasingly forward of the axle as the ground speed increases and produces the wheel spin-down moment.

Suppression of tire bow wave

Under partial and total hydroplaning, it was observed that a large bow wave forms in front of the tire for all ground speeds below the hydroplaning speed. As the ground speed increases, the angle of the bow wave with respect to the runway tends to reduce progressively until at some high ground speed in the total hydroplaning region, the bow wave disappears completely.

Scouring action of escaping fluid in tire-ground footprint region

The escaping fluid under the action of high hydrodynamic pressures developed in the tire-ground contact region tends to clean the runway surface in the tire path with the result that white streaks instead of black streaks are formed by the tires on the pavement surface. It should be pointed out that this scouring action may also develop when smooth tires are moving on wet smooth pavement surfaces at ground speeds below the tire hydroplaning speed because of viscous effects which also produce high hydrodynamic pressures in the tire-ground contact region.

Peaking of fluid displacement drag

It was shown experimentally that fluid displacement drag reaches a maximum at a ground speed near the tire hydroplaning speed. It was observed that increasing the ground speed above the critical hydroplaning speed results in appreciable reductions in fluid drag. This result is attributed to the tires lifting off the runway surface at the higher ground speeds and consequently displacing less runway fluid from the tire paths.

Loss in braking traction

Whenever a pavement surface is flooded with fluids such as slush or water to depths large enough (7.62 mm) to initiate tire hydroplaning, the loss in braking traction is more substantial than the reduction of dry-runway values, i.e., braking friction coefficients approach free-rolling friction coefficient. At this point, applying brakes to wheels that have either completely or nearly stopped rotating from hydroplaning effects cannot be expected to improve the existing tire retardation forces and friction coefficient at all.

Loss in directional stability and control

Test runs conducted by the Federal Aviation Agency with National Aeronautics and Space Administration on a four-engine jet transport show that at a speed of 120 knots (1 knot=1.852 km/h), it was observed to yaw and drift laterally on the runway while in the slush bed. The loss of tire directional stability at and above tire hydroplaning speeds could be extremely serious to aircrafts especially during take-offs.

2.3.3 Previous Studies on Hydroplaning

2.3.3.1 Model development (Three-Zone Concept)

In order to investigate the wet performance of tires, hydrodynamic lubrication, elasto-hydrodynamic lubrication (EHL) and boundary layer lubrication are employed to describe the phenomena of hydroplaning by researchers. Gough (1959) put forward a "Three-Zone Concept" to describe the sliding locked-wheel traction under wet conditions. Then Moore (1966) developed this concept further to cover the case of the rolling tire. This concept is demonstrated to be useful in understanding the effect of water and speed on hydroplaning and skid resistance. The three zones, as shown in Figure 2.18, are described as follows:

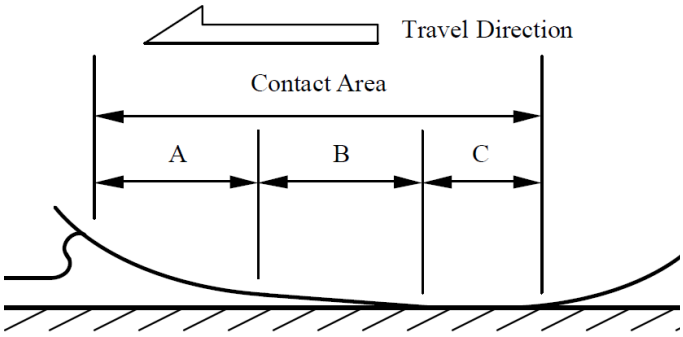

Figure 2.18 Schematic of Three-Zone Concept (A: Squeeze-film zone; B: Transition zone; C: Traction zone)

Squeeze-film Zone

This zone is governed by the EHL, where the wedge term largely predominates out of the three terms. It is called the squeeze-film zone, meaning some of the water is squeezed out from the space between tire and pavement, but some is trapped to form a water wedge. The water wedge penetrates backward into the footprint area as the speed increases. Frictional force developed in this zone is strongly dependent on the bulk properties of the lubricant, namely viscosity and velocity gradient in the

lubricant film. Total dynamic hydroplaning occurs as full separation between the tire and pavement surface takes place.

Transition Zone

The transition zone begins when the tire elements, having penetrated the squeeze-film, commence to drape dynamically about the asperities of the road surface, and make contact with the lesser asperities. In this zone, a progressive breakdown of the water film occurs down to thickness of a few layers of water molecules. Therefore, a mixed-lubrication regime exists, which is part hydrodynamic and part boundary. The effective friction coefficient varies widely from a very low value of viscous hydroplaning at the leading edge of the transition zone to the friction value of boundary layer lubrication at the end edge of this zone, which is comparable to dry friction. At ordinary speeds, this zone is common and the uplift forces are not great enough to develop full dynamic hydroplaning (Balmer and Gallaway, 1983).

Traction Zone

This region is the rear part of the contact area, beginning with the end of transition zone. The lubrication water film in this zone has been substantially removed and vertical equilibrium of the tread elements on road surface has been attained. In this zone, boundary lubrication is dominant and almost all skid resistance or traction capability is developed. The length of this region depends on vehicle speed. The frictional force is a function of the properties of the contacting solids and of the lubricant at their common interface.

The two types of rubber-pavement contact in the footprint area are EHL and boundary layer. EHL dominates in *Squeeze-film Zone*, boundary layer in *Traction Zone*. Transition zone is a mixture of both types. Based on this assumption, a

measured traction coefficient is defined by the relative proportions of these two modes i.e.

$$\mu_{wet} = (1 - F_{HL})\mu_{BL} \tag{2.5}$$

where μ_{wet} is the measured traction coefficient, μ_{BL} is boundary-layer wet friction; F_{HL} is fraction of footprint in hydrodynamic lubrication mode. At very high speeds when $F_{HL} \equiv 1$ and $\mu_{wet} \equiv 0$, total hydroplaning occurs. At low speeds, $F_{HL} \equiv 0$, and boundary-layer lubrication dominates tire pavement interaction behavior. Equation (2.5) essentially represents the simple tire traction model together with the basic rubber lubrication concepts and the ideas of the three-zone contact. It can be used to interpret wet traction behavior of tires.

2.3.3.2 Experimental Studies

The risk of hydroplaning in wet-weather driving is a function of the depth of surface water, pavement texture properties, and tire characteristics. With the aim of improving wet-weather driving safety, extensive experimental studies have been conducted to investigate how tire characteristics, inflation pressure and water film thickness in particular, would affect vehicle hydroplaning performance (Horne and Dreher, 1963; Horne and Joyner, 1965; Mosher, 1969; Yeager and Tuttle, 1972; Sinnamon and Tielking, 1974; Horne et al., 1986). These researches shed some new lights on how different factors can affect hydroplaning, and proposed certain useful measures to reduce hydroplaning occurrence, such as pavement grooving (Mosher, 1969) and air-jets (Horne and Joyner, 1965). In the following paragraph, prominent investigations conducted by former researchers have been reviewed in detail.

The first experimental demonstration for hydroplaning was observed in a tire treadmill test by Harrin (1957). He found that hydroplaning can occur at fluid depths as low as 0.02 to 0.09 inch (0.5-2.3 mm) for smooth belt-surface and tread tires. Later on, extensive experimental investigations on hydroplaning phenomenon were conducted by NASA (Horne and Dreher, 1963; Horne and Joyner, 1965; Horne, 1984 and 1986). They investigated the physical manifestations of hydroplaning and tested three major groups of the parameters, i.e. (a) tire parameters (tread pattern, inflation pressure and construction), (b) pavement surface texture, and (c) water depth and density, which were found to be important in creating the favorable conditions for the occurrence of hydroplaning. Horne and Dreher (1963) concluded that higher tire inflation pressures led to higher hydroplaning speeds. Measurements from Horne and Joyner (1965) showed that as speed increases, groove pressure builds up and the difference in pressure between groove and rib decreases. Hydrodynamic pressure in the grooves is strongly dependent on water depth at depths below the critical value. Nevertheless, it is difficult to explain precisely why wet traction performance is extremely sensitive to water depth below some critical value and relatively insensitive to water depth above the critical value.

Experimental investigations on large scales also indicated that hydroplaning speed depends primarily upon tire inflation pressure and that tread pattern, tire construction, tire load, and surface texture have only a small effect in deep water (Staughton and Williams, 1970). The same findings are also verified by experiments using scale model tires (Gilbert and Robert, 1973). It is found that the tires with larger number of ribs are superior for the same ratio of rib area to groove area with tread depth increasing and that tire pressure has the largest single effect on hydroplaning speed while tire normal load has a moderate effect on hydroplaning speed. It has been

verified, however, that it is not the case for truck tire. Horne (1984) predicted a more rapid loss of ground contact, due to hydrodynamic pressures, under lightly-loaded truck tires due to the shortened shape of the tread contact patch which results in a shortened time interval available for water expulsion.

Sinnamon and Tielking (1974) concluded that hydroplaning speed varies inversely with water depth, i.e. higher water depths accelerate the onset of hydroplaning phenomena. The critical water depth for hydroplaning can range from approximately 0.1 to 0.4 inch (2.54 to 10.2 mm) depending upon the character of tire-pavement surfaces. It was also found that hydroplaning speed decreases rapidly for water film thickness between 0.1 mm and 2 mm and tends to level-off for larger water film-thickness (Ong et al., 2005).

Leland (1972) reported that in shallow water (0.04 inch or 1mm), tread grooves are highly effective in delaying the occurrence of hydroplaning. The lateral grooves in the shoulder region of tread could provide a large improvement over the simple circumferential groove pattern. The zigzag grooves of the production tire appeared to provide less efficient drainage than straight grooves. The loss in braking traction due to partial hydroplaning effects is considerably less for rib-tread tires than for smooth-tread tires even when the fluid depth on the pavement surface is greater than the tread groove depth. Deeper tire tread depth can offer a more effective channel for water flow so that hydroplaning takes place at a higher speed due to a lower development rate of the hydrodynamic uplift force (Horne and Dreher, 1963; Gallaway, 1979).

Investigation on pavement textures indicated that pavement macrotexture is a function of aggregate size, shape, angularity, spacing and distribution of coarse aggregates (Kokkalis and Panagouli, 1998). A pavement with good macrotexture in

the form of grooving can delay the dynamic hydroplaning considerably (Horne, 1975; Ong and Fwa, 2006). It was found that the pavement microtexture in the 0.2- to 0.5-mm range delays hydroplaning by increasing the hydroplaning speed by up to 20% (Ong et al., 2005). The hydroplaning risk associated with different types of surfaces and their depths of macrotexture can be found in literatures (Yager, 1983).

2.3.3.3 Numerical Studies

The experimental research on hydroplaning had revealed valuable knowledge and deepened our understanding for the affecting factors related to it. Some useful strategies to reduce the potential of hydroplaning were proposed based on their findings. In addition, several experimental equations for determining critical hydroplaning speeds have received wide applications. However, the empirical methods have major limitations in shedding light on the intrinsic mechanism involved in hydroplaning phenomenon. Thus many researchers turned to employ analytical or numerical method to investigate this problem since 1960s.

Martin (1966) employed the potential flow theory and conformal mapping techniques to study the total dynamic hydroplaning problem. In his analysis, the two-dimensional irrotational flow problem of rigid curved surfaces with arbitrary shape placing on an incompressible inviscid fluid was solved. However, side flow and viscosity were completely neglected and no variation in gap in the direction perpendicular to the flow was incorporated in the analysis. Moore (1967) modeled a rubber sliding on a 2D smooth sinusoidal asperity separated by a thin fluid film. The correlation was obtained for load capacity, friction level, and minimum clearance by 1D Reynolds equation. The major drawbacks of his study were that it neglects the

side flow and can only be applied to the case of viscous hydroplaning due to the assumptions involved.

Eshel (1967) studied the dynamic hydroplaning problem using a three-region model in which different simplifying assumptions were applied to the flow in each region. The solutions obtained from the three regions were coupled at the regional boundaries. Simple models of tire flexibility were coupled form an elasto-hydrodynamic system. However, the model failed to consider the side flow in the inlet region under the wheel. Furthermore, the treatment of the problem as a 2D problem is inappropriate and the assumption of a laminar parabolic velocity profile is not accurate. Daughaday and Tung (1969) introduced a 3D tire surface model to deal with the hydroplaning problem by using a two-region model. The major disadvantage was that planar footprint regions cannot produce the magnitude of the recovery factor found for hydroplaning tires. Consequently, tire deformations are necessary for accurate predictions (Figure 2.19).

Later Browne (1971) proposed a 2D treatment for a 3D tire deformation model to study hydroplaning by means of the Navier-Stokes equations. In his model, inviscid, laminar and the turbulent models were explored with considering the side flow. He investigated the influence of deforming tire using Moire Fringe technique. The results revealed that tire hydroplaning must be accompanied by inward buckling of tire tread in the central portion of the contact region and that viscous effects are not important in hydroplaning where the amount of water encountered by the tire exceeds the combined drainage capacity of the tread pattern and the pavement macrotexture. Grogger and Weiss (1996, 1997) investigated the pressure distribution and the velocity field of a deformable automobile tire without rotating when hydroplaning. The 3D flow around the tire is described by an efficient free surface model and the

Navier-Stokes equations. The effects of turbulence are modeled by k-ε model. The deformation of the tire is calculated using a noncommercial finite element program. It verified that the tire deformation has a strong influence on the resulting lift forces, which had been reported by Browne (1971).

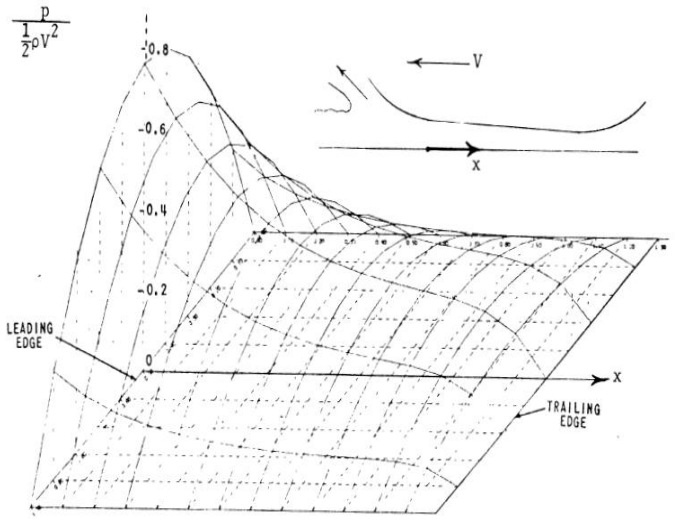

Note: p: pressure, ρ: density, V: moving velocity

Figure 2.19 Hydrodynamic pressure distributions for a totally hydroplaning tire (Sinnnamon, and Tielking, 1974).

Nakajima et al. (2000) employed FEM for tire and FVM for water to simulate tire hydroplaning. They considered fluid-structure interaction, tire rolling, and practical tread pattern in the analysis but ignored the effect of fluid viscosity. The prediction of hydroplaning velocity was not achieved. Okano and Koishi (2000) used MSC.Dytran to predict the hydroplaning speed for tires with four different tread patterns. However this study suffered a drawback in that the fluid flow was modeled using the potential flow theory. Janajreh et al. (2001) used CFD to determine the drag force, which indicates the fluid evacuation around the tread pattern. However, it takes

a long time to finish such a simulation because the model needed a great number of Lagrangian and Eulerian elements, and a contact should be defined between the two different types of elements. The simulation results of the lift force and the contact force were very oscillatory. Oh et al. (2008) adopted two separate mathematical models to simulate hydroplaning. A finite difference method (FDM) code was developed to solve Navier-Stokes and continuity equations and to obtain the pressure distribution around a tire with the inertial and viscous effects of water taken into account. An FEM tire model was used to obtain the deformed shape of the tire due to the vertical load and the pressure distribution. The two models were iteratively used until a converged pressure distribution was obtained.

Recently, Ong and Fwa (2005, 2006a, 2006b, 2007, 2008) established a numerical simulation model for hydroplaning prediction using CFD techniques implemented by Fluent to investigate the effect of different affecting factors such as grooving width, depth and spacing of pavement on hydroplaning speed of smooth passage car tires. The model is based on a 3D finite volume method and adopts the standard k-ε turbulence model. The simulation results for the case of a smooth pavement surface were found to be in good agreement with experimental results in the literature and NASA hydroplaning equation. In their studies, it was shown that the NASA equation underestimated hydroplaning speed for a passenger car tire with definite tire inflation pressure when transverse and longitudinal pavement grooving designs were used. Investigation on the groove dimensions showed that larger groove width and depth and smaller groove spacing help to reduce the occurrences of hydroplaning.

The proposed simulation model was also applied to analyze the effect of tire tread pattern and tread groove depth and inflation pressure of passenger cars on

hydroplaning for different surface water depths (Fwa et al., 2007, 2008). The analysis indicated that the groove volume per tread area of the tire is a useful performance indicator to assess the effectiveness of various tire tread groove patterns in reducing vehicle hydroplaning risk. Based on the knowledge of hydroplaning prediction, Ong and Fwa (2009) proposes a framework for runway geometric design, which involves adding an independent module for hydroplaning risk calculation to determine if a runway geometric design meets the safety requirement against hydroplaning for the selected design rainfall and aircraft traffic.

2.3.3.4 Prediction of Minimum hydroplaning speed

Hydroplaning is one of the major causes for traffic accidents during rainy weather. The prediction of minimum hydroplaning speed at various conditions is very important for safety operation of vehicles on highway. Many researches based on vast experiment investigation and field survey established several empirical equations to predict the hydroplaning speed. Some widely used ones are summarized here.

(1) NASA Hydroplaning Equations

One of the most popular hydroplaning equations is the NASA hydroplaning equation (2.6) which was first proposed according to aircraft tire experiments at Langley Center of NASA (Horne and Joyner, 1965)

$$v = 6.36\sqrt{p} \tag{2.6}$$

where p is the tire inflation pressure (kPa) and v denotes the minimum hydroplaning (km/h). It should be noted that this equation can only be applied to smooth or closed pattern tread tires or rib tires on fluid-covered runways where the water depth exceeds the groove depth.

(2) Horne's Equations for Truck Tires

Investigations on truck accidents indicated that tire footprint aspect ratio (*FAR*) has significant effect on hydroplaning performance of truck tires, and should be included in the prediction equation as a parameter (Horne, 1984; Horne et al., 1986). The proposed equation can be expressed as

$$v = 23.3\, p^{0.21} \left(\frac{1.4}{FAR}\right)^{0.5} \tag{2.7}$$

where *FAR* is defined as the ratio of the width over the length of contact area, *p* is the tire inflation pressure, and *v* is the minimum hydroplaning.

(3) Gallaway's hydroplaning equation

Gallaway et al. (1979) presented a regression equation (2.8) involving spin down percent, tire inflation pressure, tread depths, water film thickness and mean texture depth of pavement surface.

$$v = \left(SD\right)^{0.04} \left(p\right)^{0.3} \left(TRD+1\right)^{0.06} * A \tag{2.8}$$

where

$$A = \max\left\{\left[\frac{10.409}{t_w^{0.06}} + 3.507\right], \left[\frac{28.952}{t_w^{0.06}} - 7.819\right]\left(MTD\right)^{0.04}\right\},$$

v is the hydroplaning speed (mph), *SD* is the spin-down (%), t_w is the water-film thickness (inch), *MTD* is the mean texture depth (inch), and *TRD* is the tire tread depth in 1/32 inch (0.8 mm).

(4) Wambold's hydroplaning equation

Wambold et al. (1984) developed a prediction equation for low pressure tires based on 10% spin-down and 165 kPa tire pressure,

$$v = 3.5k_1[(TD/25.4+1)^{k_2} MTD^{k_3} (k_4 / WT^{k_5} + 1)] \tag{2.9}$$

where *WT* is the estimated water film thickness (mm), *MTD* mean texture depth (mm), *TD* tire tread (mm), *v* hydroplaning speed (km/h) and k_1, k_2, k_3, k_4, and k_5 are empirical coefficients with typical values 0.05, 0.01, 1.8798 and 0.01, respectively.

2.4 Skid Resistance and Hydroplaning of Truck Tires

Researches on traffic accident and vehicles types revealed that truck tires are much easier to suffer hydroplaning than passenger car tires. Compared to car tires, the wet skid resistance of truck tires has much lower values on normal highway operation speed (Figure 2.8, in section 2.2.2.3). However, previous research mainly focused on the aircraft and passage cars, little attention has been given to truck tires.

The widely adopted NASA hydroplaning equation is able to predict the hydroplaning speed for passenger cars on a wet pavement closely, but could not explain the hydroplaning behaviors of trucks and gives much higher values for truck tires. In addition, field observations and experimental studies found that lightly loaded trucks are more prone to hydroplaning than heavily loaded trucks. Ervin and Macadam (1976) investigated the longitudinal and lateral traction performance of a six-tire sample on a wet concrete surface. It is found that over the 20- to 55-mph (32-88 km/h) range of velocity, all tires exhibited the classic downward trend in shear force limits with velocity. The drainage performance of heavy truck tires would seem to be inherently high as a consequence of high contact pressures between tread and road, low values of tire deflection, and high groove volumes. Sakai et al. (1978) showed that the wet-traction level fell about 15% when the load was reduced to 0.6 times the rated load value.

Horne (1984, 1986) found that light-loaded trucks can hydroplane at highway speeds on wet pavements due to both viscous and dynamic hydroplaning mechanisms.

He attributed such reasons to hydroplaning: contact area, footprint aspect ratio, and tire inflation pressure. He also proposed a predictive regression equation for hydroplaning speed based on a series of tests on worn 10.00-20 truck tires. However, Ivey (1984) did not agree that hydroplaning of lightly loaded truck tires was related to the aspect ratio of the contact patch. He attributed to some other reasons such as vehicle stability, braking system effects, low tire-pavement friction, and the speed increases associated with unloaded vehicles. Ervin et al. (1985) postulated that the loss of truck tire traction on wetted surfaces is clearly most pronounced with the following of factors: (a) High speed; (b) Ramps having large radius curves; (c) An unloaded truck; (d) A high-speed turn; (e) Poor pavement texture; and (f) Water drainage characteristics. Several investigations on the variation of wet skid resistance with tread depth had also been carried out experimentally (Dijks, 1976; Williams and Meades, 1975). Results indicated that the influence of tread depth on skid resistance was very important, for both car and truck tires, especially in the lower tread depth range.

In the aspect of analytical investigation, Bareket and Fancher (1989) developed one semi-empirical tire model and extend it to a comprehensive one, which was capable of predicting tire traction performance during combined braking and steering. Empirical formulas from literatures were used to represent the frictional characteristics of poor wet roads. In their study, the semi-empirical model was used to illustrate the influences of tread groove depth, roadway skid number, and the mean texture depth of the pavement on the lateral and longitudinal forces generated by truck tires. However, the contact patches are divided into sliding and adhesive zones manually and the variations in pressure across the width of the contact patch are averaged together in the model so that the lateral distribution of pressure did not

appear in the analysis. In addition, a very large experimental program would be necessary to assess the accuracy attainable with this approach, in which conditions were very difficult to control.

Ong and Fwa (2008) analyzed the hydroplaning problem of smooth truck tires based on hydrodynamic theory using numerical modeling. The effects of tire inflation pressure, footprint aspect ratio and truck wheel load on truck hydroplaning speed were examined to offer some explanation to the different hydroplaning behaviors between truck and passenger car. Their study verified the fact that empty trucks are more prone to hydroplaning than loaded trucks and the conventional NASA equation over-estimates truck hydroplaning speed. Ong and Fwa (2010) examined the relationship between the AASHTO stopping distance requirements and the skid resistance threshold level adopted by several state pavement management authorities. They pointed out that it is necessary to maintain consistency between geometric design stopping distance requirements and pavement friction management to achieve safe vehicular operations.

2.5 Summary

In this chapter a comprehensive literature review on skid resistance and hydroplaning of pneumatic tire has been presented. The mechanism, affecting factors, measurements and research advancements of skid resistance is firstly summarized. The prominent findings and results from previous researches are discussed and analyzed. Also discussed are the types and manifestation of hydroplaning, followed by some important research for hydroplaning both in experimental and analytical efforts. Finally, a brief review on equations of hydroplaning prediction and skid

resistance and hydroplaning for truck tires are given. The knowledge that has become available through these studies will be a guideline for this research.

Skid resistance and hydroplaning are the two major concerns of safe travelling on wet pavements. They are highly dependent on the interaction of a broad set of factors, such as roadway geometry, surface condition, climatic variables, vehicle braking and handling properties, and various mechanisms by which these properties interact with one another. The linking of any single factor to the skid resistance is a difficult exercise since the interaction mechanisms are so strong and since the factors of potential importance are so numerous.

Experimentally derived relationships by past researchers are available to estimate the effect of rib-tire tread depth on hydroplaning risk. However, such statistical relationships have limitations in their application range and transferability. They also do not provide detailed insights into the mechanism of hydroplaning. These limitations can be overcome by developing a theoretically derived analytical model. Considerable progress has been made in the field of tire traction research. This has led to significant improvements in tire and road performance. However, it is still not possible to predict the traction performance of a tire-road system based on the many tire and surface variables. Indeed, there is, as yet, no agreement as to how to quantify many of these variables in a meaningful way. It is clear that there is a great deal of definitive work yet to be done in this field.

In this research a newly developed FSI simulation model will be employed to investigate the hydroplaning and skid resistance of rib truck tires. The turbulent fluid model k-ε is adopted and the flexible tread of tire which can deform with the water pressure is utilized. Coulomb friction model is used to consider the tire-pavement contact. The software package ADINA will be employed in modeling this problem.

CHAPTER 3 BASIC THEORY FOR FSI SIMULATION

3.1 Introduction for Fluid Structure Interaction

In the simulation of skid resistance and hydroplaning of tires, tire-water interaction (Fluid Structure Interaction) is essential for accurate results due to the large deformation of tire. When calculating the values of skid resistance, contact friction is also essential. In this chapter, the basic theory for FSI simulation used in this research is briefly outlined for reference.

Fluid Structure Interaction problems, such as sloshing of tanks, cyclic oscillations of wings, instabilities of cable stayed bridges in the wind, the inflation of an airbag and of course hydroplaning, in general are often too complex to solve analytically and so they have to be analyzed by means of experiments or numerical simulation. Research in computational fluid dynamics and computational structural dynamics is still ongoing but the maturity of these fields enables numerical simulation of FSI.

In FSI analyses, fluid forces are applied onto the solid and the solid deformation in turn changes the fluid domain. For most interaction problems, the computational domain is divided into the fluid domain and solid domain (Figure 3.1), where a fluid model and a solid model are defined respectively, through their material data, boundary conditions, etc. The interaction occurs along the interface of the two domains. Having two models coupled, we can perform simulations and predictions of many physical phenomena.

FSI problems can be handled nowadays thanks to the increase of computing power and advances in numerical methods in the last decade. FSI problems can be divided into the following parts:

- Space and time discretisation
- Structure and fluid mesh
- Coupling of non-matching meshes
- Monolithic or partitioned solver.

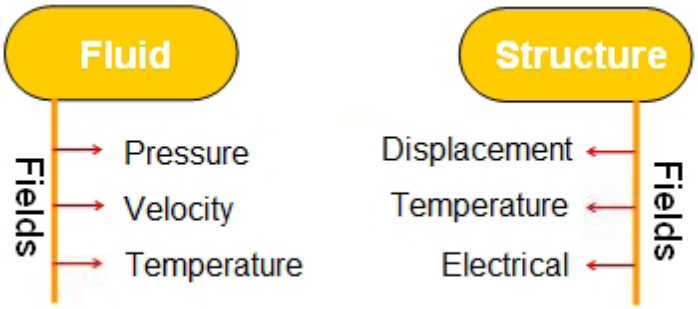

Figure 3.1 Schematic of Fluid-Structure Interaction.

3.2 Discritization Methods

Special attention should be given in meshing the structure and fluid respectively when carrying out FSI simulation. There are four different reference frames to be considered for meshing, each of which has its own merits.

3.2.1 Lagrangian Formulation

A Lagrangian frame moves with the material. In this way the interface of the material is tracked precisely, see Figure 3.2. When considering materials with high E modulus, deformations are small and the Lagrangian frame is attractive. However, when having large deformations, the accuracy will reduce dramatically due to the large distortion of elements. Thus remeshing is needed in such a case, which have to

cost a lot of computational power. For this reason, the Lagrangian frame is used widely in structure mechanics.

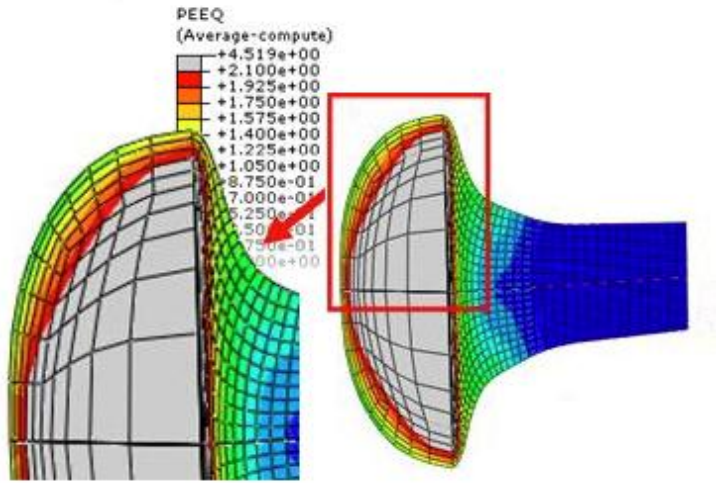

Figure 3.2 Simulation Results for Large Deformation Using Lagrangian Mesh (SIMULIA, 2008)

3.2.2 Eulerian Formulation

The Eulerian frame is fixed in space. The considered domain is divided into elements. With deformation and movement, materials flow through the elements. Where high gradients are expected, a fine mesh is needed (Figure 3.3). The advantages of this method are that the mesh does not change per time step and that large deformations do not increase the needed computation power. For this reason, the Eulerian frame is used widely in fluid dynamics. A disadvantage is that an interface is not tracked accurately, which is of importance with FSI problems.

3.2.3 Arbitrary Lagrangian-Eulerian Formulation

Because of the shortcomings of purely Lagrangian and purely Eulerian descriptions, arbitrary Lagrangian-Eulerian (ALE) technique has been developed that succeeds, to a certain extent, in combining the best features of both the Lagrangian and the Eulerian approaches. In the ALE frame, the nodes of the computational mesh

may be moved with the continuum in normal Lagrangian fashion or be held fixed in Eulerian manner, or be moved in some arbitrary specified way to give a continuous rezoning capability, as shown in Figures 3.4.

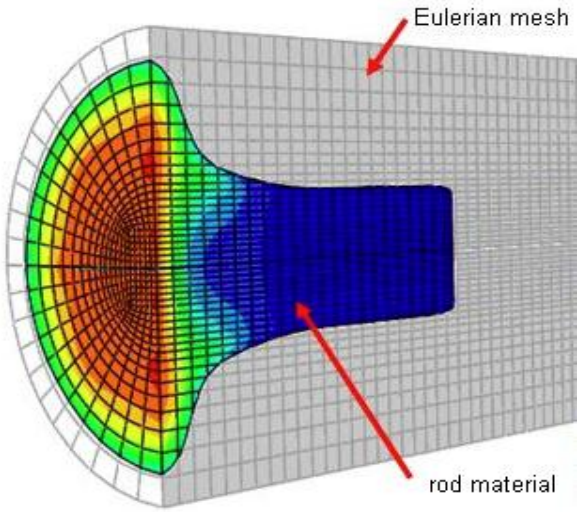

Figure 3.3 Simulation Results for Large Deformation Using Eulerian Mesh (SIMULIA, 2008)

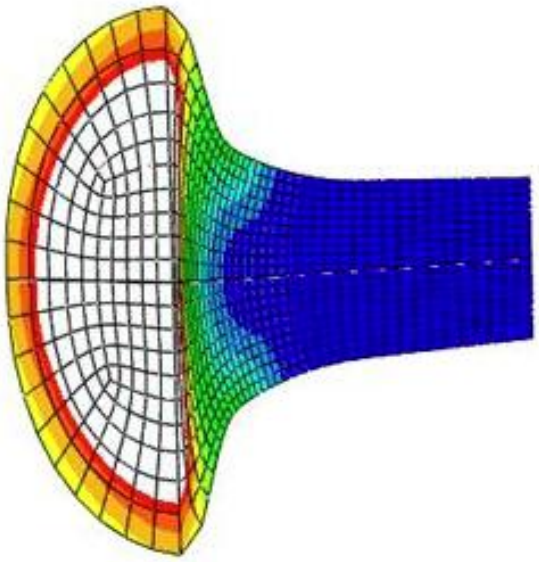

Figure 3.4 Simulation Results for Large Deformation Using ALE mesh (SIMULIA, 2008)

Because of this freedom in moving the computational mesh offered by the ALE description, greater distortions of the continuum can be handled than would be allowed by a purely Lagrangian method, with more resolution than that offered by a purely Eulerian approach. The mesh follows the boundary. However, this freedom in mesh movement has its limits. An extensive description of ALE methods can be found in the reference by Boer, et al. (2006).

3.2.4 Coupled Eulerian-Lagrangian Formulation

The coupled Eulerian Lagrangian (CEL) method also attempts to capture the strengths of the Lagrangian and Eulerian methods. In general, a Lagrangian frame is used to discretise the moving structure while an Eulerian frame is used to discretise the fluid domain. The boundary of the Lagrangian domain is taken to represent the interface between the different domains. Interface models use the velocity of the Lagrangian boundary as a kinematic constraint in the Eulerian calculation and the stress with the Eulerian cell to calculate the resulting surface stress on the Lagrangian domain (Veldman, 2006). Different CEL algorithms may be characterized by the details of how this interface condition is treated (Haberman, 2004).

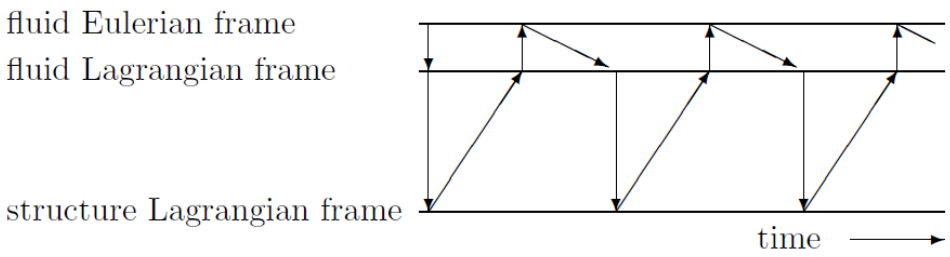

Figure 3.5 Subsequent mesh and information treatment of CEL method (Veldman, 2006)

This mesh treatment is certainly unique, but also very time-consuming, having to remesh from the Lagrangian mesh back to the original Eulerian mesh every time step, which can be seen from Figure 3.5. This partially explains the long simulation times. The displacement for the fluid is solved instead of the velocity. There is no turbulence modeling possibilities. The loose partition coupling is employed in general (Simulua, 2008).

3.3 Approaches for Solving FSI Problem

The typical task of an analysis of a FSI model is to obtain the fluid and structure response through the coupled solution. The structural model is based on a Lagrangian coordinate system and the displacements are the primary unknowns. A pure fluid model is always analyzed using an Eulerian coordinate system. However, for fluid-structure interaction problems, the fluid model must be based on an Arbitrary-Lagrangian-Eulerian coordinate system since the fluid-structure interface is deformable. Therefore, the solution variables of the fluid flow include the usual fluid variables (pressure, velocity, etc.) as well as displacements.

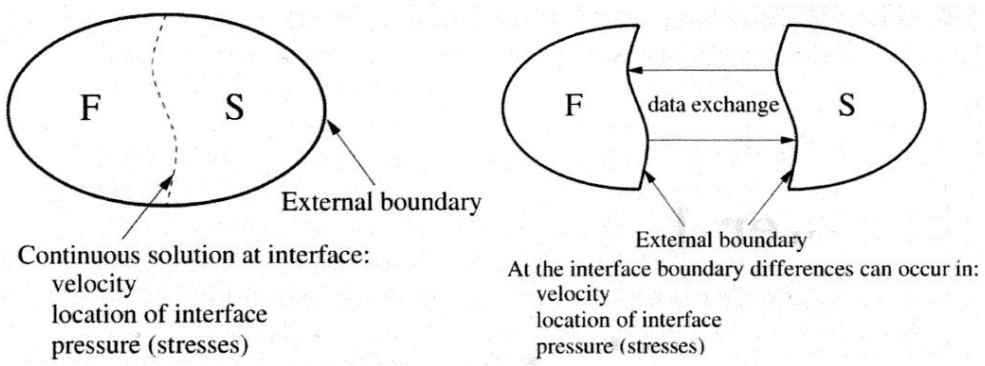

Figure 3.6 Monolithic or partitioned method for FSI simulation (Veldman, 2006).

Two main approaches for the simulation of FSI problems are:

- Monolithic approach: the equations governing the flow and the displacement of the structure are solved simultaneously, with a single solver (Figure 3.6 left)
- Partitioned approach: the equations governing the flow and the displacement of the structure are solved separately, with two distinct solvers (Figure 3.6 right)

A monolithic solver aims at putting all the necessary components (the physical modeling, discretisation and solution algorithm) into a single computational model and solver. However, the monolithic solvers encountered the difficulties in the implementation of different physical models within a single solution environment and it is hard to update the solver with the latest developments in each research field. A partitioned solver treats each physical domain separately. Thus it can use existing solvers that can be developed and maintained independently. Therefore the popular approach is to develop a partitioned solver (Zuijlen, 2006).

A partitioned FSI solver consists of a flow solver, a structure solver and a coupling algorithm that couples the solvers at the fluid-structure interface both in space and time. The coupling algorithm contains an interpolation method to transfer data from one system to the other and an iteration scheme to obtain a coupled solution that is within the desired accuracy. In the case of strong partition coupling, iterations per time step are needed before continuing to the next time step for the sake of accuracy. As shown in Figure 3.7, time progresses from left to right. The connections between the fluid and structure sides represent information exchange. As indicated by the arrows, these information exchanges also go back in time, in contrast with loose

partition coupling where the coupling is done without iterations. ADINA-FSI solver is partitioned and uses a loose partition coupling algorithm. Thus the fluid and structure equations are solved subsequently (Figure 3.8).

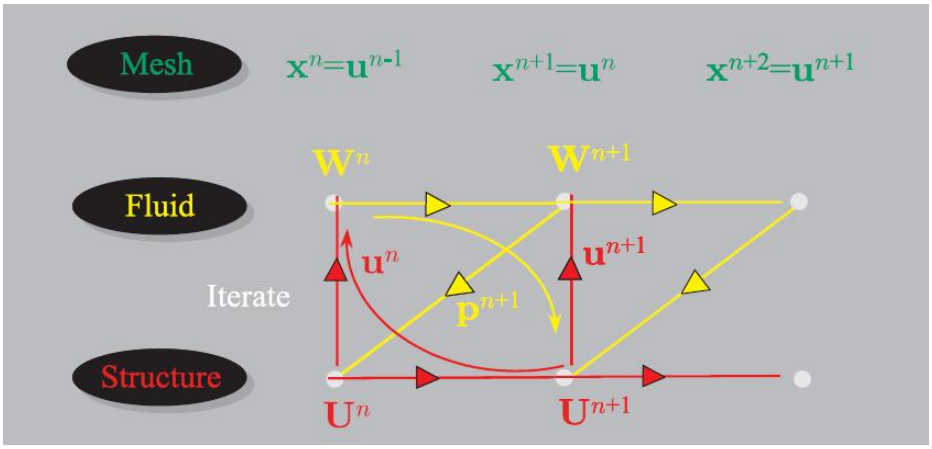

Figure 3.7 Schematic of A Strong Partition Coupling Scheme

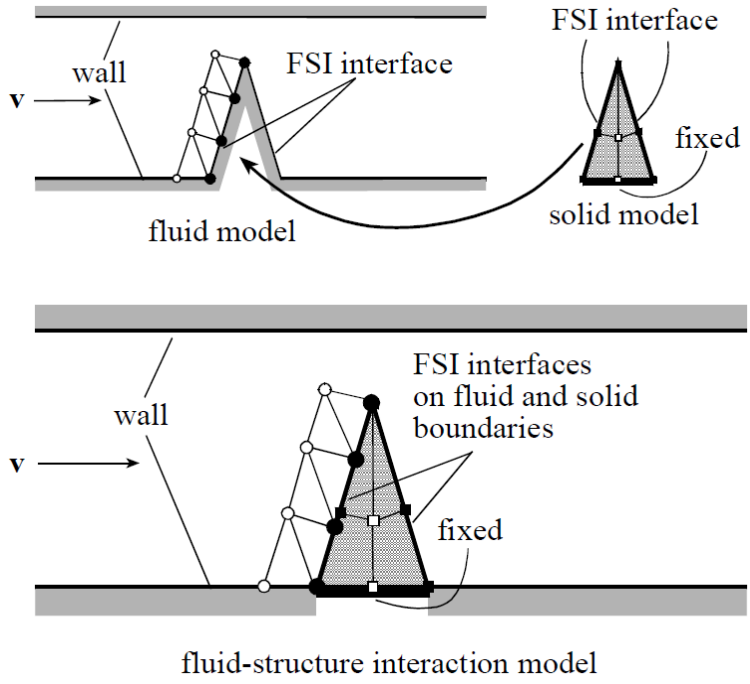

Figure 3.8 Illustration of Fluid-Structure Interaction (ADINA, 2009)

3.4 Coupling Non-Matching Meshes

The discrete meshes used in the different domains in fluid-structure interaction computations do not have to match at their common interface. Exchange of information over this interface is therefore no longer trivial (Boer et al., 2006). In Figures 3.9 and 3.10, non-matching discrete interfaces between flow and structure domain are shown. For information transfer, FSI computations require that pressure loads are transmitted from the fluid side of the fluid-structure interface to the structural nodes on that interface. Once the motion of the structure has been determined, the motion of the fluid mesh points on the interface has to be imposed. In FSI simulations generating matching meshes at the fluid structure interface is usually not desirable, because the flow generally requires a much finer mesh than the structure. When meshes are non-matching, an interpolation or projection step has to be carried out to enable transfer of information between the two domains.

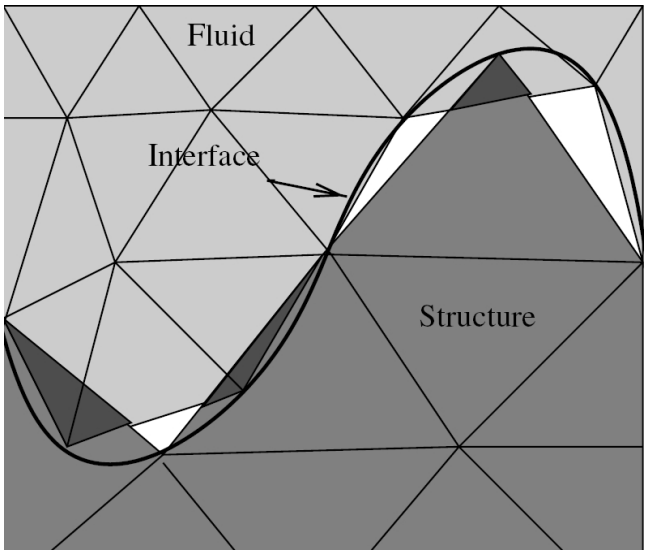

Figure 3.9 Non-Matching Meshes in 2D (Boer et al., 2006)

There are several criteria which such a data exchange or coupling method ideally should satisfy. The most important are

- Global conservation of energy over the interface,
- Global conservation of loads over the interface,
- Accuracy,
- Conservation of the order of the coupled solvers,
- Efficiency, which is defined as a ratio between accuracy and computational costs.

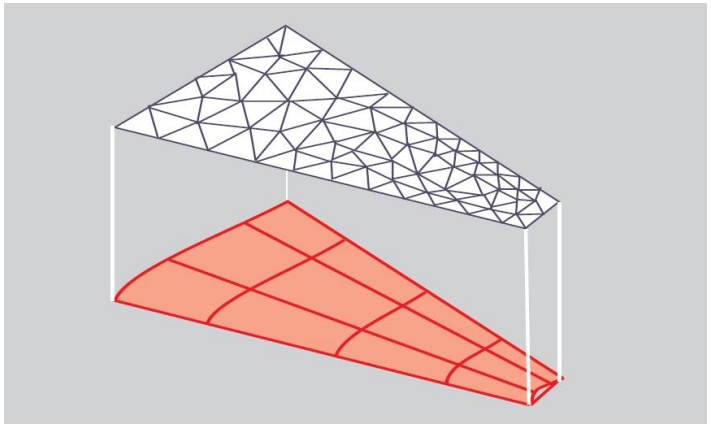

Figure 3.10 Non-matching Meshes between Fluid Model and Solid Model

The simplest and fastest way to perform the information transfer is to obtain the information from the closest point in the other mesh. However, this only provides satisfactory results if the two grids are almost matching. A more accurate way of handling the data transfer is by projection, as shown in Figure 3.11. To obtain information from the other mesh, a point can be orthogonally projected on that mesh and the information in that projection point can be used in the original point. Similarly, a whole element can be orthogonally projected on the other mesh and the

size of the area of intersection can then be used to define to what degree the values of that element have to be taken into account. The third way to exchange data is using spline based methods. These are often applied in interpolation schemes in finite element methods, for example, radial basis functions interpolation.

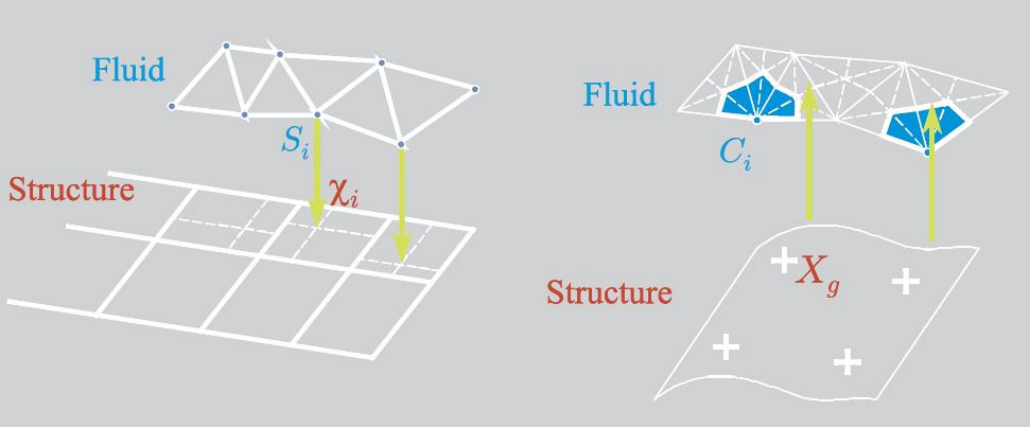

Figure 3.11 Information Transfer by means of Projection (Boer et al., 2006)

3.5 Summary

The FSI simulation is a very challenging and complex problem. Many researchers both academic and industrial in the world are exploring new methods, such as XFEM (Mayer et al., 2010), mesh free method (Quarantay et al., 2005) and SPH method (Carla et al., 2007), aiming to solve this problem more efficiently.

In this research, the computational domain is divided into the fluid domain and solid domain. A fluid model and a solid model are defined respectively in ADINA and ADINA-F, through their material data, boundary conditions, etc. The Navier-Stokes equations governing the water flow behaviors are discritized using the ALE Discritization Method. The detail formulations are given in Chapter 4.

The interaction occurs along the interface of the two domains. Different mesh densities are utilized for truck tire (solid part) and water film (fluid part), in which the fluid meshes used are much smaller than those in solid model in order to enhance the accuracy. A loose partition coupling algorithm (ADINA-FSI) is used in this thesis. It consists of a flow solver, a structure solver and a coupling algorithm that couples the solvers at the fluid-structure interface both in space and time. An iteration procedure must therefore be used to obtain the solution at a specific time.

CHAPTER 4 HYDROPLANING ANALYSIS OF WIDE-BASE TRUCK TIRE

4.1 Introduction

Wide-base truck tire have been widely used on trucks in Europe since the early 1980s. In 1997, around 65% of trailers and semi-trailer tires in Germany used wide-base tires (COST 334, 2001). Although it is expected to take several years to build acceptance and confidence in this new technology in the U.S., the use of the new generation of wide-base tires has been growing exponentially in recent years. Wide-base truck tire has struck the interest of trucking and tire industries as well as highway agencies and pavement engineers since their introduction over 30 years ago. Compared to conventional dual tires, wide-base tires offer the trucking industry significant economic advantage such as improved fuel efficiency, increased hauling capacity, reduced tire cost and repair, and superior ride and comfort (AI-Qadi and Elseifi, 2007). However, the wet performance of wide-base truck tires, especially the hydroplaning performance, which is very important for rainy weather travel safety, has been known little by people and even has not been carefully investigated by pavement engineers. The researches on this topic rarely can be found in literatures based on the knowledge of the author.

Experimental investigations have contributed a lot to the prediction and prevention of hydroplaning. For example, the famous NASA hydroplaning equation, derived from plenty of experimental tests, can give a satisfactory hydroplaning prediction for both aircrafts and passenger cars (Horne and Dreher, 1963); Pavement grooving, firstly invented in UK for pavement construction, can permit at least partial

elimination of hydroplaning (Yager, 1968; Williams, 1969). However, the theoretical analysis of hydroplaning phenomenon encounters some more complex problems because the equations describing the fluid flow system are non-linear and no accurate mathematical model for tire deformation exists. Previous researches for hydroplaning, both theoretical and analytical, mainly concentrated on the numerical method. Rare satisfactory results, however, have been given due to the complexity of the problem and the limited capability of computer (Daughaday and Tung, 1969; Groger and Weis, 1996; Zmindak and Grajciar, 1997; Seta, E. et al., 2000; Okano and Koishi, 2001; Ong and Fwa, 2006a, 2006b, 2008). Attempts to formulate a description for hydroplaning, which can be employed to analyze the relative importance of the parameters involved in tire, fluid and pavement, have been unsuccessful in general (Daughaday and Tung, 1969).

Observations have revealed that trucks more easily developing hydroplaning at normal highway speeds than passenger cars. It is also found that the empty trucks usually have three times higher propensity for single-truck accident involvement on wet pavements than loaded trucks (Chira-Chivala, 1986; Ivey et al., 1986), which differs from what people thought before. Horne (1984, 1986) predicted a more rapid loss of ground contact, due to hydrodynamic pressures, under lightly-loaded truck tires due to the peculiarly for shortened shape of the tread contact patch which results in a shortened time interval available for water expulsion. Based on this observation, he broadened their prior work to involve the aspect ratio of footprint as a effective variable in determining hydrodynamic pressure development in addition to tire inflation pressure. Ivey (1986) also confirmed that the complete hydroplaning of lightly loaded truck tires does relate to the aspect ratio of the contact patch as had been predicted by Home's analysis. Ong and Fwa (2006, 2008) investigated the

hydroplaning problem of smooth truck tire employed the Fluent and ADINA, respectively. They also investigated the skid resistance of the smooth truck tire using FEM simulation (Ong and Fwa, 2010a and 2010b).

It is believed that accurate quantification of hydroplaning performance of wide-base tire due to various tire configurations would provide many benefits to the suggestion for tire development and policy decision for pavement agencies. Thus, in this chapter the hydroplaning performance of wide-base tire 425/65R22.5 was analyzed using the proposed fluid structure interaction (FSI) model. In order to give a general concept of its hydroplaning performance, the traditional dual truck tire 11R22.5 is also analyzed for comparison. The two-way Fluid-Structure-Interaction (FSI) method is utilized for hydroplaning simulation. One FSI simulation model employing the k-ε turbulent model is used to consider the effects of tire deformation and the turbulence flow in this research in order to overcome the limitations of previous studies by Martin (1966), Tsakonas et al. (1968), Browne (1971), Groger and Weis (1996), and Zmindak and Grajciar (1997), Seta, E. et al. (2000), Okano and Koishi (2001), Ong and Fwa (2005, 2006), and Fwa and Ong (2006).

This chapter firstly addressed a detailed introduction for modeling and the related theories. Then the tire models were verified by comparing the predicted contact areas under different loads and inflation pressures with the measured contact areas in the literatures. Later the verified tire model was combined with the fluid model to verify the effectiveness of the FSI simulation model by using the measured hydroplaning speeds. The results indicated that the model can be used to predict the hydroplaning speed with a good agreement with the measured data. The effects of tire inflation pressure and wheel load on hydroplaning speed of wide-base truck tire are discussed in detail. Finally, the performance comparison for the wide-base

425/65R22.5 and traditional 11R22.5 tires was performed under the same tire inflation pressure and axle loads in order to check if the wide-base truck tire has a better hydroplaning performance.

4.2 Wide-Base Truck Tire

Historically, wide-base tires have evolved considerably since the introduction of the first generation in the early 1980s. Over the years, wide-base tires have become increasingly wider than their predecessors shown in Figure 4.1, which indicates the general trend in wide-base technology (different patterns of dual and wide-base tires exist and are not shown in this figure for simplicity).

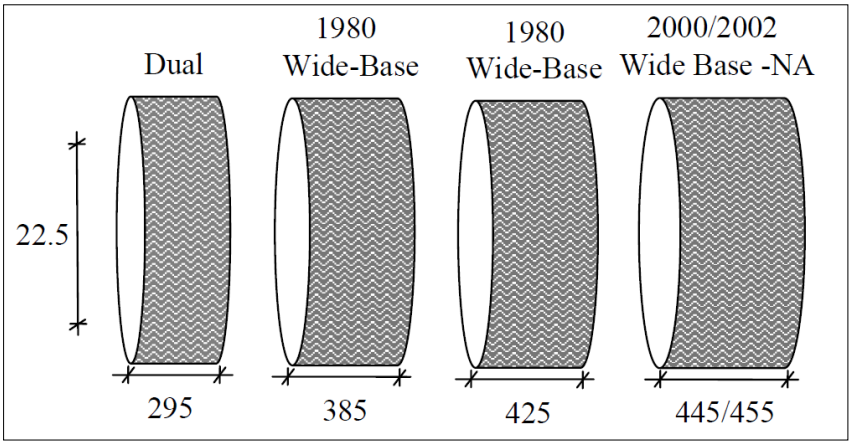

Figure 4.1 Evolution of Wide Base Tires

As mentioned before, wide-base tire has many advantages compared to the traditional dual tires. A single wide-base tire and wheel is lighter than two standard tires and wheels. The weight savings would reduce fuel consumption, or increase cargo capacity for truck trucks that are weight-limited. Wide-base tires have lower rolling resistance and aerodynamic drag, and generate slightly less pass-by noise than

dual tires. Wide-base tires have been found on average to produce between 4% and 5% fuel savings compared to conventional duals. By using wide-base tires, a combination long-haul truck could save over 400 gallons of fuel per year and cut emissions of carbon dioxide as well as NO_x (the most common greenhouse gas) by more than four metric tons annually. Most importantly, these environmental benefits can be achieved while cutting costs because a single wide-base tire costs about the same as two equivalent dual tires and a single wide-rim wheel typically costs about $130 less than two standard wheels (AI-Qadi et al., 2002). Figure 4.2 shows two common types of wide-base truck tire, 425/65R22.5 and 455/55R22.5.

Figure 4.2 Wide-Base Truck Tires (425/65R22.5 and 455/55R22.5)

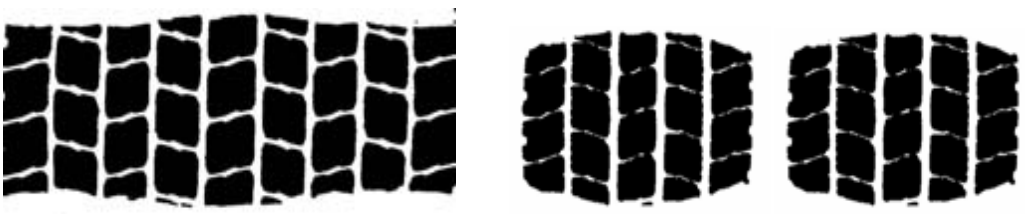

Figure 4.3 Footprints of Dual-Tire Assembly and Wide-Base Tires

It is also noticed that the tire footprints of Dual-Tire Assembly and Wide-Base Tires are different, as shown in Figure 4.3. The detailed dimensions of wide-base 425 tire and 11R22.5 dual-tire assembly used in this study are summarized in Table 4.1.

Table 4.1 Dimensions of Wide-Base and Dual Truck Tires used

Tire type	Loaded Radius		Overall Diameter		Overall Width		Tread Depth	
	(in)	(mm)	(in)	(mm)	(in)	(mm)	(in)	(mm)
WB-425/65R22.5	20.6	523.2	44.5	1130.3	16.6	421.6	0.7	17.8
Dual 11R22.5	19.2	487.7	41.3	1049.0	11.2	284.5	0.9	22.9

4.3 Modeling of Hydroplaning for Rib Truck Tire

In the phenomenon of hydroplaning, the inertial effects of the water are dominant, producing changes in momentum which cause a reaction force normal to the tire tread. Increasing speed causes an increase in the hydrodynamic pressure and a water wedge penetrating into the tire contact patch, which leads to a decrease in the contact area between tire and pavement. If the velocity continues to increase, the uplift force of water (mainly initial force) will rise to the weight of wheel and the applied load, and then full hydroplaning occurs as the water wedge penetrates through to the rear of the contact patch and the tire surface is completely separated from the pavement surface (Horne et al., 1986).

During this process, it is necessary to consider the interaction between the tire and the water film for an accurate simulation. Thus in FSI simulation three major components, i.e. pneumatic tire sub-model, pavement surface sub-model, and fluid film sub-model should be involved and the interactions between water film and tire tread must be considered. Figure 4.4 illustrates the relation of the different components in the FSI numerical model and the parameters needed to be input. The

finite element method is employed for solid parts: tire structure and pavement structure; while control volume method is harnessed for fluid part: water film. The software package ADINA is used to implement the coupled tire-water interaction (ADINA R&D Inc., 2009).

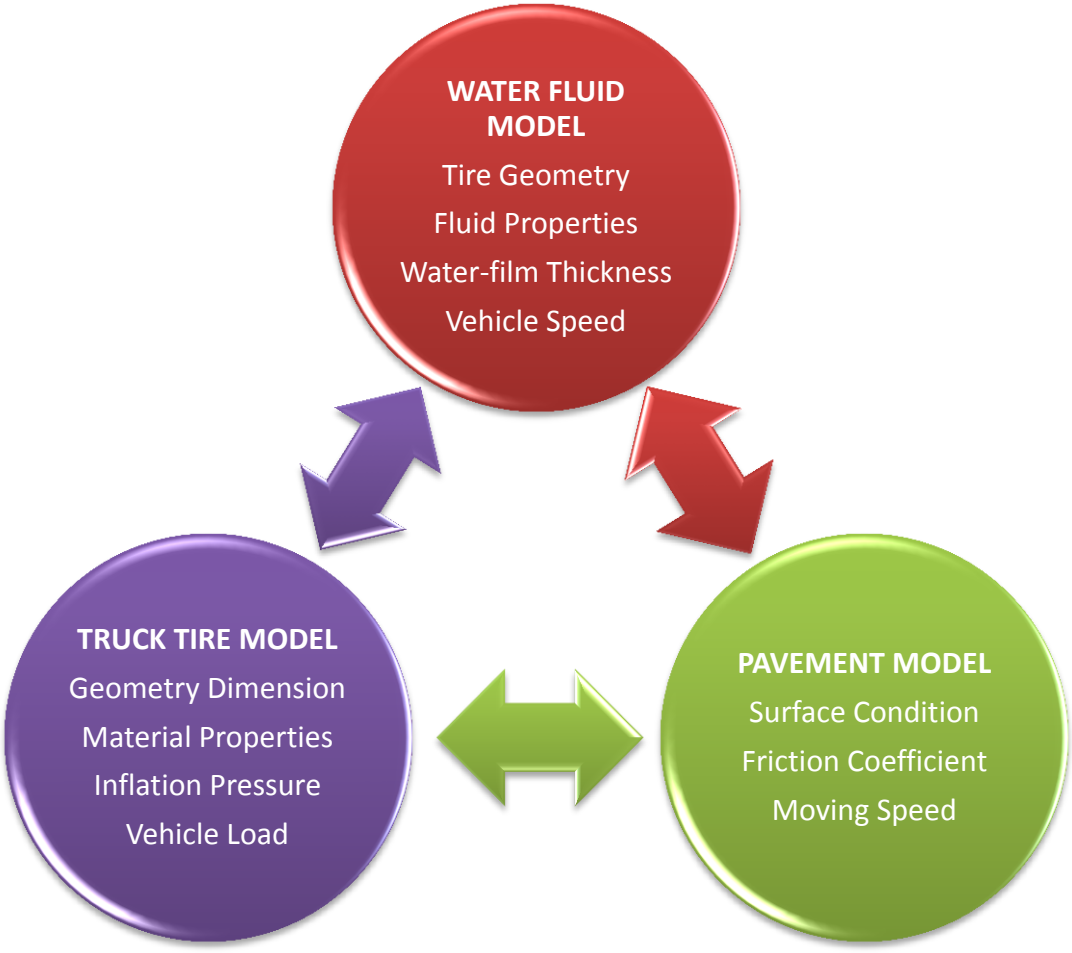

Figure 4.4 Relationships of Sub-Models in Tire Hydroplaning Simulation

The simulation process starts from the static state, and then an increasing inlet water velocity is applied on the fluid model step by step. The coupling of the CFD model and the FEM model is implemented by transferring the displacements or forces through the predefined FSI fluid-structure interaction interfaces in FEM and CFD models. The fluid pressure force calculated by the CFD model is transferred to the

FEM model and applied as external loads, and then the corresponding tire deformations are computed by the FEM tire model under the fluid pressure loads. The computed tire deformation data are in turn transferred to CFD model through the FSI interface. The revised tire deformation profile will serve as the new boundary wall for fluid pressure calculation. This iterative process is repeated until the force residuals and displacement residuals reach a pre-defined convergence criterion.

For a given sliding speed, the output from the FSI model includes the following useful information: tire deformation profile, the tire contact footprint, the pressure and velocity fields of water body, the fluid uplift force and the drag force at the tire-fluid interface. Figure 4.5 summarizes the solution process described in the preceding paragraphs.

4.3.1 Truck Tire Model

Tire constructions for aircraft, automobiles and other vehicles are quite complex, and the typical tire cross-section includes several layers of cord rubber composite material, reinforcing plies and strips, a rubber tread area, and wire beads (The Tire and Rim Association, 1995). Accurate three-dimensional modeling of truck tire involves significant challenges and requires a fairly detailed representation of the cross-section. Despite the numerous components and various material properties contained, exact material parameters and actual structure configuration are not available to the public for the reason of commercial secret.

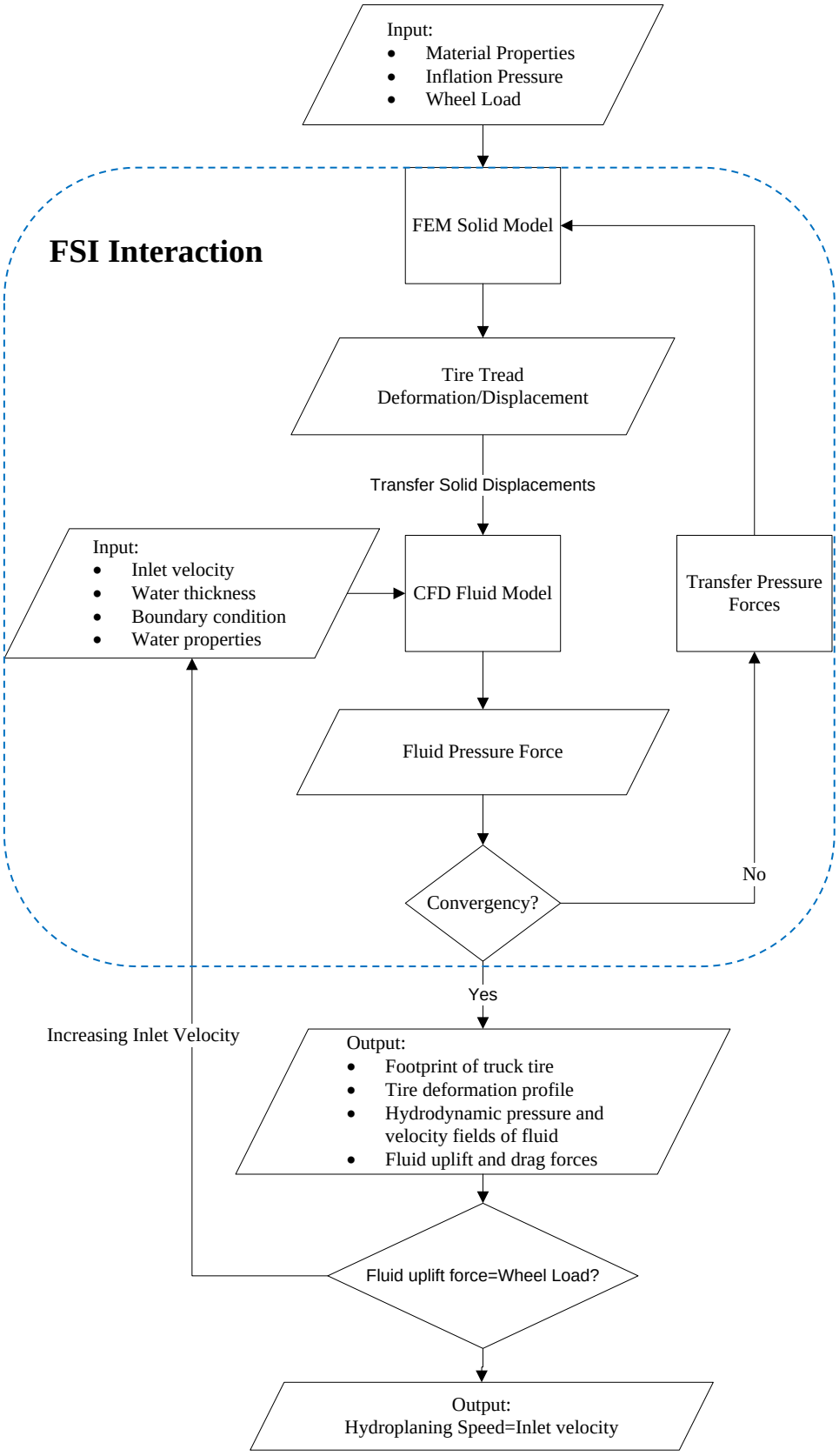

Figure 4.5 Flow Chart of Hydroplaning Simulation

However, some basic response data, including general structure made-up, load-deflection response and footprint, can be used for parameter determination modeling the tires. Therefore, in this chaper a simplified tire model, consisting of three major structural components, namely tire rim, sidewalls and tread with elastic or orthotropic elastic materials, was employed. Since the tire footprint (contact area) is the critical and crucial factor for assuring the simulation as accurate as possible in the hydroplaning analysis, the contact areas should be carefully verified by experiment results.

Figure 4.6 Truck Tires 425/65R22.5 (Left), 11R22.5 (Right)

The wide base tire (425/65R22.5) and the conventional dual tire configuration (11R22.5) are analyzed in this research (Figure 4.6). The load limit of the wide base truck tire (425/65R22.5) is close to twice the load limit of the traditional dual truck tire (11R22.5), and the wide base truck tire has about the same air volume as two traditional dual truck tires (Sinnamon and Tielking, 1974). The tires selected have similar highway-type tread patterns and the same groove depth of 19mm and nearly the same percent 16% footprint void (ratio of groove area to gross contact area). But it is found that usually the footprint area of a single wide-base tire is less than twice the footprint area of a single conventional tire.

Table 4.2 Parameters of Truck Tire Components used for Different Inflation Pressures

Truck Tire	Inflation pressure (psi)	Tire Parts	E_a (Mpa)	E_b (Mpa)	E_c (Mpa)	G_a (Mpa)	G_b (Mpa)	G_c (Mpa)	μ
425/65R22.5	80	Tread	510	493	493	30	30	30	0.45
		Sidewall	420	410	410	24	24	24	0.45
	100	Tread	640	600	600	44	40	40	0.45
		Sidewall	440	425	425	35	29	29	0.45
	120	Tread	685	650	650	43	41	41	0.45
		Sidewall	480	465	465	43	43	43	0.45
11R22.5	85	Tread	100	600	220	14	15	15	0.45
		Sidewall	100	130	130	12	15	15	0.45
	105	Tread	150	600	260	20	20	20	0.45
		Sidewall	130	150	150	20	20	20	0.45
	125	Tread	168	610	270	24	23	23	0.45
		Sidewall	145	160	160	23	22	22	0.45

The dimensions for the two types of truck tires can be found from the 1995 Tire Year Book (The Tire and Rim Association, 1995). The material parameters of different tire components are listed in Table 4.2, which should be determined according to the measured contact areas. The differences derived from the non-linear response behaviors of the tire which is affected by tire inflation pressure. However, in all cases, the rim is assumed to be rigid with the elastic modulus of 100 GPa, Poisson's ratio of 0.3, and density of 2,700 kg/m^3. The truck tire models were discretized using 4-node isoparametric single-layer shell elements MITC4 (ADINA R&D Inc., 2009), which have been successfully used for tire friction analysis by others (Tanner, 1996).

4.3.2 Pavement Model

The pavement surface can be considered to be rigid compared to the flexible tire. For simulation purposes, it is assumed to have an elastic modulus of 30 GPa, a Poisson's ratio of 0.15, and a density of 2,200 kg/m^3. It is also discretized using shell elements (MITC4), which have been demonstrated suitable for analysis of plates or shells (ADINA R&D Inc., 2008).

4.3.3 Tire-Pavement Contact Algorithm

Constraint-function algorithm (ADINA R&D Inc., 2009) was used for contact calculation in this chaper. In this algorithm, the following normal constraint function is used to enforce the no-penetration and the frictional contact conditions.

$$w(g,\lambda) = \frac{g+\lambda}{2} - \sqrt{\left(\frac{g-\lambda}{2}\right)^2 + \varepsilon_N} \tag{4.1}$$

where g and λ are tangential and normal contact force, respectively. ε_N is a small user-defined parameter, whose value is 1.0×10^{-12} by default and can be set via the EPSN variable in the CGROUP commands in ADINA. The advantage of this constraint function is it involves no inequalities, and is smooth and differentiable which is shown in Figure 4.7(a).

Define a non-dimensional variable $\tau = \frac{F_T}{\mu\lambda}$, where FT is the tangential force, μ is the coefficient of friction and λ is the normal contact force. The Coulomb frictional constraint function takes the form $f(\dot{u},\tau) = 0$. A multi-linear frictional constraint function is used in the friction algorithm as shown in Figure 4.7(b), where u is the sliding velocity and ε_T is a small parameter (EPST parameter in the CGROUP commands) which provides some elastic slip to the Coulomb friction law.

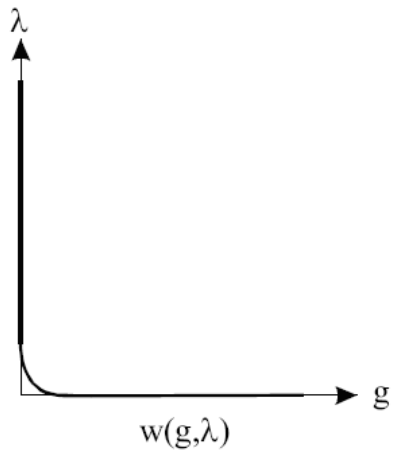

(a) Constraint Function for Normal Contact Algorithm

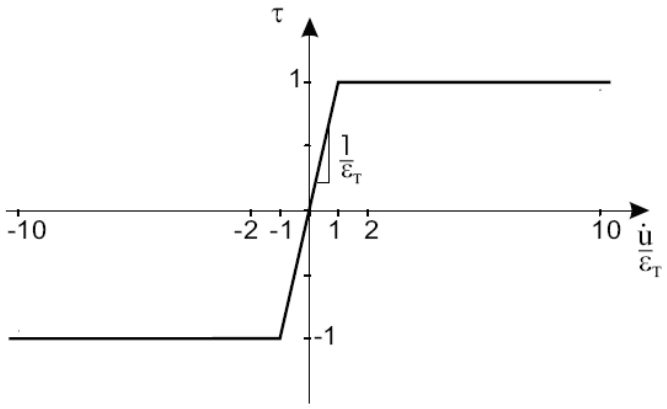

(b) Frictional Contact Constraint Function for Tangential Friction Algorithm

Figure 4.7 Contact Constraint Functions Used in the Analysis

4.3.4 Water Film Model

The behavior of fluid flow near the tire pavement contact patch has to be illustrated by turbulence model (Wallace and Trollope, 1969). In this simulation, the standard *k*-*ε* turbulence model (ADINA R&D Inc., 2009), which is a semi-empirical model based on model transport equations for the turbulence kinetic energy *k* and its dissipation rate *ε*, is employed to illustrate the fluid flow with a high Reynolds number when

hydroplaning occurs (Ong and Fwa, 2006). *k* and *ε* are determined by the following two equations:

$$\frac{\partial\left(y^a \rho K\right)}{\partial t} + \nabla\bullet\left[y^a(\rho v K - q_K)\right] = y^a S_K \tag{4.2}$$

$$\frac{\partial\left(y^a \rho \varepsilon\right)}{\partial t} + \nabla\bullet\left[y^a(\rho v \varepsilon - q_\varepsilon)\right] = y^a S_\varepsilon \tag{4.3}$$

where $q_k = \left(\mu_0 + \frac{\mu_t}{\sigma_K}\right)\nabla K$, $q_\varepsilon = \left(\mu_0 + \frac{\mu_t}{\sigma_\varepsilon}\right)\nabla \varepsilon$,

$$S_K = 2\mu_t D^2 - \rho\varepsilon + B,\ S_\varepsilon = \frac{\varepsilon}{K}\left[2c_1\mu_t D^2 - c_2\rho\varepsilon + c_1(1-c_3)B\right],$$

$$B = \left(\mu_0 + \frac{\mu_t}{\sigma_\theta}\right)\beta g\bullet\nabla\theta,$$

where *K* and *ε* are kinetic energy and rate of dissipation of the turbulence respectively; *a* is zero for two- and three-dimensional flows and one for axisymmetric flows; where μ_0 and μ_t are the laminar viscosity and its turbulent counterpart. c_1, c_2, c_3, c_μ, σ_k, σ_ε, σ_θ are model constants and their default values are c_1 = 1.44, c_2 = 1.92, c_3 = 0.8, c_μ = 0.09, σ_k = 1, σ_ε = 1.3, σ_θ = 0.9.

For fluid structure interaction (FSI) simulation, the Arbitrary Lagrangian-Eulerian (ALE) formulation should be used for the fluid. The incompressible Navier-Stokes equations governing the water flow behaviors in a general ALE coordinate system can be expressed as

$$\frac{\partial}{\partial t}\int_V U dV + \oint_{\partial V}[(v - v')U - G]dS = \int_V R dV \tag{4.4}$$

where

$$U=\begin{bmatrix}\rho\\ \rho v\\ \rho E\\ \rho\varphi\\ 0\end{bmatrix},\ G=\begin{bmatrix}0\\ \tau\\ \tau\bullet v+k\nabla\theta\\ d_{\varphi}\nabla\varphi\\ d_{\psi}\nabla\psi\end{bmatrix},R=\begin{bmatrix}0\\ f^{B}\\ f^{B}\bullet v+q^{B}\\ S_{\varphi}\\ 0\end{bmatrix}$$

where τ, v, v', ρ, E, θ, f^B q^B are the stress tensor, the velocity vector, the moving mesh velocity vector, density, specific energy, effective viscosity, the body force per unit volume, and the rate of heat generated per unit volume, respectively. V and ∂V are an arbitrary integral volume and its boundary surfaces. ϕ is the specific rate of heat generation, represents any other variables governed by convective-diffusive equations with d_ϕ and S_ϕ being its diffusion coefficient and source term respectively, and ψ represents any other variables governed by the Laplace equations, with $d\psi$ being its diffusion coefficient. The variables that ϕ might represent are the turbulence kinetic energy K and the turbulence dissipation rate ε for the K-ε turbulence model. The variables ψ represents the increments of fluid displacement for the moving boundary condition.

The physical parameters of water at 25℃, density 997.1 kg/m^3, dynamic viscosity 0.894×10^{-3} Ns/m^3 and kinematic viscosity0.897×10^{-6} m^2/s are used in the simulation (Chemical Rubber Company, 2003). The fluid domain is discretized by 8-node hexahedral elements. The flow-condition-based interpolation (FCBI) approach proposed by Bathe (2007) is used to numerically solve this equation. The detailed boundary conditions of the fluid model are given in the following section.

4.3.5 Formulation of Fluid-Structure Interaction

Considering FSI between pneumatic tire and water flow, the tire tread deformations can be complex and be highly affected by the turbulence water flow that takes place

as the sliding speed of the wheel increases. Of course, the water flow can also be highly affected by the tire deformations. For this problem, the two-way coupling method should be used, which is an iterative process to couple the responses of the fluid model and the tire model. The governing finite element equations coupling the fluid flow and tire structural response can be written as (Bathe and Zhang, 2004)

$$\mathbf{F(X)} = \begin{bmatrix} \mathbf{F_f(X_f, X_s)} \\ \mathbf{F_s(X_f, X_s)} \end{bmatrix} = \mathbf{0} \tag{4.5}$$

where $\mathbf{F_f}$, $\mathbf{F_s}$ represent the equation systems for the water fluid and tire models, and $\mathbf{X_f}$, $\mathbf{X_s}$ are the fluid and tire parts solution variables, including the displacements of the FSI interface. It contains all momentum, energy and continuity conditions of the fluid and structure, and all interface conditions between the fluid and the structure. In the coupling analysis, the kinematic condition, or the displacement compatibility is ensured. This is achieved with the condition that the stresses on the tire face and tire face displacements are equal to the corresponding responses in the fluid model.

4.3.6 Load and Boundary Conditions

Figures 4.8(a) and 4.8(b) show the two tire models with their boundary conditions used in the simulation: wheel load acting on the rim, and tire inflation pressure acting on the inner faces and fluid-structure interface at the tread surface of the tire. The rim was fixed except for vertical transform degree of freedom. For convenience and reducing the calculation time consideration, the moving coordinate system was used so that we can move the pavement and water instead of tire to simulate the relative movement between them.

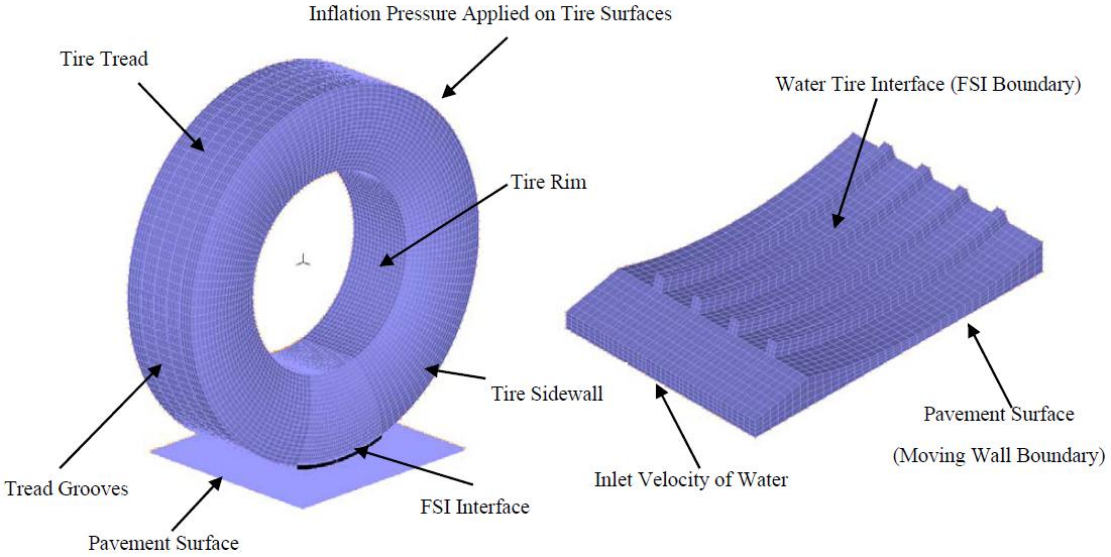

(a) 11R22.5 Truck Tire and its Corresponding Water Film Model

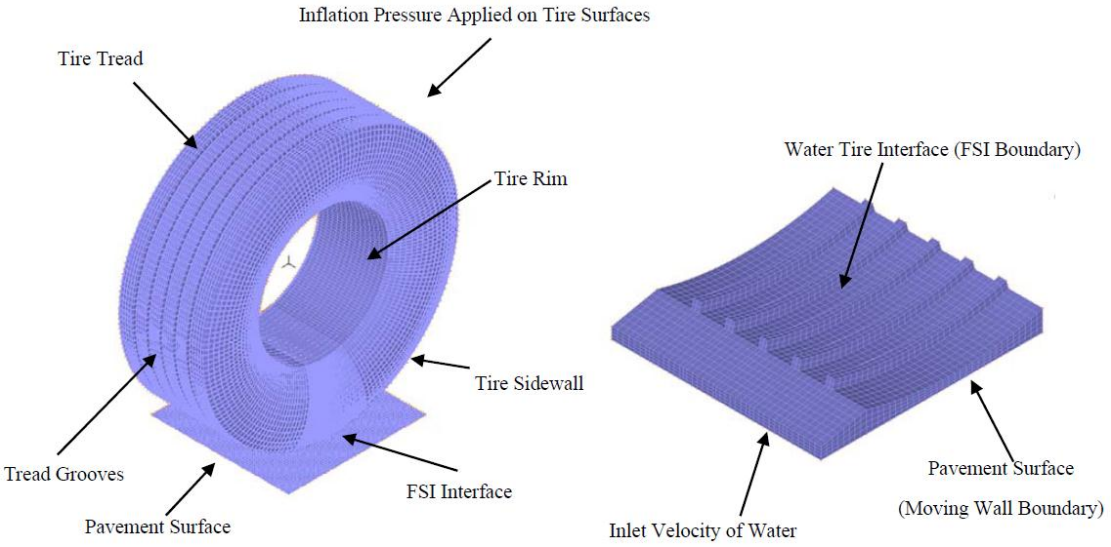

(b) 425/65R22.5 Truck Tire and its Corresponding Water Film Model

FIGURE 4.8 3D Truck Tire Models and Their Corresponding Water Fluid Models

The boundaries for water fluid include: Inlet velocity at the front surfaces to simulate the vehicle speed; Fluid-Structure Interface at the tread face of the tire; and Outlet pressure at the back of the wheel to simulate the splash. Moving wall boundary condition is used for water and pavement interface while other surfaces of the water part are subject to the atmospheric pressure boundary condition. The finite-element mesh together with the loads and boundary conditions in the fluid flow model is also shown in Figure 4.8. The inlet velocity is increased gradually until up to the hydroplaning speed. The water-film thickness is controlled by the inlet condition to the desired thickness.

4.4 Model Calibration Using Contact Area

Since a finite element model approximates a structure displacement using node points and element domains, the mesh can be a major source of model errors. The more elements used in the model, the more accurate the model converges to the solution. The trade-off is that the more elements the bigger is the model, and the longer the solution time. The rate of convergence of most FEA models will plateau at a certain number of elements, i.e. no further mesh refinement will improve the results. The required number of elements used in this analysis was determined according to this criterion. It is found that using 14,630 shell elements for the tire model and 3,600 shell elements for the pavement surface would be sufficient to give satisfactory results, as shown in Table 4.3.

Figure 4.9 and Figure 4.10 show the differences between the simulated contact areas and the experimental contact areas of 425/65R22.5 and 11R22.5 tires under different loads and different inflation pressures, respectively. It indicates that the model employed can accurately predict the contact patches.

Table 4.3 Comparison of Measured and Predicted Contact Area

Type of Truck Tire	Inflation Pressure (psi)	Applied Load (kN)	Measured Contact Area (cm^2)	Predicted Contact Area (cm^2)	Error (%)
425/65R22.5	80 (550kPa)	8.9	406	410	-0.98
		17.8	658	656	0.31
		26.7	825	796	3.52
	100 (690kPa)	8.9	365	339	7.12
		17.8	567	584	-3.00
		26.7	753	760	-0.93
	120 (830kPa)	8.9	345	325	5.78
		17.8	538	576	-7.06
		26.7	730	731	-0.14
11R22.5	85 (580kPa)	5.6	268	271	-1.12
		7.8	326	330	-1.23
		10	393	387	1.53
		13.3	445	450	-1.12
		16.7	503	496	1.39
	105 (720kPa)	5.6	226	220	2.65
		7.8	297	290	2.35
		10	342	344	-0.58
		13.3	406	413	-1.72
		16.7	471	472	-0.21
	125 (860kPa)	5.6	213	214	-0.47
		7.8	271	288	-6.28
		10	324	326	-0.62
		13.3	384	391	-1.82
		16.7	432	429	0.69

It can be seen from the figures that the tire inflation pressure has much less effect on contact area of wide-base truck tire compared to the traditional dual truck tire, especially in the cases of higher inflation pressure. Figure 4.11 shows the gross

contact areas measured for a single 11R22.5 tire and a 425/65R22.5 wide-base tire at the indicated inflation pressures of 690kPa (100psi). Since dual tires carry twice the load of a single 11R22.5 tire, and produce twice the footprint area, the data may be plotted to compare the footprint area of dual tires with that of a single wide-base tire at the same load. As shown in Figure 4.11, the footprint area of the wide-base tire is, at most, 12% less than that of the dual tires, which agrees well with the experimental results (Tielking, 1992).

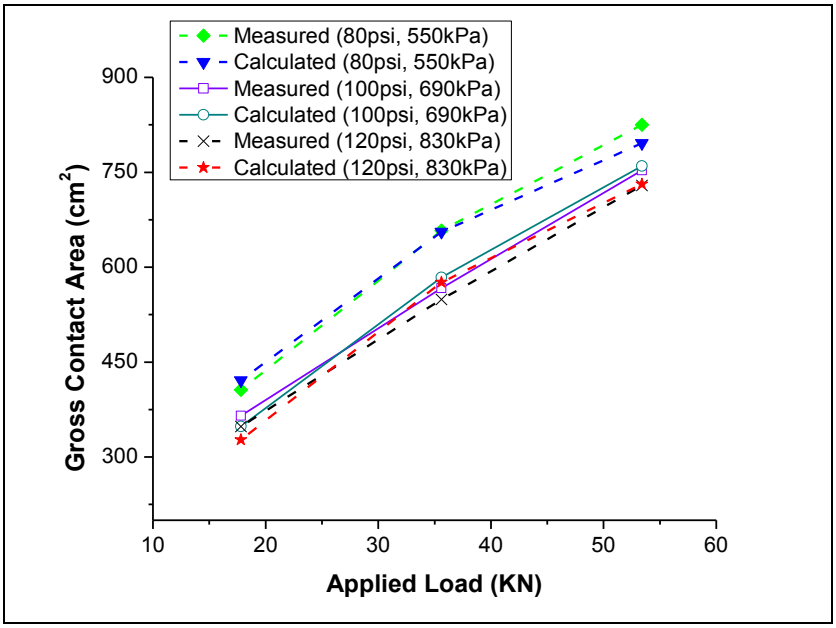

Figure 4.9 Comparisons of Contact Areas between Experimental and Simulated Results for Wide-Base Truck Tire (425/65R22.5)

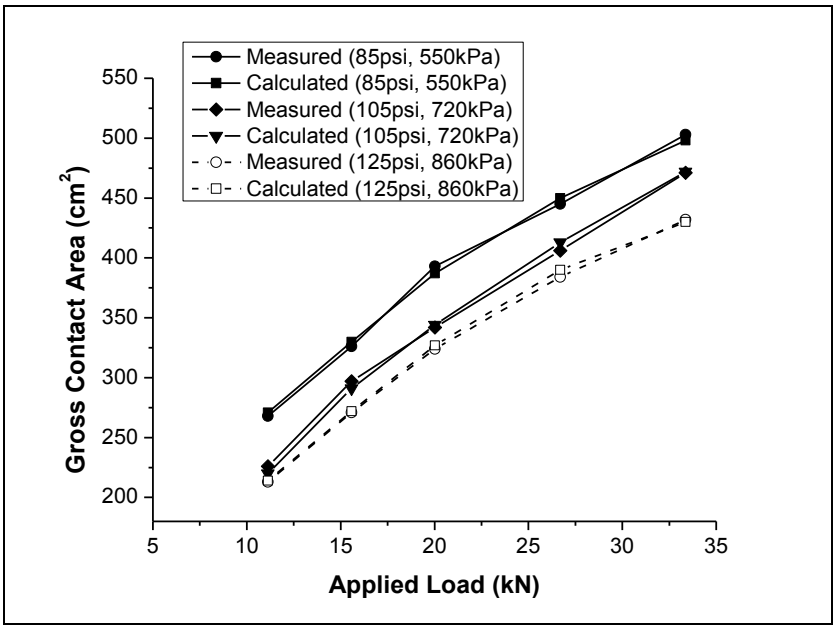

Figure 4.10 Comparisons of Contact Areas between Experimental and Simulated Results for 11R22.5 Tire

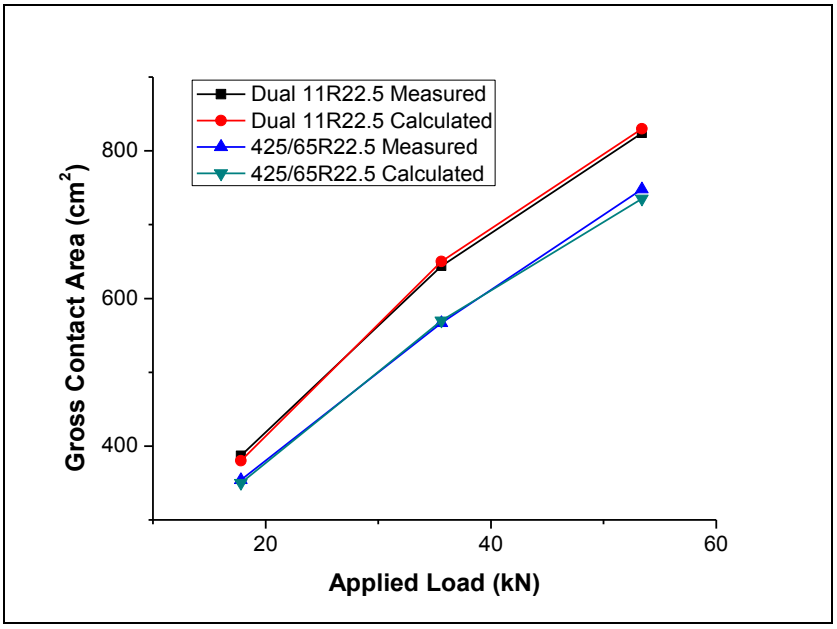

Figure 4.11 Comparison of Contact Areas between Tire 425/65R22.5 and Tire 11R22.5 at Inflation Pressure of 690kPa (100psi)

4.5 Validation of FSI model with experimental data

In order to verify the FSI simulation model, the situations according to the literature (Tielking, 1992) are simulated firstly. In the experiments of Texas Transportation Institute, the hydroplaning tests were conducted by towing a single test tire in a water trough, in which uniform water depths up to 19mm was maintained to allow tires to be tested with the grooves completely flooded. Tire hydroplaning is detected in their experiment by an abrupt spin-down of the test wheel. Thus the same condition as used in their experiments is adopted in our simulation. It has been demonstrated that flooding the grooves minimizes tread pattern influence on hydroplaning (Tielking, 1992). Due to the fact that the tread depth of the tire is 15mm while the water film thickness is 19mm, the tire grooves are modeled using straight grooves in this analysis.

Similarly with the validation of truck tire models in the former section, the convergence test was also conducted in FSI simulation for fluid mesh density. The results indicated that the number of 8,400 hexahedral FCBI elements is enough for FSI simulation. For verification of the model, two cases were simulated: wide-base 425/65R22.5 Truck Tire, 690kPa (100psi) inflation pressure under two tire loads 11kN (2500lb) and 18kN (4000lb); traditional 11R22.5 truck tire, 690kPa (100psi) inflation pressure under two tire loads 9kN (2000lb) and 22kN (5000lb). The measured and the predicted hydroplaning speeds were given in Table 4.4 in which dual-tires data are the single 11R22.5 tire speeds plotted at twice the single tire load.

It can be seen that the predicted values for the investigated cases agree well with the measured data within an error of less than 5%. This difference may mainly derive from the different criterion of hydroplaning determination besides the errors from the numerical model. It is noted that in their experiment (Tielking, 1992) tire

hydroplaning was detected by the abrupt spin-down of the rolling test tires while in our simulation it is determined by the fluid uplift force equaling the vehicle load applied on locked sliding tire. Actually, when the tire abrupt spin down occurs, it can only demonstrate that the traction force between the pavement and tire cannot supply enough resistance to support the nonslip state of tire, i.e. the frictional force contributed by the pavement surface have reduced to small enough while the fluid uplift force may be less than the tire load at this moment.

Table 4.4 Validation of Hydroplaning Speed for 425/65R22.5 and 11R22.5 Tires

Type of Truck Tire	Applied Load (kN)	Measured Speed (km/h)	Predicted Speed (km/h)	Error (%)
425/65R22.5	11.1	90.7	94.0	3.6
	17.8	100.4	102.3	2.8
Dual 11R22.5	8.9	84.5	88.2	4.3
	22.2	94.7	97.1	2.5

4.6 Analysis and Discussion of Results

4.6.1 Effect of Wheel Load on Hydroplaning

As one of the major affecting factors to truck tire hydroplaning, wheel load is investigated in this study. The range studied in this simulation is from 11.1kN (2500lb) to 44.5kN (10000lb), which is the load range commonly carried by wide-base truck tires. The inflation pressure is kept constant at 690kPa (100psi) for all the cases. The water thickness is also constant at 19mm while the tread grooves are 15mm. The variation of the hydroplaning speed for different wheel loads is given in Figure 4.12.

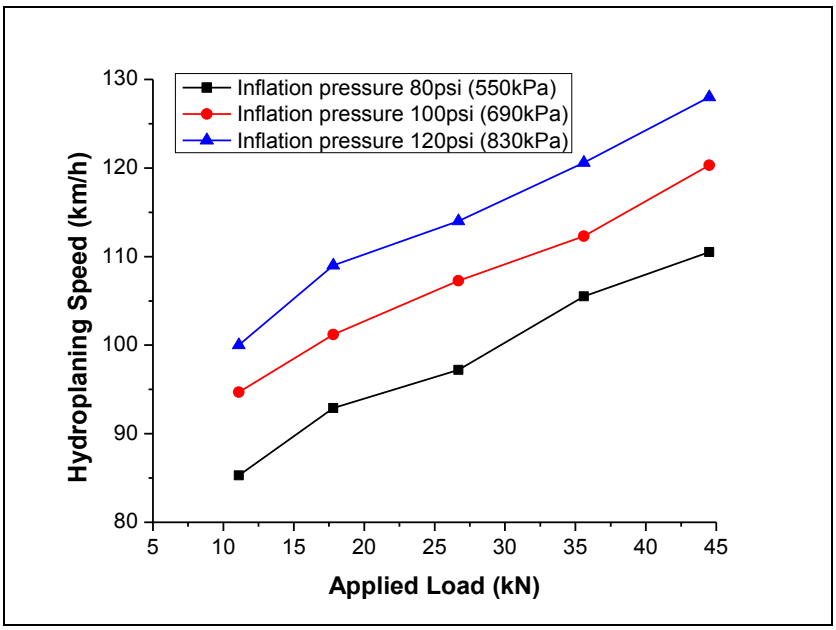

Figure 4.12 Effect of Wheel Load on Hydroplaning of Wide-base Tire 425/65R22.5

It can be seen from the figure that the predicted hydroplaning speed increases with the increasing applied load. An increase in wheel load from 11.1kN to 44.5kN, about four time of initial load, would causes an increment of approximately 25km/h for hydroplaning speed when the tire inflation pressure was definite. It is noted that the wheel load 11.1kN (22.2kN, 5000lb axle load) are realistic for empty trucks. This may give some explanation for the observation that the empty truck tire is easier to hydroplaning than full loaded trucks.

4.6.2 Effect of Inflation Pressure on Hydroplaning

Previous study (Ong and Fwa, 2008) has revealed that the tire inflation pressure has significant influence on the hydroplaning speed of truck tires. Therefore, the effect of tire inflation pressure on wide-base tire's hydroplaning is also investigated in this research. Figure 4.13 depicts the variation of hydroplaning speed for truck tire

425/65R22.5 at different tire inflation pressures. It is observed that the predicted hydroplaning speed increases as the increasing tire pressure when keeping the load constant. As shown in the Figure 4.13, it can be seen that an increase in tire inflation pressure from 550kPa (80psi) to 830kPa (120psi), about 1.5 time of initial inflation pressure, would cause an increase in hydroplaning speed by about 15 km/h under the same load condition.

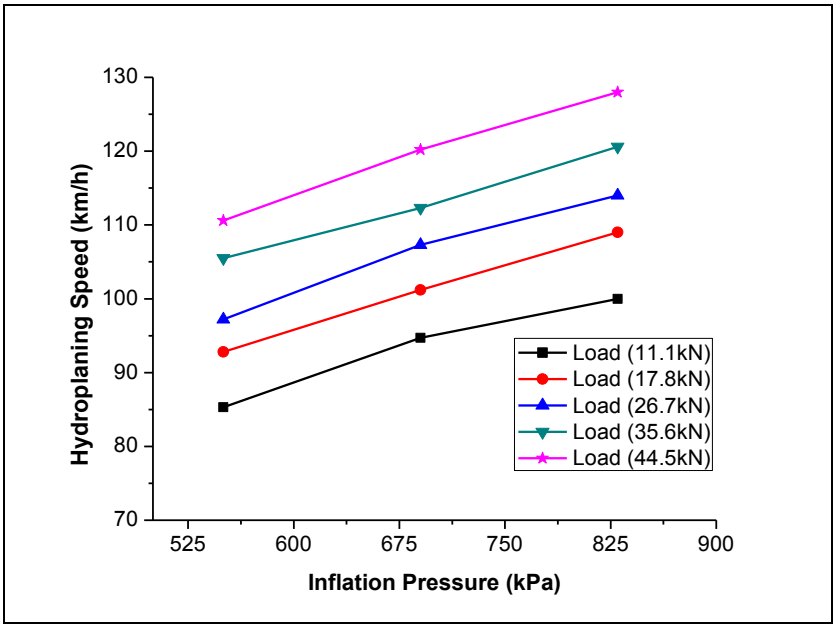

Figure 4.13 Variation of Hydroplaning Speed for Wide-base Tire at Different Inflation Pressures

Compared with the influence of wheel load, it seems that the effect rate of inflation pressure is larger than that of wheel load. However, it is found that hydroplaning of wide-base truck tire is not more sensitive to the tire inflation pressures than the traditional truck tires as previous investigation by Ong and Fwa (2008) using the smooth truck tire 10.00-20.00. This may be contributed by the different tire properties (material properties, bias or radial, smooth or treaded) and the

different water-film thickness. Another reason may be the fact that, as mentioned before, the contact area of the wide-base truck tire is less sensitive to the inflation pressure compared to the traditional truck tire. Thus there is a motivation for us to investigate other factors of hydroplaning involving tire sizes and grooves, water film thickness and pavement surface profile in the future work.

4.6.3 Effect of Water Film Thickness on Hydroplaning

Investigations have demonstrated that even a very thin water film resting on pavement may dramatically reduce the traction force and leads to hydroplaning at higher speeds. In this section, the effect of water-depth on hydroplaning speed is studied. Six different water-depths: 2mm, 4mm, 7mm, 10mm, 15mm and 19 mm are employed as inlet water depth in the simulation. The tire inflation pressure is kept at 690 kPa (100psi) and the wheel load increases from 11.1 kN to 44.5kN.

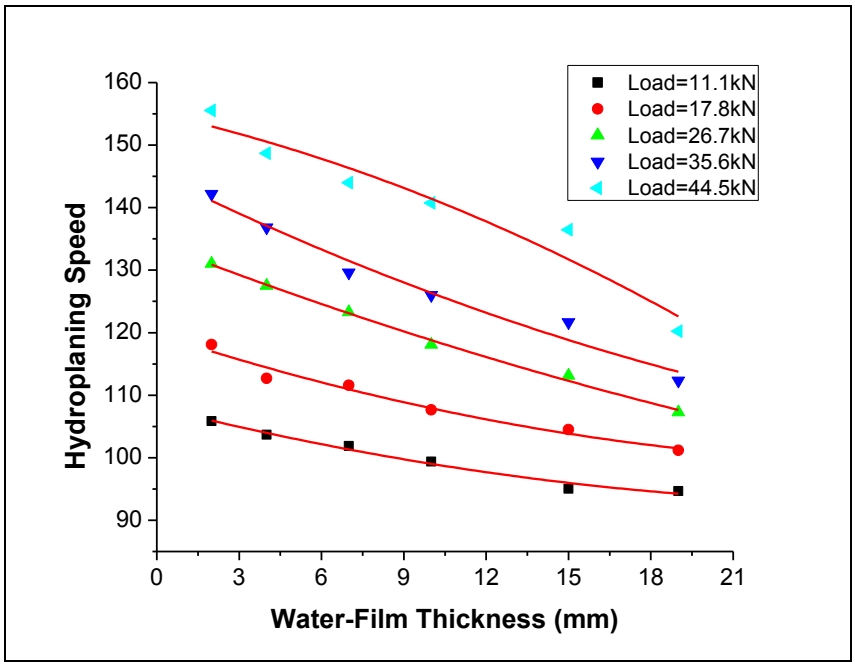

Figure 4.14 Variation of Hydroplaning Speed for Wide-base Tire at Different Inflation Pressures

The variation of hydroplaning speed with water film thickness at different wheel loads are shown in Figure 4.14. It can be seen that for the wide-base truck tire the hydroplaning speed reduces with increasing water depth. When the load is larger, the rate of decreasing is higher, for example, when wheel load is kept at 44.5kN, the drop of hydroplaning speed is about 30km/h whereas the drop of hydroplaning speed is only about 12km/h when wheel load is kept 11.1kN. However, even if the larger drop in hydroplaning speed at larger load, the minimum hydroplaning speed still remains above 120km/h. Thus it indicates that when it is fully loaded, the truck equipped with wide-base tires will usually not suffer hydroplaning even at the normal traffic speed of highway.

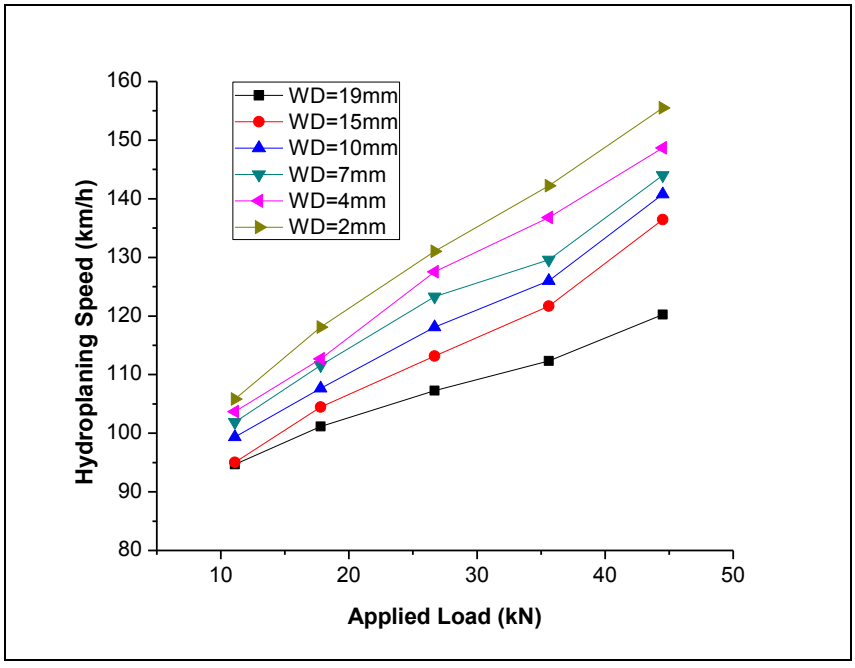

Figure 4.15 Variation of Hydroplaning Speed for Wide-base Tire at Different Inflation Pressures

4.6.4 Comparison between Wide-Base and Traditional Truck Tire

As shown in Figure 4.16, it is obvious that both the wide-base 425/65R22.5 truck tire and traditional 11R22.5 truck tire can develop hydroplaning at highway speeds. However, the wide-base tire was not apt to hydroplaning than two conventional tires under the same vehicle load. The difference for hydroplaning speed is about 10 km/h when keeping other conditions the same. The reason may come from the fact that the contact pressure of wide-base truck tire is larger than the traditional duals under the same load condition. This finding indicates that the wide-base truck tire has the potential capability in favor of hydroplaning performance to substitute conventional dual truck tire.

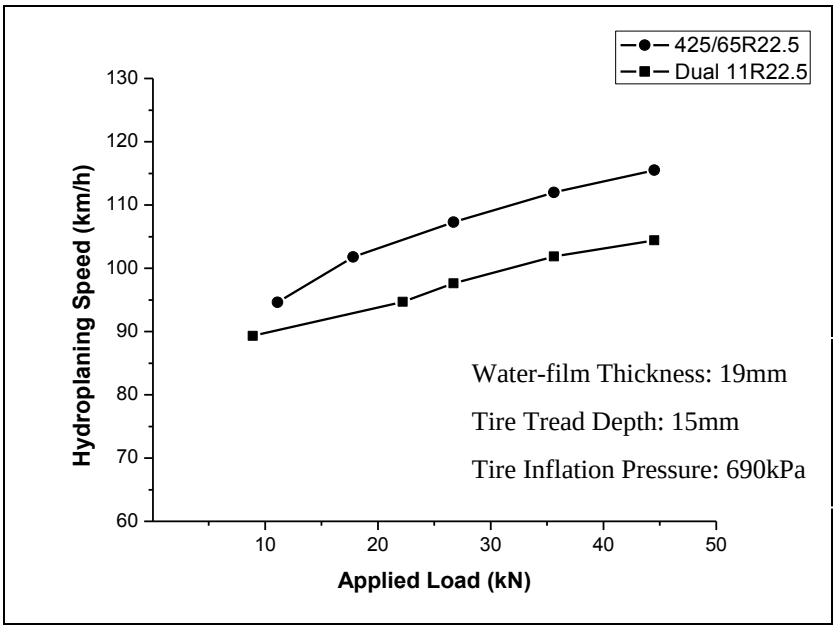

Figure 4.16 Comparison of Hydroplaning Speed for Different Truck Tires

4.7 Summary and Conclusion

The three-dimensional FSI simulation, considering the interactions of tire, water and pavement, was performed to analyze the hydroplaning phenomenon of wide-base

truck tires. The verification of the FSI model using the experimental data indicated that the proposed models can be used to simulate truck hydroplaning phenomenon and to predict truck hydroplaning speeds satisfactorily. Without assuming the tire deformation profile, the model can be easily and effectively employed to investigate the hydroplaning variations contributed by the changes of different related factors, such as material properties, tire sizes, and tread dimensions, applied wheel load, and water film thickness on pavement surfaces.

The simulation results for the investigated cases indicated that the hydroplaning speed increases with wheel load and tire pressure. It was observed that for wide-base truck tire, inflation pressure is still the major factor and has larger influence on hydroplaning speed than wheel load. The analysis has also confirmed the following observation from past field experience and experimental tests, i.e. empty trucks are more prone to hydroplaning occurrences than loaded trucks, even for the wide-base truck tire; and the single wide-base tire 425/65R22.5 has better hydroplaning performance than conventional truck tire 11/R22.5.

This chapter indicates the ability of FSI model in simulating hydroplaning phenomenon and conducting valuable sensitivity analysis that are often complex and difficult to obtain in practice unless large-scale experiments are conducted. The effects of tire tread pattern, groove depth and water film thickness on hydroplaning speed of wide-base truck tire will be investigated in the future work.

CHAPTER 5 SKID RESISTANCE ANALYSIS OF RIB TRUCK TIRES

5.1 Introduction

Skid resistance, as one of the most important factors for travelling safety, has been attracted much attention over the past century. Numerous measurements and experiments have been conducted for a wide range of interest throughout the world. Most of them are focusing on pavement parameters such as microtexture and macrotexture and are mainly concentrating on standard test tires and passenger car tires. However, it has been reported that tires of trucks have significantly different performance of skid resistance compared with those of passenger cars, which may derived from the differences between operating conditions of trucks and cars such as tire size and design, tire inflation pressures, wheel load and so forth (Dijks, 1974; Ervin, 1977; Williams, 1977). Therefore, there is strong interest for engineers to investigate the difference between truck tires and car tires and to identify the skid resistance performance of truck tire under different operation conditions.

Experiments have revealed that the wet skid resistance of smooth tires is poorer compared with tires with full tread depth. The decrease in skid resistance, however, is not linearly dependent on the tread depth (Allbert and Walker, 1965). Experiments conducted in UK using passenger car tires had shown that a sharp drop in skid resistance will occur under certain conditions when the car tire wears to a tread depth below 1 or 2 mm (Staughton, 1970). Studies conducted by Dijks (1974) investigated the braking force coefficients as well as cornering force coefficients

using four types of car tires and found that skid resistance values decrease progressively as the tread depth decreases. Based on the experiments, they proposed one empirical formulation to predict the drop value of skid resistance based on vehicle speed and road surface average texture depth

$$\Delta\mu = -20\mathrm{TD} + 0.5V \tag{5.1}$$

in which $\Delta\mu$ is the percentage drop in friction value for a bald tire compared with a new one. *TD* is the average texture depth of the road surface in mm, *V* is the vehicle speed in km/h. This formula is applicable within a speed range of 50-130 km/h and a *TD* range of 0.1-1.5 mm.

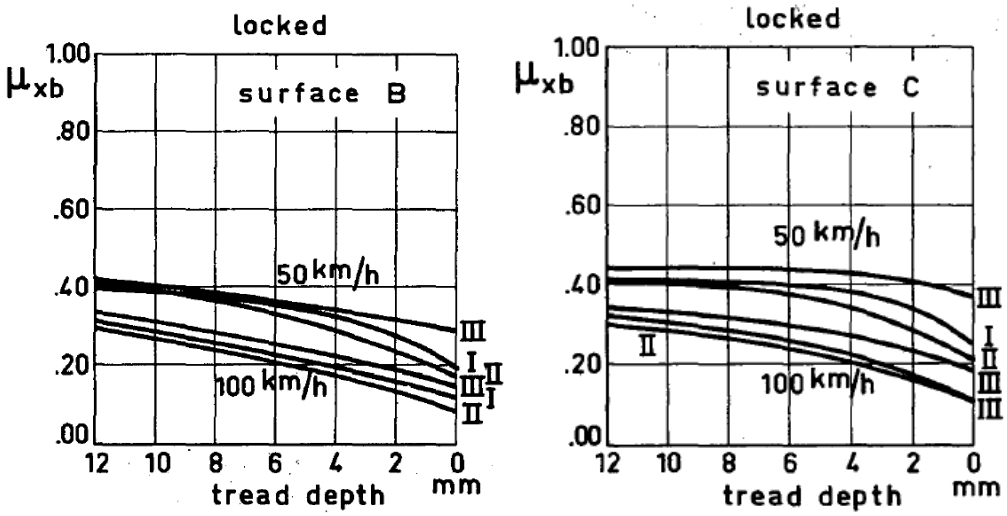

Note: I: 11R20 Truck Tire, II: 10R20 Bus Tire, III: 10R20 Retreaded Truck tire;Surface B: Cement Concrete, Surface C: New Asphalt Concrete; Refer to Figure 2.7 in Chapter 2 for definition of symbol μ_{xb}.

Figure 5.1 Variation of Skid Resistance with Tread Depths (After Dijks, 1974)

Research conducted in Netherlands (Dijks, 1974) using three types of truck tires on different road surfaces showed that the sliding resistance values decreases gradually with tire wear at all speeds and it decrease sharply when the tread depth is

reduced below 2mm (Figure 5.1). They also verified that the skid resistance of truck tires are very low compared to car tires, about half that of car tires (as shown in Figure 2.8). They attributed the difference in skid resistance between car tires and truck tires to three sources: tread compound, higher loads and inflation pressure of truck tires, and tread pattern.

Results (Figure 5.2) for truck tire 9.00-20 with a load of 21 kN and an inflation pressure of 515 kN/m from TRRL of UK gave a similar decreasing trends like Dijks' results (1974).

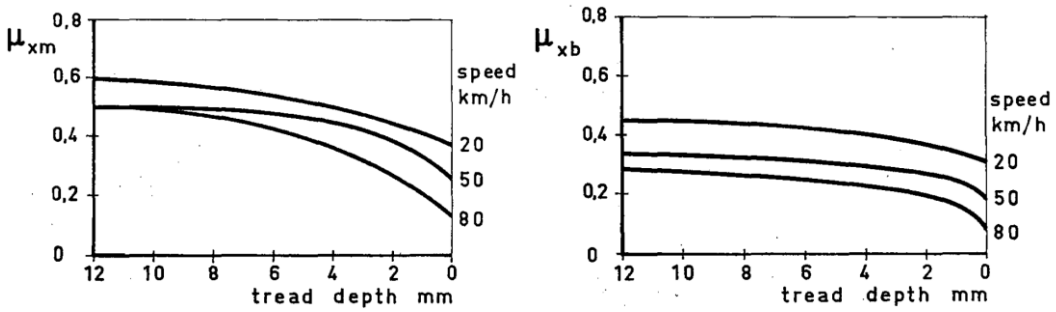

Note: Definitions of symbol μ_{xm} and μ_{xb} are the same as those in Figure 2.7.

Figure 5.2 Variation of Skid Resistances of Truck Tires with Tread Depths (After Williams and Meades, 1975)

It should be noted that compared with the wide exploration of experimental studies, less efforts have been given to analytical research to reveal the mechanism of skid resistance. Two possible reasons are the complexity of this problem and the limitation of mathematical tools and computation power. Even the several important attempts in this effort were all focused on passenger cars, rare or none for trucks. Browne (1971) and Groger and Weis (1996) had developed hydroplaning models using fluid dynamics without considering the effects of tire deformation. Zmindar and

Gradjar (1997) and Okano and Koishi (2000) employed computational fluid dynamics (CFD) to simulate tire hydroplaning with considering the fluid-structure interaction. However, their flow was assumed to be laminar and skid resistance was not investigated due to the limitation of their models. The previous studies conducted by Ong and Fwa (2008, 2010b) have employed a FEM simulation model to simulate the hydroplaning and skid resistance of smooth truck tires on wet pavements with considering tire-fluid interaction. However, the model cannot be used to investigate the effect of tire rib geometry.

In this chapter, the skid resistance of rib truck tires will be simulated and discussed in detail. The similar FSI simulation model as depicted in Chapter 4 will be employed. Though both tire hydroplaning and skid resistances involve tire-water-pavement interaction, the modeling of skid resistance is analytically more complex than that of hydroplaning because it is essential to consider the tire-pavement interaction. In the previous Chapter 4, the FSI model has been demonstrated to be able to simulate the hydroplaning phenomenon. In this chapter, the model was extended to simulate and investigate skid resistance of rib truck tires under different situations. The validation of the model is carried out using the experimental data reported in the literatures. The effects of affecting factors, including tread depth, width and number of grooves, wheel load, inflation pressure, water-film thickness and sliding speed, are also discussed in detail to get some new insight of skid resistance of truck tires with ribs.

5.2 Rib Truck Tire Description

In this analysis, SP321 truck tire (Figure 5.3), one of the most commonly used for medium trucks in Europe, are employed as the prototype of tire FEM sub-model. The

tread pattern is a 3/6 rib pattern configuration, having two wide grooves that divide the tread pattern into three ribs, each of which is in turn divided by a narrow groove. The geometry profile of the tire can be found in the guidelines published by the Tire and Rim Association Inc. (1995).

Figure 5.3 3D Profile and Cross Section of Medium Truck Tire

Tread Depth

One of the major tasks of this research is to investigate the effect of tread depth on skid resistance of truck tires. It should be noted that the depth of the tread pattern is to be measured in the grooves or sipes; bridge-like protrusions or reinforcements in the tread base should be ignored in this context (Figure 5.4). As depicted in the former section, the tread depth is an important index for assuring traffic safety in wet weather. Therefore, it is necessary and beneficial to rule a definite minimum tread depth for operating vehicles. The following requirements are law in the majority of European countries:

- Pneumatic tires on trucks and trailers have to feature tread grooves or sipes round their entire circumference and over the whole width of the tread area.

• The main grooves on truck tires have to have a tread depth of at least 1 mm, 1.6 mm or 2 mm, depending on the law in each country.

Figure 5.4 Schematic of Tread Depths Measurement

5.3 Model Description

The 3D modeling of tire-water-pavement system is a complex task. The coupled description and realistic interaction of the sub-systems represent even a larger challenge to computation. Generally, one of the components, either pavement or tire, is simplified. Similarly to the hydroplaning model, as shown in Figure 5.5, the FSI modeling for skid resistance of truck tires is also involved three components: pneumatic truck tire sub-model, pavement surface sub-model, and fluid sub-model.

For truck tire sub-model, three structural components are modeled, namely tire rim, tire sidewalls and tire tread. Tire rim is assumed to be rigid while tire sidewall and tire tread are considered to be homogeneous, orthotropic elastic materials. The structural properties of the tread and sidewall components are characterized by the following parameters: elastic module E_a, E_b and E_c (where subscripts a and b refer to the in-plane orthogonal material axes and subscript c is the third material axes which is perpendicular to the plane defined by a and b), shear module G_a , G_b, G_c, Poisson's ratio and material density. The calibration of these tire properties for the simulation

model has been given in the Chapter 4 when doing the simulation of hydroplaning. The properties of the water fluid model and pavement model are the same as those used in the Chapter 4.

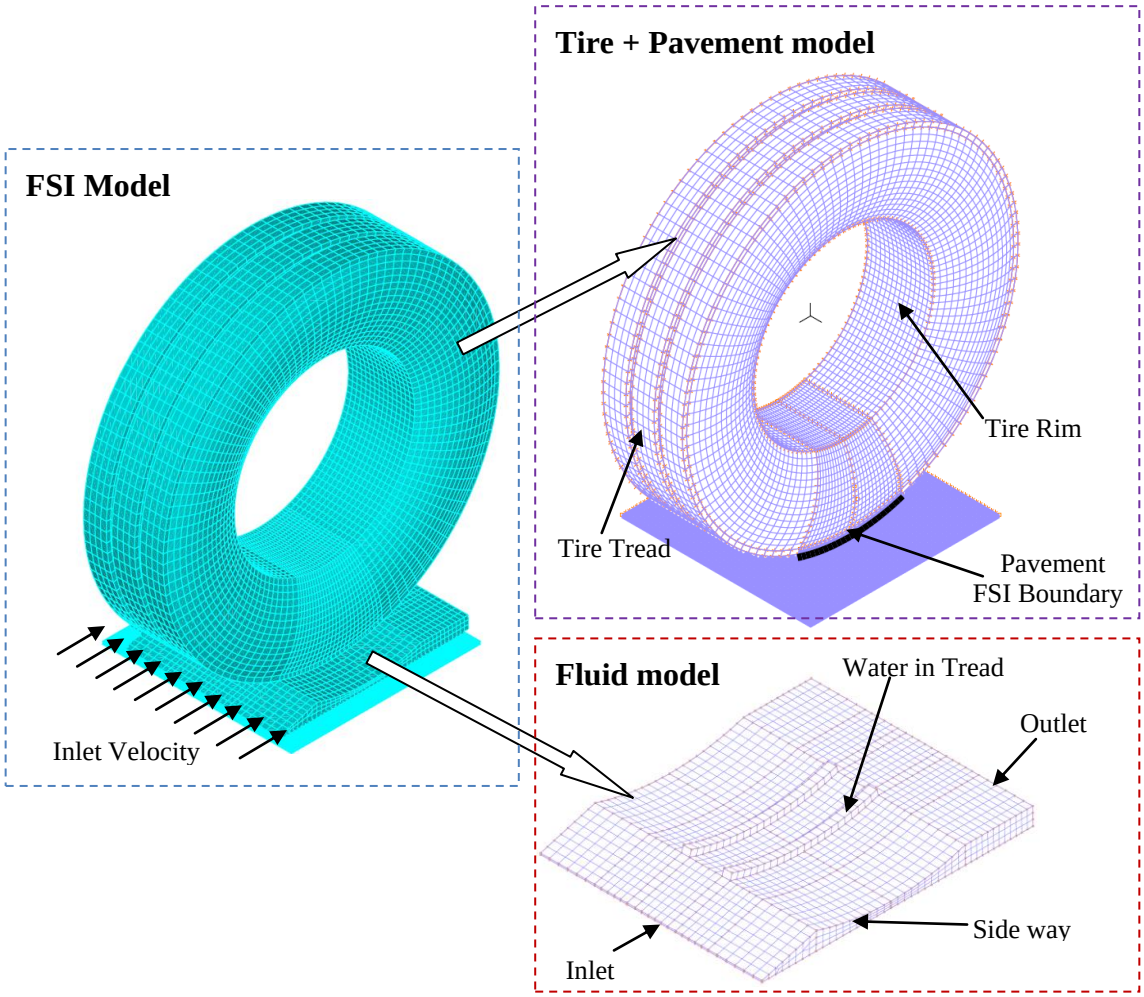

Figure 5.5 Fluid Structure Interaction Model used for Skid Resistance

Compared with hydroplaning simulation, the main difference of skid resistance simulation is the necessity of considering the interaction between tire and pavement. A plane pavement surface with a tire-pavement friction coefficient μ is involved. The pavement is assumed to be a rigid surface without deformation. The

tire-pavement friction coefficient μ is defined as the ratio of the tangential force, F, required to produce sliding divided by the normal force N,

$$\mu = \frac{F}{N} \tag{5.2}$$

where μ is numerically equal to the skid number at zero speed when the actions of fluid and other dynamic forces are absent.

In this chapter, the behavior of rib truck tire sliding on a wet pavement surface is investigated by using the proposed FSI model. The problem is modeled as a water film with given thickness resting on the pavement surface, and moving together towards the locked wheel at a given speed. The finite element analysis computer software, ADINA-FSI (2009) is used to solve the coupled tire-fluid interaction problem. The key input parameters needed for the FSI simulation model are listed below:

- Geometry profile and dimensions of truck tire;
- Material properties of three components of truck tire: elasticity modulus and Poisson's ratio;
- Tire inflation pressure;
- Wheel load magnitude;
- Physical properties of water fluid: density, dynamic viscosity, kinematic viscosity;
- Water film thickness;
- Sliding speed of rib truck tire;
- Static frictional coefficients between tire and pavement.

The simulation begins with a wheel sliding speed of zero and the static tire footprint. The sliding speed is increased in a predefined increment until hydroplaning takes

place. The solution procedure involves determining the deformation profile of the tire, under a given wheel load sliding at a given speed, through iterative coupling of the three sub-models. First, tire-pavement interaction analysis gives a tire deformation profile. With this profile, the interaction of fluid and tire generates the hydrodynamic forces acting on the tires and pavement. These are in turn fed to the tire pavement interaction model where the interface contact forces and a new tire deformation profile are generated. Upon convergence, the solution yields tire deformation profile, fluid drag and uplift forces, tire-pavement normal reaction and traction forces.

5.4 Definition of skid resistance

Wet skid resistance is usually characterized by three coefficients, that is, average braking coefficient when wheel is locked, maximum braking coefficient before locking and cornering coefficient. In this research, we mainly concentrated on the longitudinal average braking coefficient when wheel is locked, i.e. μs, which is defined as

$$\mu_s = \frac{F_x}{F_z} \tag{5.3}$$

However, when carrying out measurement of pavement skid resistance, it is common to report it as Skid Number (*SN*) at speed v (km/h) as

$$SN_v = 100 \times \frac{F_x}{F_z} \tag{5.4}$$

where F_x is the horizontal resistance force to motion acting on the axle of the tire and F_z is the vertical loading acting on the tire. The horizontal resistance force F_x is equal to the traction forces developed between the tire-pavement contact surface and the fluid drag forces derived from the water inertial forces. The relative contributions of the two components and their respective variations with the sliding speed will have

direct influence on the overall value of horizontal resistant force F_x. The vertical loading F_z is equal to the sum of the normal contact force and the fluid uplift forces, and remains constant throughout the simulation.

It can be seen from Equation (5.4) that the only variable that is responsible for the changes in the measured skid resistance is the horizontal resistance force F_x since the vertical loading F_z remains constant throughout the sliding process. As the wheel sliding speed increases, there will be a gradual loss in the horizontal traction force. The mechanism for this variation in *SN* can be seen from the re-written form of Equation (5.4)

$$SN_v = 100 \times \frac{F_x}{F_z} = 100 \times \frac{\mu(F_z - F_{up-lift}) + F_{drag}}{F_z} \tag{5.5}$$

where μ is the friction coefficient between tire and pavement surface. Therefore, the skid resistance of the simulation can be obtained after getting the required values of fluid drag forces and up-lift forces under different conditions. Given a defined speed, the vertical fluid uplift force, the horizontal drag force, the vertical tire-pavement contact force and the horizontal traction force developed between tire and pavement surface can be obtained. Then the *SN* values can be calculated based on these data.

5.5 Validation of Skid Resistance Using Experimental data

The proposed FSI simulation model for predicting skid resistance for truck tires was verified using the measurement data from literature (Kemp, 1989) in this section. The effect of temperature was ignored in the investigated cases because little variation of the properties of water with the temperature varying between 15 to 35oC has no significant impact on the simulation results (Ong and Fwa, 2006). So the density, dynamic viscosity and kinematic viscosity of water at 25 were employed, which are

998.1 kg/m^3, 0.894x10^{-3} Ns/m^3 and 0.897x10^{-6} m^2/s, respectively (Chemical Rubber Company, 2003). Determination of the tire-pavement friction coefficient, which is a material property between the tire rubber and moist pavement surface, is essential for the calculation of horizontal friction force.

Table 5.1 Verification of Predicted Skid Resistance Values Using Experimental Data

Pavement type	Tread depth (mm)	Speed (km/h)	Experimental *SN* (Kemp, 1989)	Predicted *SN*	Error (%)
Smooth Concrete Pavement	2.7	50	19.2	18.5	3.6%
	2.7	60	17.3	17.4	-0.6%
	4.2	50	20.5	19.8	3.4%
	4.2	60	18.1	17.9	1.1%
	7.8	50	25.2	24.3	3.7%
	7.8	60	22.3	22.0	1.3%
	13.6	50	26.0	25.4	2.3%
	13.6	60	25.1	23.4	6.8%
Sand Asphalt Pavement	2.7	50	25.2	24.5	2.7%
	2.7	60	21.3	22.4	-0.2%
	4.2	50	26.8	25.7	4.1%
	4.2	60	21.5	22.0	-0.3%
	7.8	50	29.7	28.6	3.7%
	7.8	60	25.4	25.6	-0.1%
	13.6	50	30.0	29.5	1.7%
	13.6	60	27.6	28.1	-0.8%

Note: Inflation Pressure: 720kPa Wheel Load: 29.4kN Water Depth: 2mm

In this analysis, the static frictional coefficient SN_0 was back-calculated trial and error based on the method previous used by Ong and Fwa (2006). In all the investigated cases, the water film thickness is kept constant at 2mm, and the inflation pressure and wheel load is using 720kPa (105psi), 29.4kN, respectively. The predicted skid resistance values and the experimental data measured by previous researchers are given in Table 5.1.

It can be seen from Table 5.1 that the predicted values of skid resistance agree well with the measured data in the literatures. The numerical differences between the predicted and measured SN are at most 1.7, which is less than 10% of the value in terms of percentage error. It indicated that the simulation model is capable of predicting wet-pavement skid resistance at a given sliding locked speed with good accuracy.

5.6 Analysis and Discussion of Results

One of the main advantages of numerical simulation is its convenience and usefulness for parametric study to consider a wide range of different influence parameters encountered both in practice an extreme conditions. Thus a parametric study was conducted in this analysis using the established simulation model to explore the effect of various factors on wet-pavement skid resistance experienced by trucks.

Table 5.2 lists the factors studied and their variation ranges investigated in this research. The detailed discussions about the simulation results are given in the following sections. It should be noted that all the simulations are based on smooth pavement surface with negligible microtexture and macrotexture.

Table 5.2 Parameter Ranges Investigated in the Analysis

Investigated parameters	Variable Range
Tread depth	0 mm-13.6 mm
Groove width	2 mm-10 mm
Tread groove position	25 mm-85 mm
Tread groove number	0-6
Wheel load	10 kN-30 kN
Inflation pressure	85 psi-105 psi
Water film thickness	2 mm-15 mm

5.6.1 Effect of Tread Depth on Skid Resistance

On smooth pavement surfaces, the tread grooves are the main drainage system and a reduction in tread depth results in a drastic drop in skid resistance values, especially at higher speeds. Thus there is a strong motivation for us to investigate the effect of tread depths of truck tire on skid resistance. In this section, several cases with different tread depths: 13.6mm, 10mm, 7.8mm, 4.2mm, 2.7mm, 0mm are studied and discussed. The schematics of the different tire cross-section are given in Figure 5.6. In all the cases simulated in this section, except the tread depth, all other conditions such as inflation pressure, wheel load and water-film thickness on pavement are kept constant at 720kPa (105psi), 29.4kN and 2mm, respectively.

Figure 5.7 gives the variations of skid resistance with tread depth. It can be seen that the skid resistance values decrease with the reducing tire tread depth at all speeds, especially at higher speeds. It demonstrates that the influence of tread depth for truck tires is similar to the situation for car tires, but the decreasing rate is more gradual. It is noted that when the tread depth is less than 2 mm, there is relatively larger drop of skid number in the *SN*-tread depth curves compared with other

segments in these curves. However, there is no definite tread depth value at which the sharp drop will be found and it is hard to definite a minimum safe tread depth, which was also illustrated by Dajia (1976).

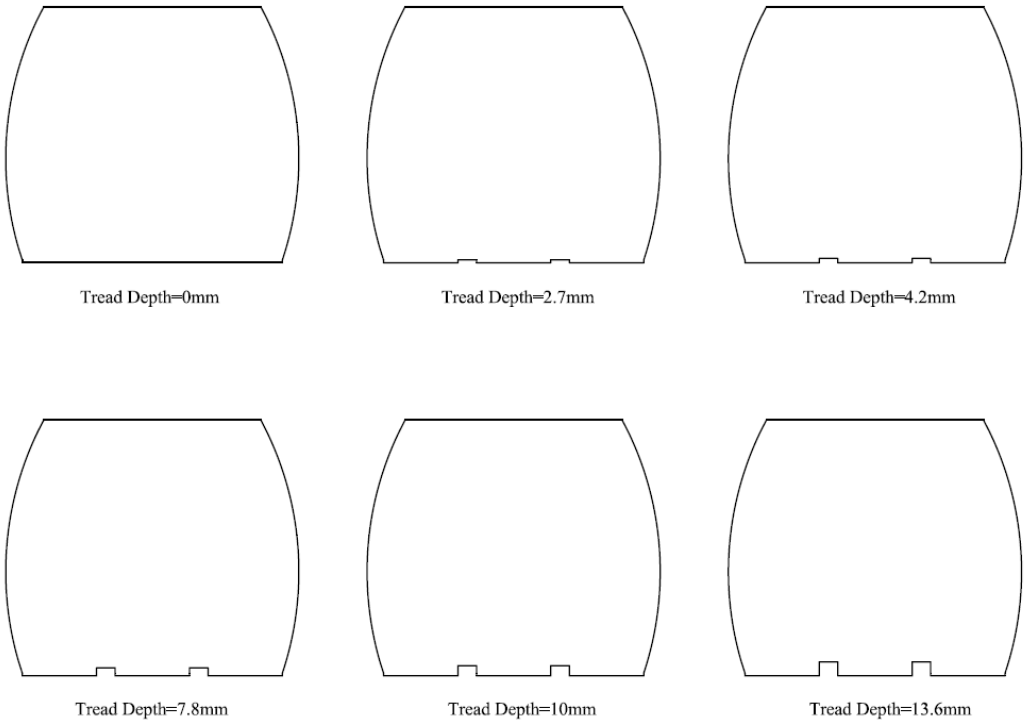

Figure 5.6 Schematic of Different Configurations of Tread Depths in Simulations

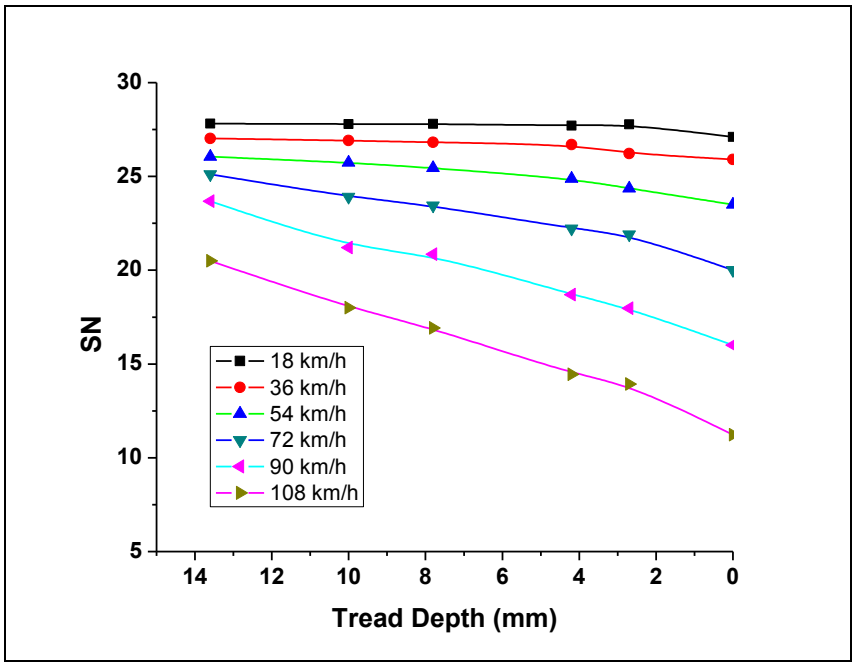

Figure 5.7 Variation of Skid Resistance with the Tread Depths of Truck Tire

It is observed that skid number decreases little when the travelling velocity is less than 15m/s (54km/h) while the skid number of bold tire is only about half of truck tires with full tread depth when the wheel speed is at 30m/s (108km/h). Therefore, when truck is traveling on wet pavements, even if the tire is new, it is still necessary for drivers to keep a lower speed less than 60km/h for safety.

5.6.2 Effect of Tread Groove Width on Skid Resistance

In this section, different configurations of tread groove width (as shown in Figure 5.8) are explored using the FSI model. The five investigated cases are respectively the truck tires with tread groove widths 5.0mm, 10mm, 18mm, 25mm, and 35mm under the same operating condition of 720kPa (105psi) inflation pressure, 29.4kN wheel load, and 2mm water-film thickness on pavement.

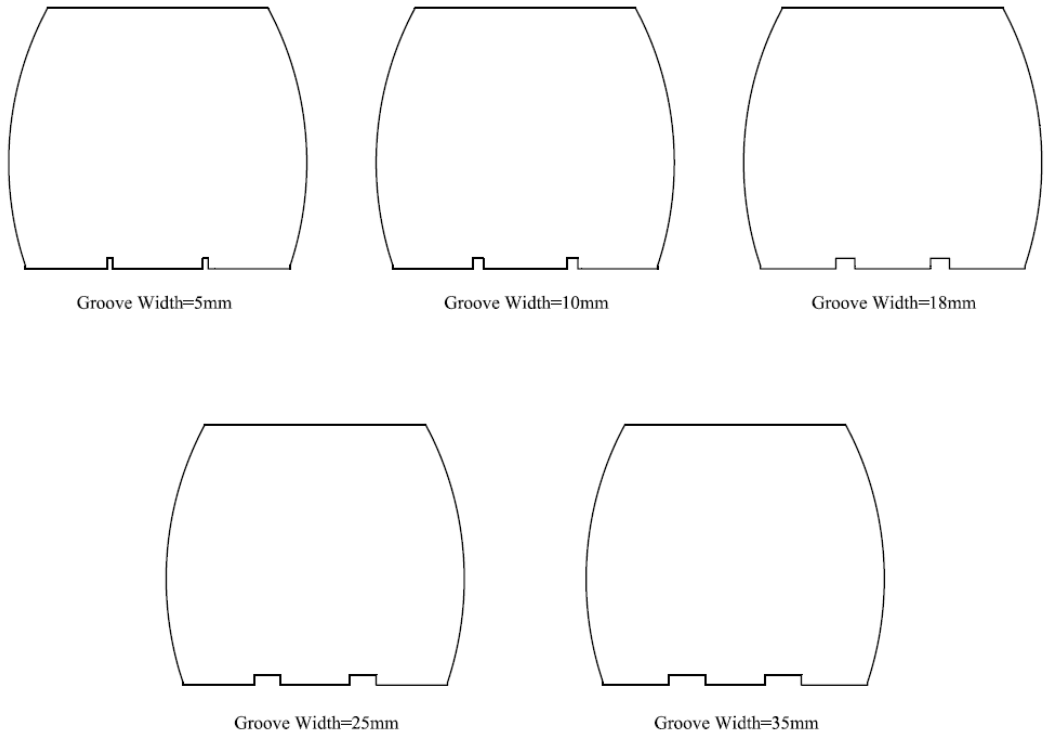

Figure 5.8 Schematic of Different Tread Groove Widths for Investigated Truck Tire

The variation of skid resistance with tread groove width is shown in Figure 5.9. It can be seen that the increasing of tread width has a positive effect on skid resistance values though the positive effect is not significant in the investigated ranges. When the sliding speed is higher than 72km/h, the positive benefit will become obvious. The margin is about 2 at 90km/h when groove width changes from 5mm to 35mm. However, at lower speed, for example less than 54km/h, nearly no difference can be found when increasing the width of tread groove.

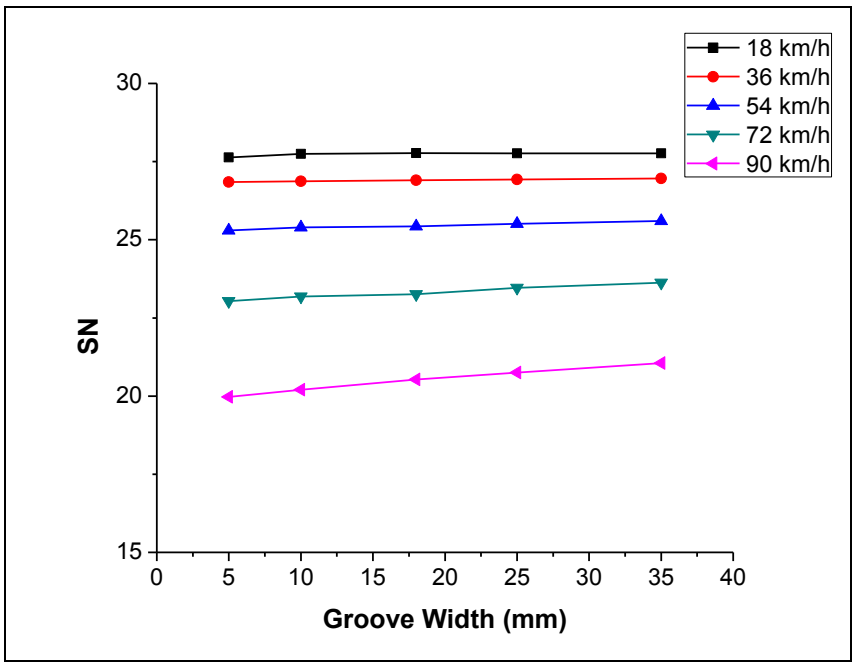

Figure 5.9 Variation of Skid Resistance with Groove Width at Different Velocities

Figure 5.10 shows the variation of skid resistance with sliding velocity at different tread widths. It is obvious that the SN-velocity curves for different tread groove widths are rather close to one another, which also indicates that tread groove width has no significant effect on the skid values of truck tire at the investigated conditions. Whereas it is noticed that for all the cases sliding velocity is still a

significant factor affecting skid resistance. The drop of skid number can be up to 80% of the total skid resistance at 0 km/h when speed rising from 0km/h to 120km/h. It can be concluded that it is not necessary for manufacturers to produce truck tires with large width grooves. However, it should be noted that the simulation results also indicated that hydroplaning speed of truck tires with width 25mm and 35mm has a higher margin value up to 10-15 km/h than those with 5mm tread groove width. In addition, it can be inferred that when traveling on muddy road, the wider grooves will be much better than narrower grooves for mud escaping.

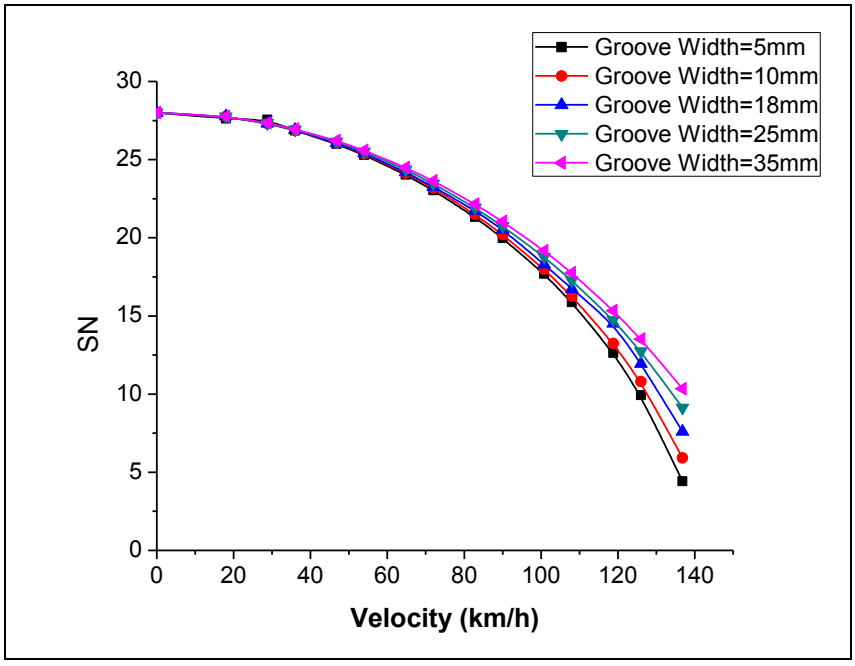

Figure 5.10 Variations of Skid Resistance with Sliding Speed at Different Tread Widths

5.6.3 Effect of the Position of Tread Grooves on Skid Resistance

In order to check whether the position of grooves in the tread has any effect on the skid resistance, effort has been taken to shed some light on this issue. Four configurations of tread grooves are discussed in this section which is shown in Figure

5.11. The offset distance is the interval distance from the central line for the groove to the central line of the tread. The groove depths and widths are all 10mm in the studied cases. The water depth is 2mm thickness and the inflation pressure and wheel load are kept 720kPa (105psi) and 29.4kN, respectively.

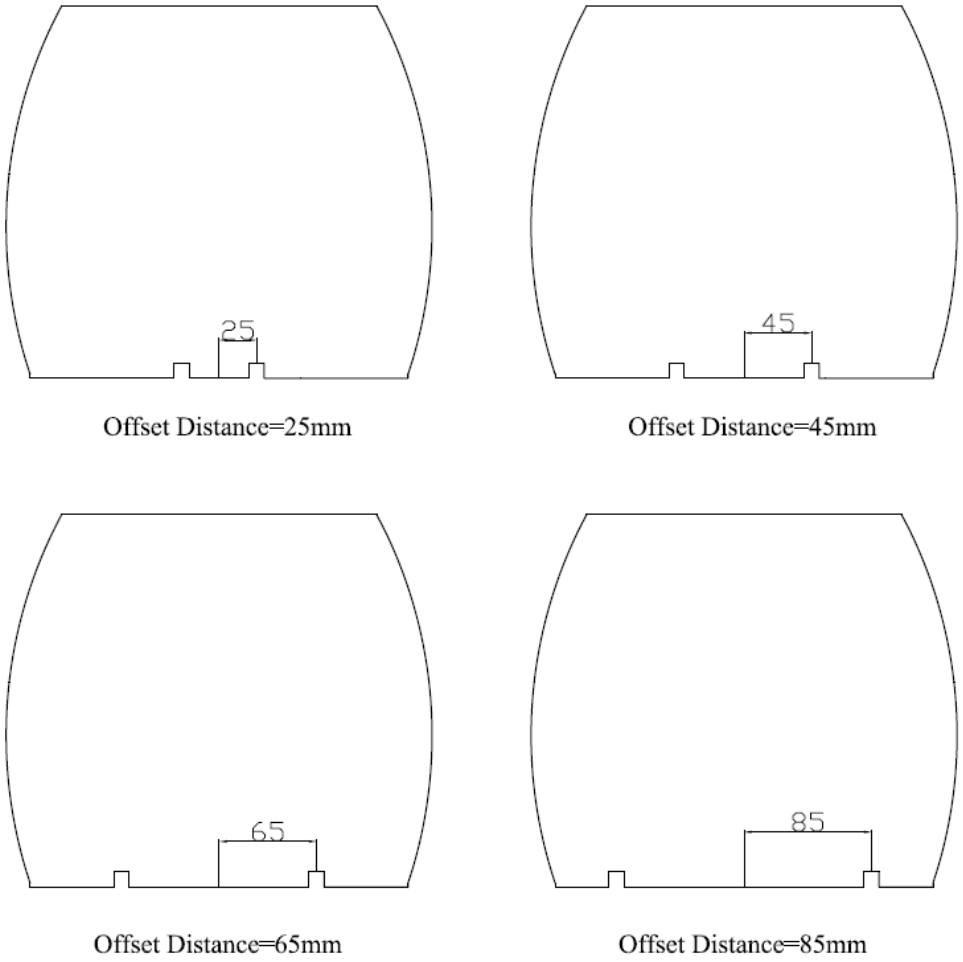

Figure 5.11 Schematic of Position Configuration of Grooves in Tire Tread

Figure 5.12 depicts the variation of skid resistance with the offset distance of grooves at different sliding velocities. It is obvious that the groove position of the grooves has no much effect on the skid number of truck tires under the adopted conditions. When the sliding speed is small, for example 36km/h, there is no effect observed for the investigated cases. While at higher speed such as larger than 72km/h,

the SN will become slightly higher when the grooves locate between 45mm-65mm in the tread surface. The reason may be that when grooves locate at near center part of tread surface, there will be a longer pathway for water expelling and when grooves locate at margin section of tread surface, it will be hard to explore the contribution of the grooves in expelling the water at contact patch. However, it is obvious that the sliding speed has significant effect on SN for all cases. When sliding speed is raised from 18km/h to 90km/h, the variation of SN is up to about 10. Herein it should be pointed out that the results may be significantly different when introducing the transverse grooves because the transverse groove can effectively reduce the length of path for water expelling when the longitudinal grooves are arranged at shoulder region of the tread.

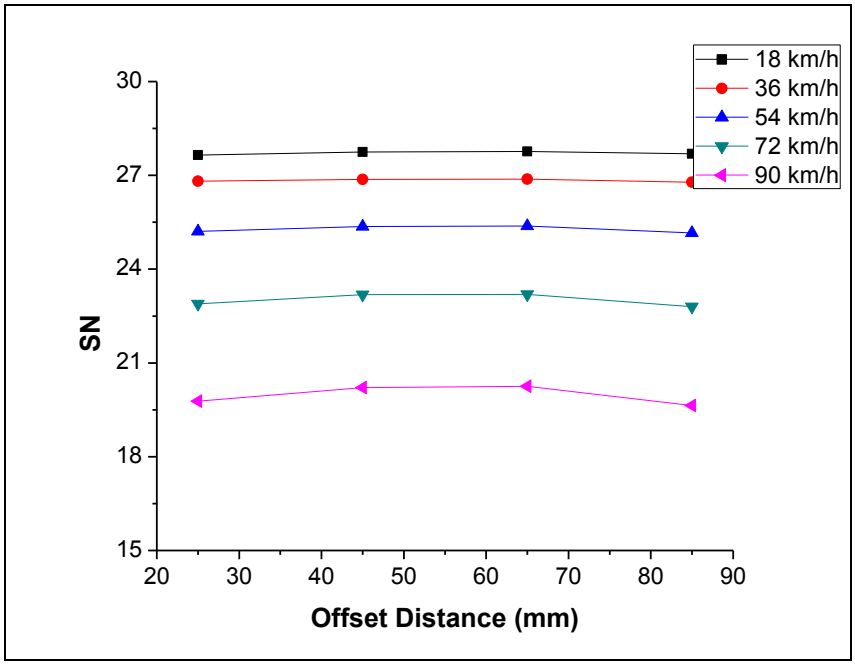

Figure 5.12 Variation of skid Resistance with the Offset Distance of Grooves at Different Sliding Speeds

Figure 5.13 shows the variations of skid resistance with increasing velocity at different offset distances of grooves. The *SN*-velocity curves for four different offset displacements are very close each other. The difference is very small for them. It can be seen that SN values of 45mm and 65mm offset distance of grooves is slightly higher than those of 25mm and 85mm offset distance of grooves.

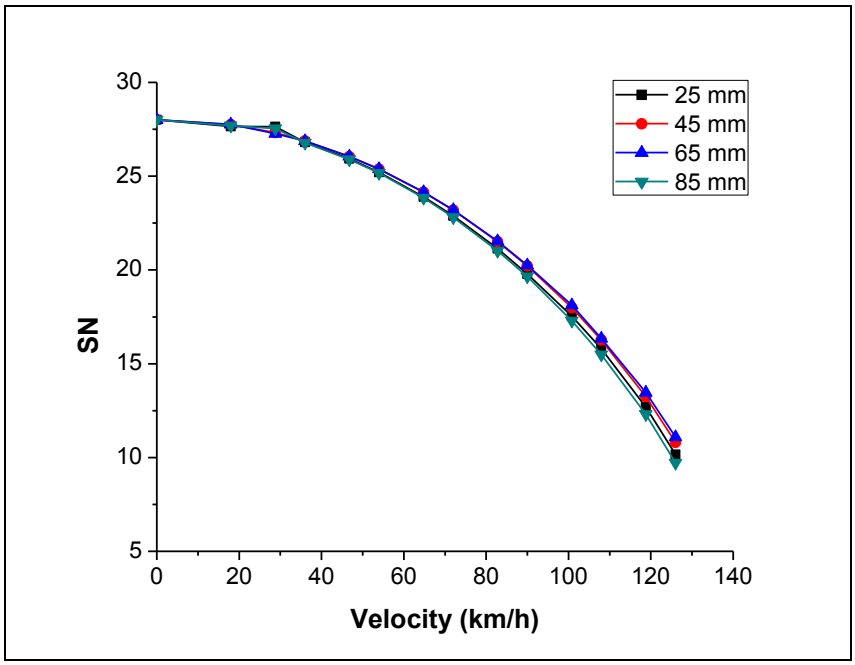

Figure 5.13 Variations of Skid Resistance with Increasing Velocity at Different Offset Distances of Grooves

5.6.4 Effect of Numbers of Groove on Skid Resistance

Besides the previous mentioned rib dimensions, the number of grooves was also investigated in this research. Four different cases with different number of grooves (0, 2, 4 and 6) symmetrically distributed in tread were simulated in this section (Figure 5.14). The truck tire inflation pressure of 720 kPa, wheel load of 29.4 kN and water depth of 10 mm were kept constant during the simulation.

The simulation curves of skid resistance with the velocity at different number of grooves are given in Figure 5.15. It can be seen that the number of ribs has no much effect when the sliding velocity is less than 54 km/h. However, it seems that the configuration with four grooves (five ribs) has a slightly better performance in skid resistance when the sliding velocity exceeds 72 km/h. The skid resistances of 2-groove configuration and 6-groove configuration nearly have the same values, as shown in Figure 5.16.

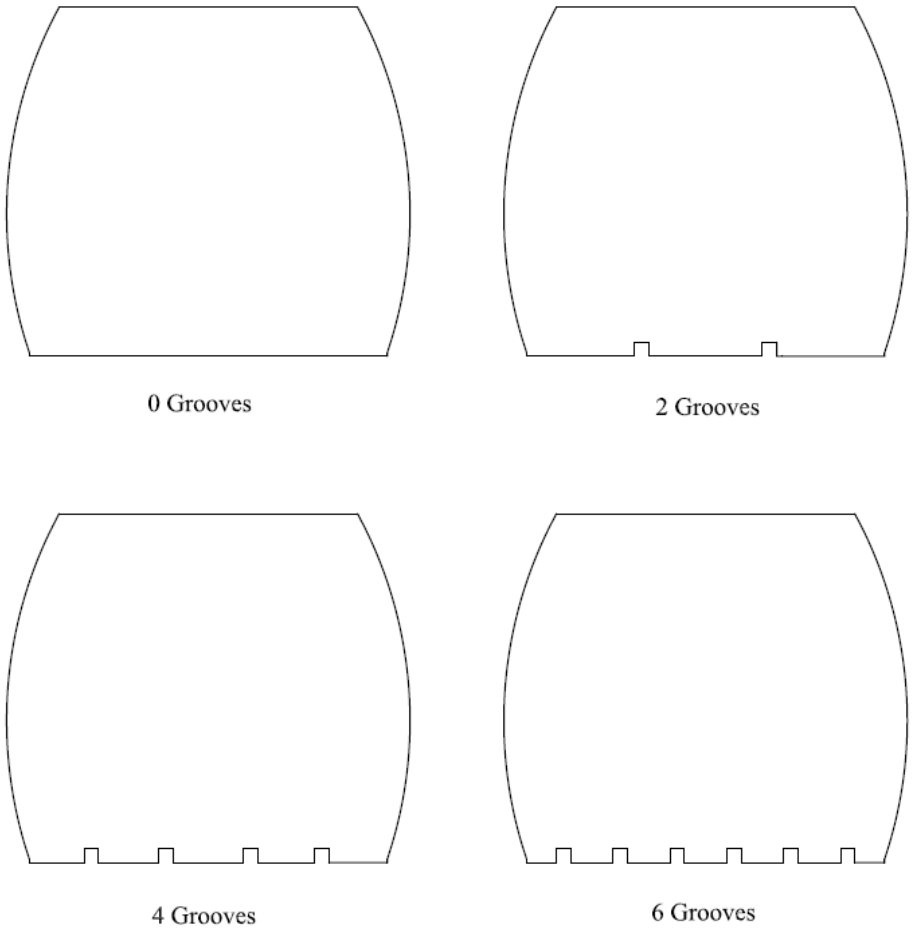

Figure 5.14 Schematic of Groove Configuration with Different Ribs

It can be seen from Figure 5.16 that the four configurations have no much difference generally. But the skid values of smooth truck tire are obviously less than those with grooves.

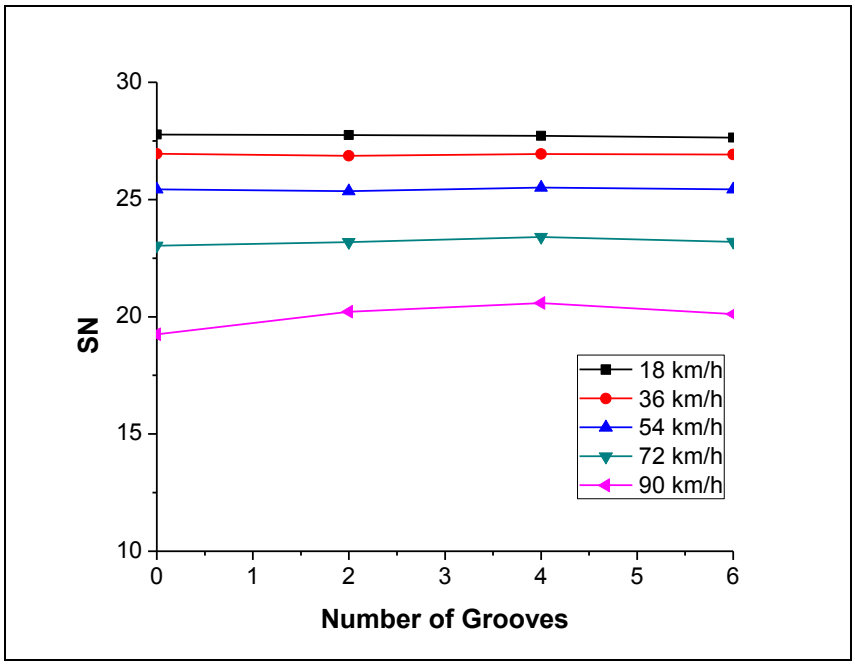

Figure 5.15 Variation of Skid Resistance with Number of Grooves at Different Speeds

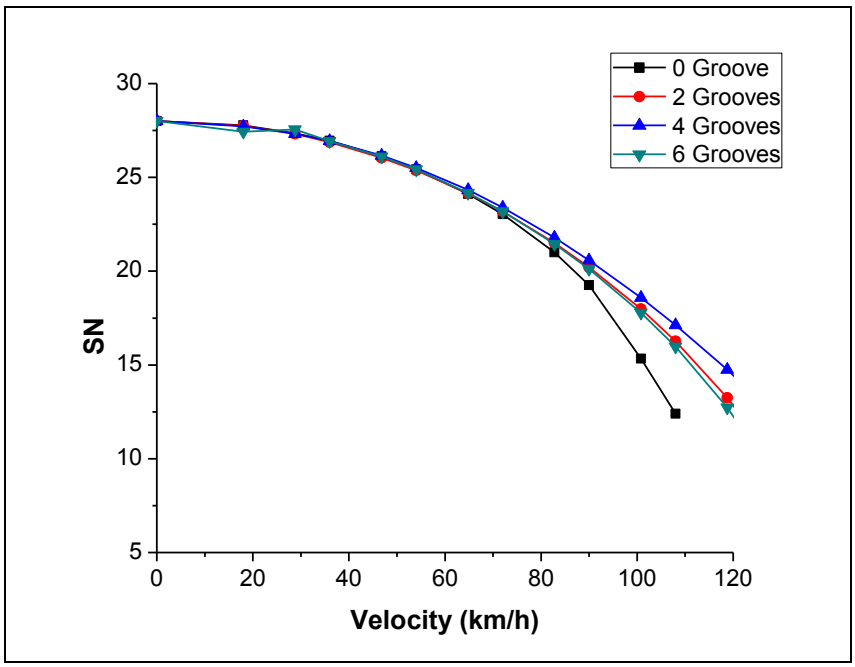

Figure 5.16 Variation of Skid Resistance with Increasing Speed at Different Numbers of Grooves

5.6.5 Effect of Wheel Load on Skid Resistance

It has been reported by previous researchers that wheel load has significant effect on hydroplaning speed of truck tires. The lightly loaded trucks have much higher risk in occurrence of hydroplaning than fully loaded trucks. However, rare literatures can be found to illustrate the effect of wheel load on skid resistance. In this research, we investigated the influence of the wheel load on skid resistance using the FSI simulation model. The water-film thickness is kept at 2mm and the inflation pressure is 720kPa. The simulation results are given in Figures 5.17 and 5.18.

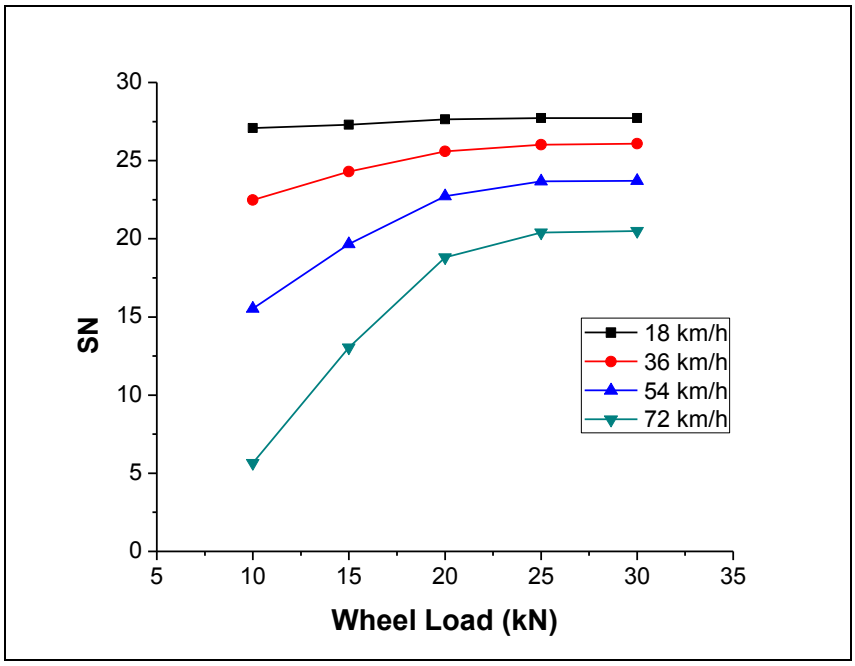

Figure 5.17 Effect of wheel load on skid resistance

As shown in Figure 5.17, the skid resistance of truck tires traveling on wet pavement generally increases with the wheel load when keeping all other parameters constant. However, the rate of changing with wheel load is not the same for different velocities. It is found that the wheel load would have much larger effect on skid

number when increasing sliding speed. At a lower speed of 18 km/h, SN is not affected much by changes in wheel load. At a higher sliding speed more than 50km/h, there are significant decreases in skid resistance when the wheel load is small. For instance, the skid number at wheel load of 10 kN is only 25% of that at 30kN when speed is 72km/h. It can be concluded that the positive effect resulted from increasing wheel load becomes more significant with higher sliding speed. This may be due to the fact that F_x comes from two parts: the water drag force and the tire pavement contact friction force. When F_x increase by a definite value, SN will be lead to a higher fall for a lighter wheel load than a heavier wheel load due to the smaller F_z. The larger the reduction in F_x, the bigger the difference between the *SN* values of a light and a heavy wheel load.

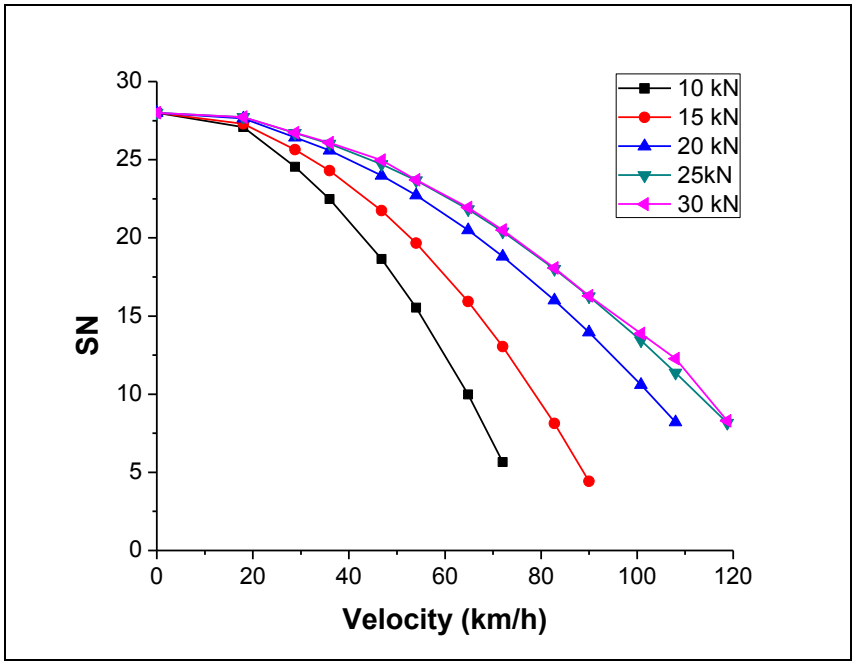

Figure 5.18 Variation of Skid Resistance of Truck Tire with Increasing Sliding Speed at Different Wheel Loads

As illustrated in Figure 5.18, skid numbers decrease at an increasing rate with the sliding velocity when the truck wheel load decreases from 30 kN to 10 kN. The decreasing rate of skid number at 10kN is much larger than the decreasing rate at 30kN. When the load is less than 10kN, trucks will definitely encounter hydroplaning at a common highway operation speed of 60km/h-80 km/h when travelling on wet pavements, which agrees very well with the observations from traffic monitoring by past investigators (Horne, 1984).

5.6.6 Effects of Water-Film Thickness on Skid Resistance

Figure 5.19 describes the variation of skid resistance with increasing water-film thickness when keeping the sliding speed constant at 18 km/h, 36km/h, 54km/h, 72km/h and 90km/h, respectively.

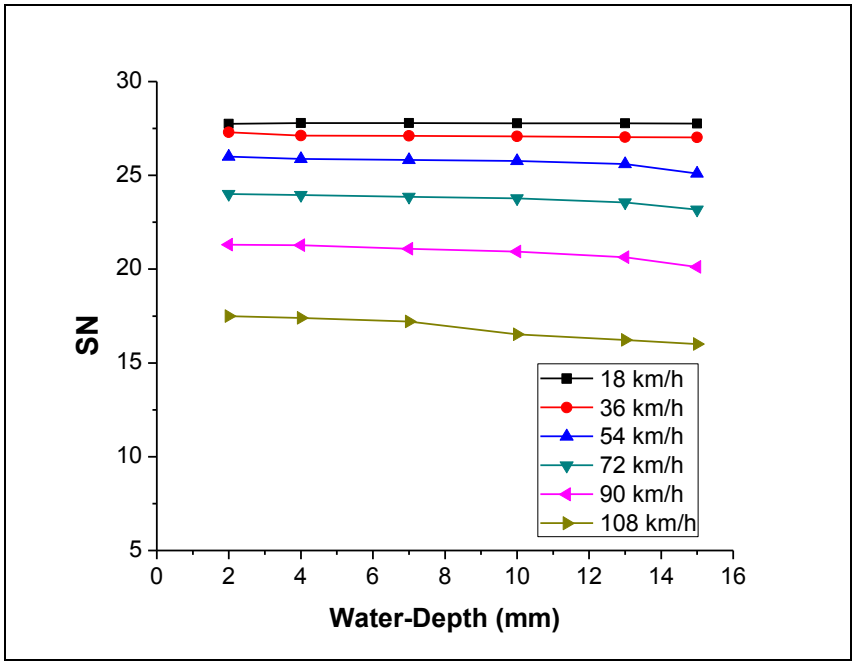

Figure 5.19 Variation of Skid Resistance with Water-Film Thickness at Different Velocities

It can be seen that skid resistance generally decreases with increasing water-film thickness when keeping all other parameters constant. When the speed is high, for example exceeding 90km/h, a slightly larger drop can be found when increasing the water-film thickness. It is also noted that when the water-film thickness exceed the tread depth of the truck tire a relatively larger drop in SN values can be observed.

The reason could be that thicker water-film reduce the water-expel function of tread grooves and results in a higher hydrodynamic force and a larger penetration of water wedge into the contact area between tire tread and pavement surface, which ultimately leads to a larger reduction in the tire footprint area and a heavier loss in skid resistance.

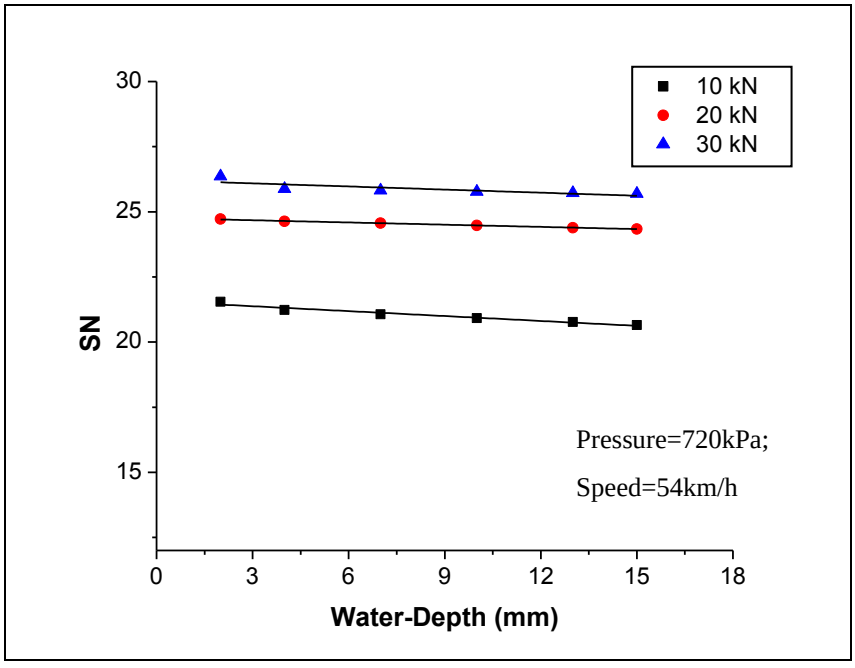

Figure 5.20 Variation of Skid Resistance with Water-Film Thickness at Different Loads

Figure 5.20 shows the variation of skid resistance with water depths at different wheel loads. It can be observed that *SN* reduces linearly with the water depth

though the absolute reduction of *SN* is not significant. And when the load is smaller, the effect of water-film thickness will become more obvious, that is, the slope of the line will become larger. The increase of skid resistance is about 1-2 for the water-film thickness ranging between 2mm to 15 mm. Figure 5.20 also indicates that wheel load is a significant factor for skid resistance.

5.6.7 Effect of Tire Inflation Pressure on Skid Resistance

The variation of skid resistance with the inflation pressure at different loads and sliding velocities are given in Figures 5.21 and 5.22, respectively. The water depth is kept at 2mm. It can be found that the skid resistance of truck tire increases marginally as tire inflation pressure increases. It can be seen from Figure 5.21 that the skid resistance of truck tire is more sensitive to inflation pressure at lighter wheel loads than heavier wheel loads.

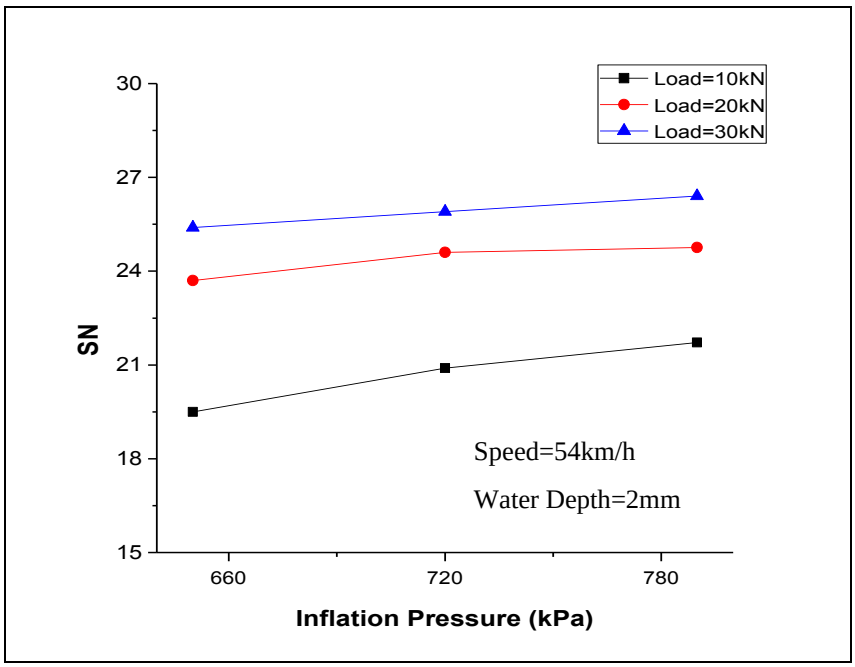

Figure 5.21 Variation of Skid Resistance with Increasing Inflation Pressures at Different Wheel Loads

As shown in Figure 5.22, the skid resistance nearly remains the same at speeds less than 36km/h when increasing the inflation pressure. When the speed is higher than 54km/h, the beneficial effect of inflation pressure will become obvious. The reason may be that at higher speed the larger inflation pressure will have an obvious influence on preventing the tread upward under large hydrodynamic force. That will lead to smaller water penetration into the tire footprint area and hence a higher skid resistance value.

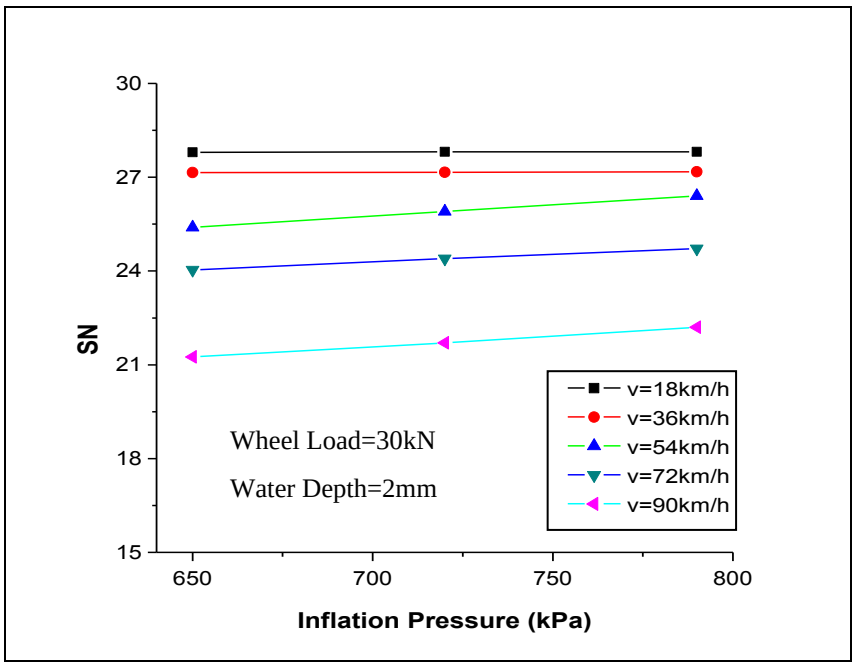

Figure 5.22 Variation of Skid Resistance with Increasing Inflation Pressures at Different Sliding Speeds

5.6.8 Effects of Vehicle Speed on Skid Resistance

As shown in Figures 5.10, 5.13, 5.16, 5.18, 5.20 and 5.22 of former sections, the skid resistance decreases with increasing truck speed when keeping all other parameters constant. The possible reason comes from the fact that while the horizontal traction force decreases with the sliding wheel speed, the fluid drag force actually increases as

the speed of fluid flow rises. However, the magnitude of the increase of the drag force with speed is rather small compared with the corresponding loss of traction force at any given speed. The increase in drag force is insufficient to compensate for the loss of traction force. As a result, there is a net loss in the total horizontal resistance force F_x as the locked-wheel sliding speed increases. It can be seen that the curves initiated from the static coefficients of friction and ended at the hydroplaning speeds. The value of SN_0 is determined by the surface characteristics of tire and pavement while the residual skid resistance at hydroplaning is contributed mainly by the fluid drag force.

5.6.9 Discussion and Comments

The skid resistance trends which are obtained from parametric analysis using the simulation model in the preceding sections are in good agreement with the experimental data obtained by previous researchers (Erwin et al., 1976; Dijks, 1976; Ervin, 1977; Thurman and Leasure, 1977 and Fancher, 1981). The effect of tread depth on skid resistance of truck tires is similar to the situation for car tires, but the drop in skid resistance is more gradual. In most cases there is no definite tread depth below which the drop in skid resistance is very pronounced.

From the previous discussion, it has been found that the tread depth, groove width, groove position, numbers of grooves, tire inflation pressure, wheel load, water-film thickness are all found to have some effect on skid resistance especially for higher velocities. The wheel load and sliding velocity are the two most significant factors for skid resistance. The simulation results indicate that at very low sliding speeds less than about 30 km/h, the longitudinal skid resistance is not much affected by tread groove width, groove position, number of grooves, tire inflation pressure and

water-film thickness, although it is sensitive to wheel load and tread depth. This may be explained by the reason that at low sliding speeds, there would be sufficient time for the water between the tire and pavement surface to escape, and then permit the tire-pavement contact to remain unaffected. Whereas at higher sliding speeds, skid resistance becomes sensitive to the all the investigated factors because some water would be trapped between the tire and pavement surface without enough time to escape or expel. When only one factor is allowed to vary and all other conditions remain constant, the analysis indicates that skid resistance varies positively with tread depth, groove width, tire inflation pressure and wheel load, but negatively with water-film thickness and truck sliding speed. It indicated that there may be an optimal groove number and position in groove configurations.

The observation that empty trucks are more prone to skidding accidents than fully loaded trucks was also verified in this simulation (Chira-Chivala, 1986; Ivey et aI., 1986). As shown in Figures 5.17 and 5.18, the differences in SN for full and lightly loaded truck tires are rather significant. For instance, at a sliding speed of 72 km/h, the skid number of trucks with 10kN load would be only 25 percent of that of trucks with 30kN load. The difference in SN is up to 17 at a water-film thickness of 2 mm, and even larger when the water-film thickness exceeds the tread depth. What is more, the lightly loaded trucks (10kN) will suffer hydroplaning at a common highway operation velocity of less than 70km/h. So for lightly loaded trucks it must be assured to keep lower speed on wet pavement to reduce the risk of accidents.

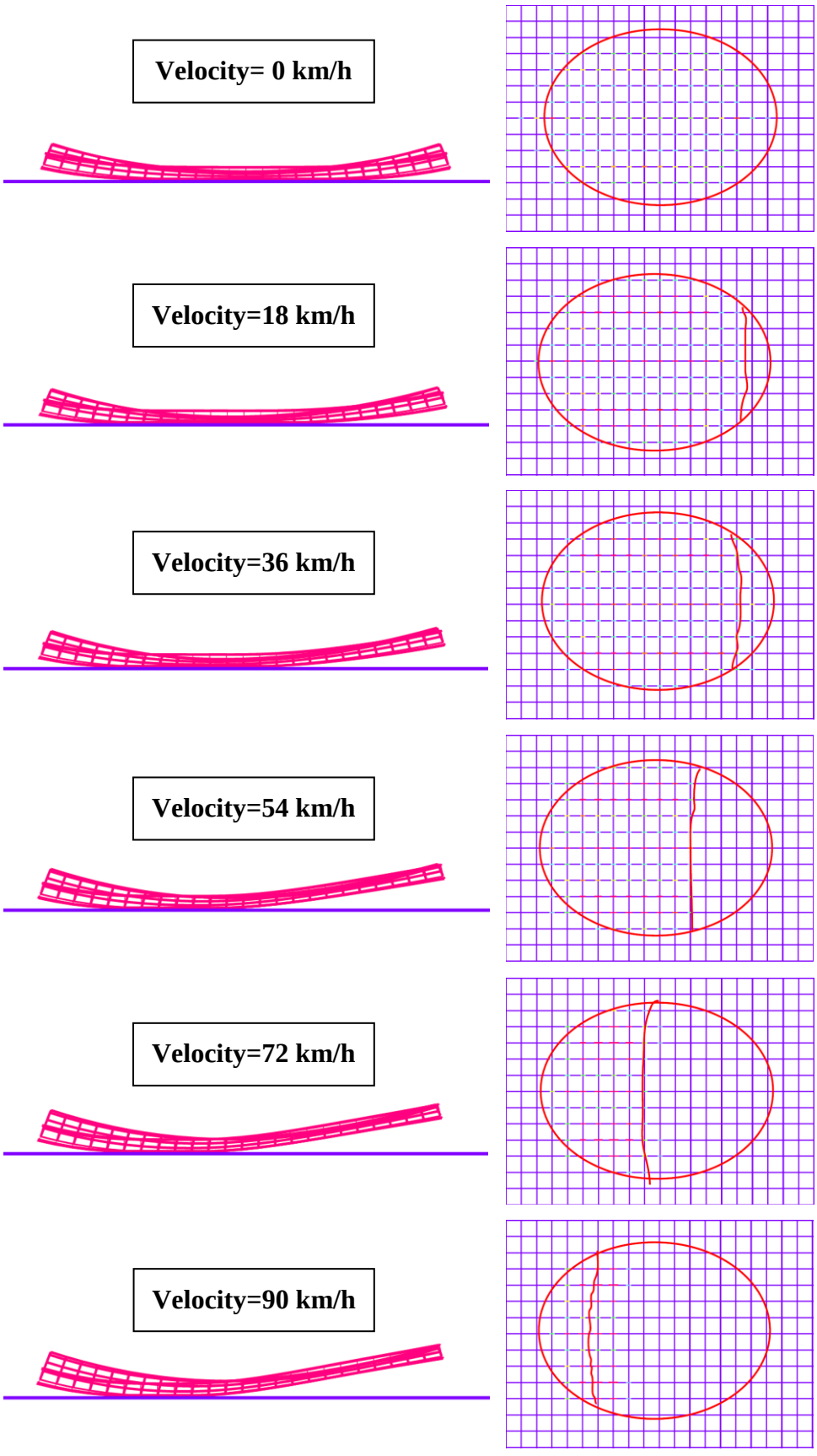

Figure 5.23 Variation of Tire Profile with Increasing Speed

5.7 Variation of contact areas between tire and pavement

The reduction of skid resistance is mainly due to the decreasing of contact force and the lubrication of water-film. The contact force between tire and pavement decreases with the reduction of contact area and increasing sliding speed. This reduction is basically derived from the development of fluid uplift force arising from the relative movement between water and tire tread. As the sliding speed increases, higher water flow speed causes a larger uplift force and leads to a larger upward deformation of tire tread, thereby reducing the contact area (i.e. tire footprint) at the tire-pavement interface. With the reduced contact area, both the vertical normal force and the horizontal traction force between tire and pavement interface are reduced.

In such a process, the tire contact patch can be divided into two zones: contact zone and the water-film zone. The friction contribution to skid resistance can be correlated with the actual contact area between tire and pavement. The reduction of contact force leads to the decreasing of contact area and then the horizontal traction force will also reduce in accordance with the Coulomb friction law.

Figure 5.23 shows the reduction process of the tire-pavement contact patch as the sliding speed increases from static to 90km/h. It indicates that as the sliding speed increases, the tire-pavement contact patch gradually retreats to the rear of truck tire. This variation can also be viewed from the variation of vertical displacements of tire contact patch with increasing velocity, as shown in Figure 5.23.

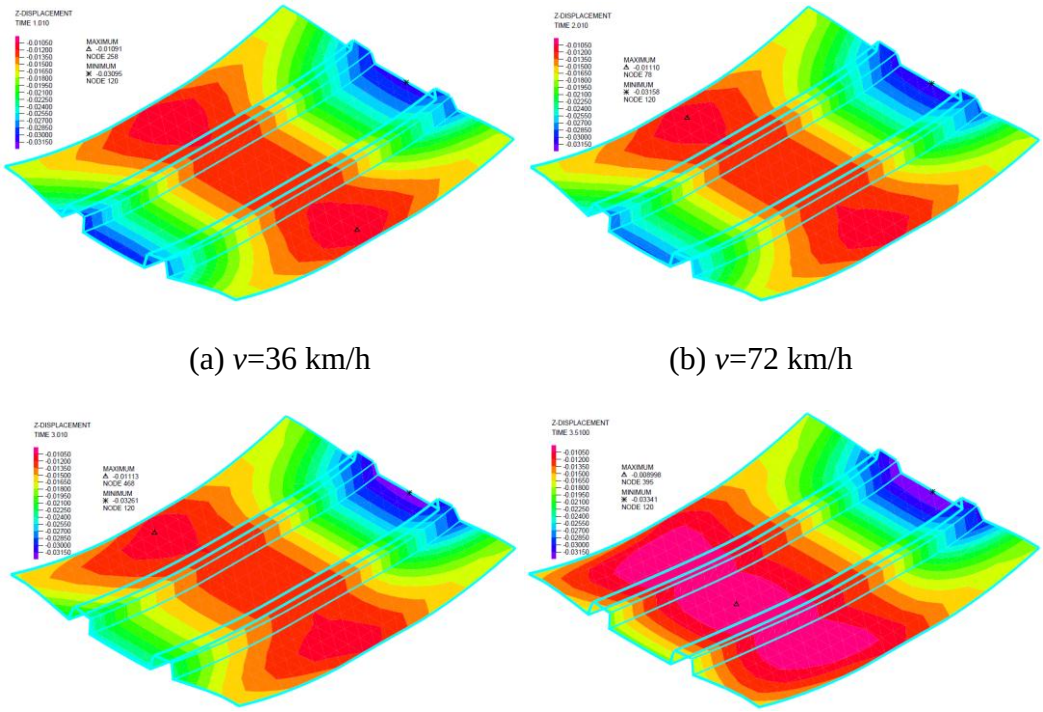

(a) *v*=36 km/h (b) *v*=72 km/h

(c) *v*=108 km/h (d) *v*=126 km/h

Figure 5.24 Vertical Displacements Distribution of Tread Contact Patch

It can be seen from Figure 5.24 that the vertical displacements are changed with the velocity. The initial displacements are mainly due to the initial contact between the tread and pavement surface, which makes the tread surface upward. Then as the velocity increases, vertical displacements of front part of the tread contact patch increases. An upward boot shape distribution of displacements is formed when hydroplaning occurs.

Figure 5.25 and Figure 5.26 show the contours of fluid pressure field and fluid velocity field in the water sub-model. It is obvious that the pressure of the front part of the water-film will dramatically increase when the relative velocity between water and tire increases. When the increasing pressure force applied on the tread surface exceeds the inflation pressure force acted on it, the tread will become upward and lead

to the separation of tire tread and pavement surface and then the reduction of contact area.

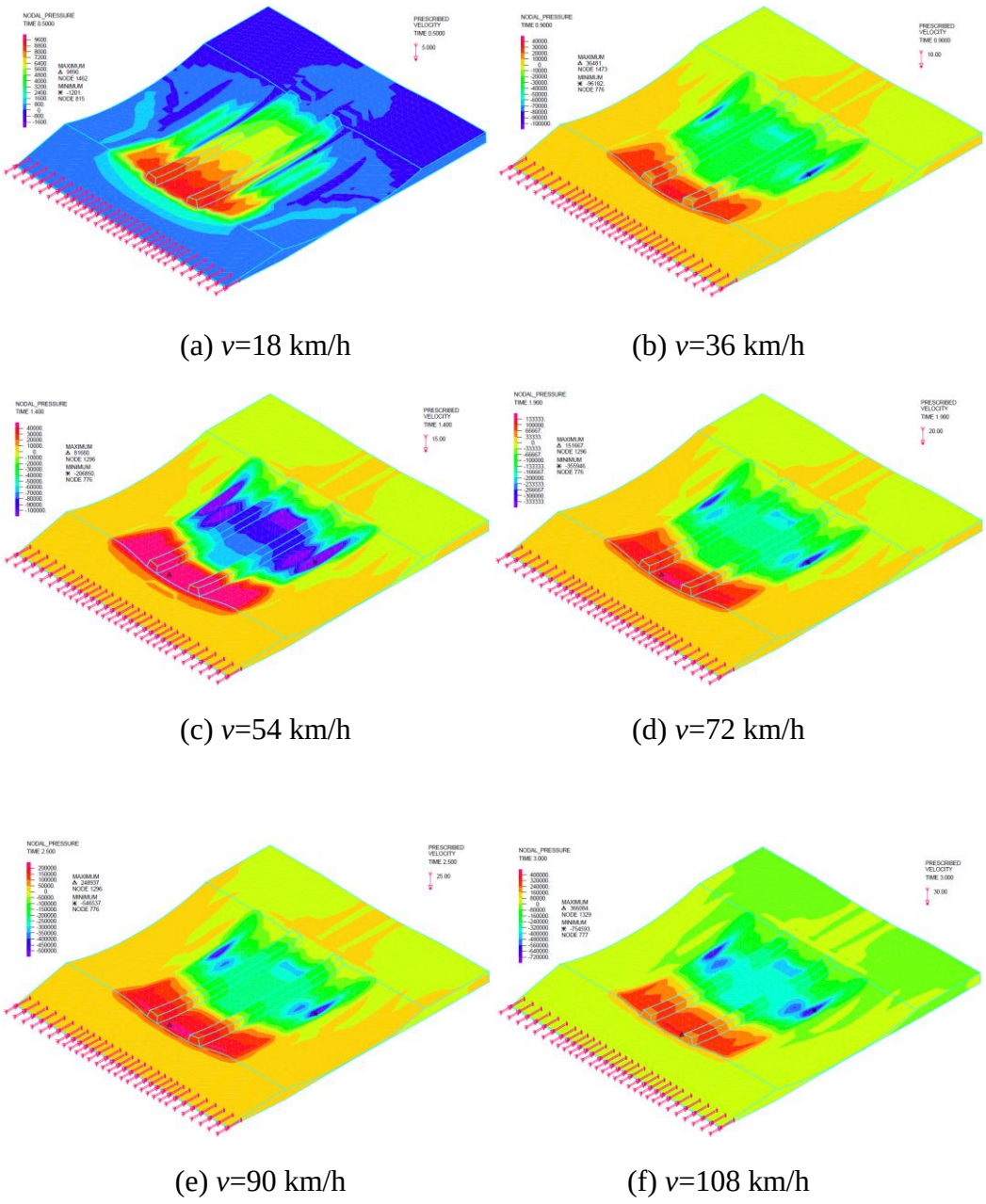

(a) v=18 km/h (b) v=36 km/h

(c) v=54 km/h (d) v=72 km/h

(e) v=90 km/h (f) v=108 km/h

Figure 5.25 Contour of Pressure Distribution at Different Velocities for Truck Tire

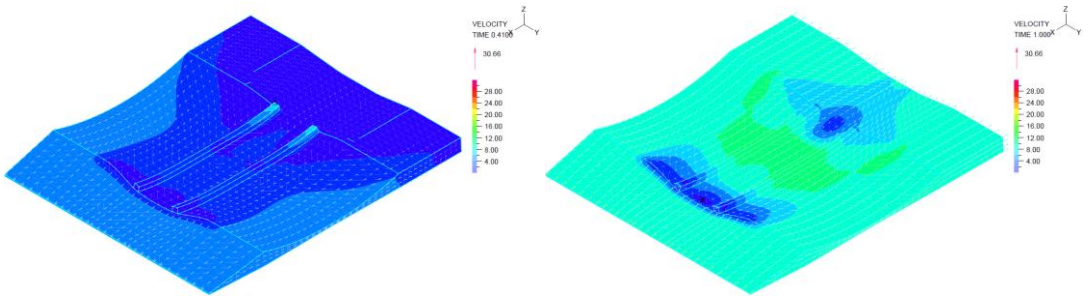

(a) *v*=18 km/h (b) *v*=36 km/h

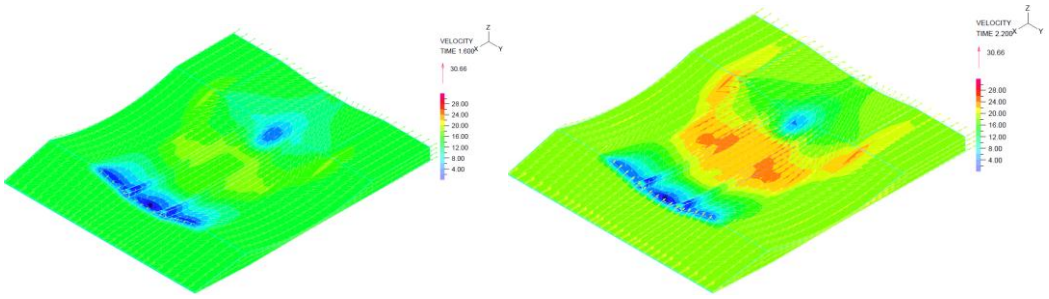

(c) *v*=54 km/h (d) *v*=72 km/h

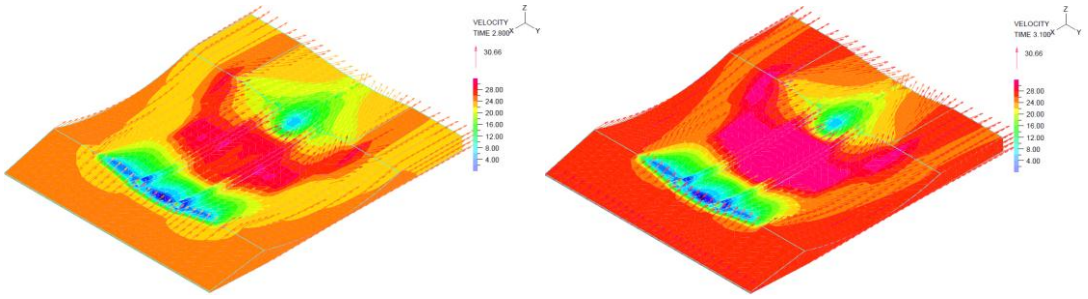

(e) *v*=90 km/h (f) *v*=108 km/h

Figure 5.26 Contour of Velocity Field at Different Velocities for Truck Tire

5.8 Summary and Conclusion

In this chapter, the proposed FSI numerical model was extended to simulate and investigate the skid resistance of rib truck tire sliding on wet pavements. The methodology used for establishing the model is the same as that employed in the previous Chapter 4 to investigate the minimum hydroplaning speed. The numerical

model was verified against experimental data measured by previous researchers. Good agreement has been found between the predicted values and the measured results. It has demonstrated that the proposed FSI simulation model is able to predict longitudinal skid resistance values at different operation conditions.

The effects of different factors that affect the skid resistance performance of trucks have been investigated in detail, such as tread depth, groove width, position of tread grooves, numbers of tread grooves, wheel load amplitude, tire inflation pressure, water-film thickness, and sliding speed. It is found that all the above factors have some effects to some extent, more or less, on the skid resistance (better or worse) experienced by truck. The skid resistance is found to increase with tread depth, groove width, tire inflation pressure and wheel load, but decrease with the sliding speed and water-film thickness. It also indicated that some optimal configuration for groove numbers and positions exist in practice. The analysis shows that vehicle speed and wheel load are the two most important factors affecting the skid resistance of truck tires, followed by water-film thickness, wheel load and tire inflation pressure.

The variation of contact areas between tire and pavement are vividly given by the simulation in this chapter. Contours of pressure and velocity fields are also given to show a clear insight for the phenomenon of FSI which is difficult to obtain from measurements in field. It should be beneficial to understand the deterioration mechanism of pavement skid resistance. The different characteristics of skid resistance between heavy and light trucks are also verified by the simulation model. The results can provide an engineering explanation to the higher skid accident propensity of empty trucks.

CHAPTER 6 CONCLUSION AND OUTLOOK

6.1 Research Overview

The main objective of this research is to simulate the skid resistance and hydroplaning phenomenon of rib truck tires and explore the effect of different affecting factors on them. The scope of the thesis consists of the following parts: to develop a FSI numerical model suitable for hydroplaning and skid resistance of rib truck tires; to evaluate the hydroplaning performance of wide-base truck tires under different operation conditions; and to simulate and predict skid resistance of rib truck tires under different operation conditions. The findings and conclusions from this research are summarized in this chapter. The recommendation and outlook for future research are also given in the last part of the chapter.

6.2 Summary of Present Research

6.2.1 Hydroplaning analysis of wide-base truck tire

In Chapter 3 an effective three dimensional FSI numerical model, considering the interactions among tire, water and pavement, was developed to analyze the hydroplaning phenomenon of wide-base truck tires. The verification of the FSI model in subsequent chapters using experimental data indicated that the proposed models can be used to simulate truck hydroplaning phenomenon and to predict truck hydroplaning speeds satisfactorily. Several cases were simulated and discussed, which involved different wheel loads, tire inflation pressures and water film thickness on

pavement surface. The major contents and findings are summarized in the following sections.

Wheel load

The range of wheel load studied in this simulation is from 11.1kN to 44.5kN at tire inflation pressure of 690 kPa which is the load range commonly wed by trucks with wide-base tires. The results showed that an increase in wheel load from 11.1kN to 44.5kN would cause an increment of approximately 25km/h for hydroplaning speed when the tire inflation pressure was constant. This can explain the observation that the empty truck tire is easier to hydroplaning than full loaded trucks.

Tire inflation pressure

The effect of tire inflation pressure, ranging from 550kPa (80psi) to 830kPa (120psi), on wide-base tire's hydroplaning is investigated. The results demonstrated that the predicted hydroplaning speed increases as the increasing tire pressure when keeping the load constant. It is found that an increase in tire inflation pressure from about 1.5 time of initial inflation pressure would cause an increase in hydroplaning speed by about 15 km/h under the same load condition. However, it is found that hydroplaning of wide-base truck tire is less sensitive to the tire inflation pressures than the traditional truck tires as previous investigation by Ong and Fwa (2008) using a smooth truck tire.

Water film thickness

Water-depths ranging from 2 mm to 19 mm are employed as inlet water depth in the simulation to study the effect of water-depth on hydroplaning speed. The tire inflation pressure is kept at 690kPa (100psi) and the wheel load increases from 11.1kN to

44.5kN. The results indicated that for wide-base truck tire the hydroplaning speed reduces with increasing water depth. When the load is larger, the rate of decrease is higher. However, even with the larger drop in hydroplaning speed at larger load, the minimum hydroplaning speed still remains above 120km/h. Thus it indicates that when it is fully loaded, the truck equipped with wide-base tires will usually not suffer hydroplaning at normal traffic speed of highway. The simulation revealed that a single wide-base tire 425/65R22.5 has better hydroplaning performance than the conventional dual truck tires 11/R22.5.

6.2.2 Skid Resistance Analysis of Rib Truck Tire

Skid resistance of rib truck tire was simulated in this research. The extended FSI simulation model involving friction contact was employed for this purpose. The proposed model was verified against the measurements of skid resistance from rib truck tires. The simulation results were analyzed to evaluate the performance of skid resistance of rib truck tire. The effects of tread depth, tire groove width, position and number of tire grooves, water depth, inflation pressure, wheel load and sliding speed on skid resistance were then studied. It has given a better insight than experiments which cannot supply information of detailed velocity and hydrodynamic pressure distribution to researchers. The findings are summarized as follows:

Tread depth

The characteristics in skid resistance of rib truck tire (SP321) were studied for tire tread depths from 0 to 13.6 mm. The simulation results indicated that the skid resistance values decrease with reducing tire tread depth at all speeds, especially at higher speeds. It demonstrates that the influence of tread depth for truck tires is similar to the situation for car tires, but the decreasing rate is more gradual. It is noted

that when the tread depth is less than 2 mm, there is a relatively larger drop of skid number in the SN-tread depth curves compared with other segments in these curves. However, there was no definite tread depth value at which the sharp drop would be found. It can be conclude that with a deeper tire tread depth which can offer a more effective channel for water flow, skid resistance values remain lager than those with lower tread depths due to a lower development rate of hydrodynamic uplift force. It is observed that the skid number decreases little when the travelling velocity is less than 15m/s (54km/h), while the skid number of bold tire is only about half of truck tires with full tread depth when the wheel speed is at 30m/s (108km/h). Therefore, for truck traveling on wet pavements, even if the tire is new, it is still necessary for drivers to keep a lower speed less than 60km/h for safety.

Groove Width

Truck tires with tread groove widths 5.0mm, 10mm, 18mm, 25mm, and 35mm are respectively investigated. The results showed that increasing of tread width had a positive effect on skid resistance values although the positive effect was not significant in the investigated ranges. When the sliding speed was higher than 72km/h, the positive benefit becomes obvious. The margin is about 2 at 90km/h when groove width changes from 5mm to 35mm. However, at lower speed, for example less than 54km/h, nearly no difference can be found when increasing the width of tread groove. It can be concluded that it is not necessary for manufacturers to produce truck tires with large width grooves. However, it should be noted that the simulation results also indicated that hydroplaning speed of truck tires with widths of 25mm and 35mm has a higher margin value up to 10-15 km/h than those with 5mm tread groove width.

In addition, it can be inferred that when traveling on muddy road, the wider grooves will be much better than narrower grooves for mud escaping.

Groove Position

Simulation results indicated that the groove position of the grooves has no much effect on the skid number of truck tires under the adopted conditions: groove depths and widths are all 10mm, water depth is 2mm and the inflation pressure and wheel load are kept 720kPa (105psi) and 29.4kN, respectively. When the sliding speed is less than 36km/h, there is no effect observed for the investigated cases. While at higher speed such as larger than 72km/h, SN will become slightly higher when the grooves are located between 45mm-65mm in the tread surface. The reason may be that when grooves are located near the center part of tread surface, there will be a longer pathway for water expelling and when grooves are located near the edge of tire tread, it will be hard to explore the contribution of the grooves in expelling the water at contact patch. However, the results may be significantly different when introducing transverse tread grooves because transverse grooves can effectively reduce the length of path for water expelling when the longitudinal grooves are arranged at the shoulder region of the tread.

Numbers of Tread Grooves

The benefit of having more grooves in rib tire was demonstrated by considering 0, 2, 4 and 6 grooves. It was found that adding grooves to a smooth tire has the beneficial effect on increasing skid resistance and reducing hydroplaning risk. However, it is noted that the number of ribs has no much effect when the sliding velocity is less than 54km/h. The results indicated that the configuration with four grooves has a slightly better performance in skid resistance when the sliding velocity exceeds 72km/h. The

skid resistances of 2-groove configuration and 6-groove configuration nearly have the same values.

Wheel Load

It is found that the skid resistance of truck tires traveling on wet pavement generally increases with the wheel load when keeping all other parameters constant. However, the rate of changing with wheel load is not the same for different velocities and the skid numbers decrease at an increasing rate with the sliding velocity when the truck wheel load decreases. It is found that wheel load would have a much larger effect on skid number when increasing sliding speed. At a lower speed of 18 km/h, SN is not affected much by changes in wheel load. At a higher sliding speed more than 50km/h, there are significant decreases in skid resistance when the wheel load is small. It can be concluded that the positive effect resulted from increasing wheel load becomes more significant at higher sliding speeds. It also showed that when the load is less than 10kN, trucks will encounter hydroplaning at the common highway operation speeds from 60 km/h to 80 km/h when travelling on wet pavements, which agrees very well with the observations from traffic monitoring by past investigators.

Water Depth

The skid resistance characteristics with respect to surface water film thickness were studied for a wide range of 2 mm to 15 mm water depths such that it covers a range of rainfall and flooded conditions. Numerical simulation has demonstrated that skid resistance generally decreases with the increasing water-film thickness when keeping all other parameters constant. When the speed is high, for example exceeding 90km/h, a larger drop can be found when increasing the water-film thickness. It is noted that when the water-film thickness exceeds the tread depth of the truck tire a relatively

larger drop in SN values can be observed. The reason could be that thicker water-film reduces the water-expel function of tread grooves and results in a higher hydrodynamic force and a larger penetration of water wedge into the contact area between tire tread and pavement surface, which ultimately leads to a larger reduction in the tire footprint area and a heavier loss in skid resistance.

Tire Inflation Pressure

The variation of skid resistance with the inflation pressure at different loads and sliding velocities indicated that the skid resistance of truck tire increases as tire inflation pressure increases. It is found that the skid resistance of truck tire is more sensitive to inflation pressure at lighter wheel loads than heavier wheel loads. The skid resistance nearly remains the same at speeds less than 36km/h when increasing the inflation pressure. When the speed is higher than 54km/h, the beneficial effect of inflation pressure will become obvious. The reason may be that at higher speed the larger inflation pressure will have an obvious influence on preventing the tread upward under large hydrodynamic force. That will lead to less water penetration into the tire footprint area and hence a higher skid resistance value.

Sliding Speed

In all the investigated cases, the skid resistance decreases with increasing truck speed when keeping all other parameters constant in each case. It demonstrated that sliding velocity is a more important factor than any other factors except the wheel load. It can be explained by the fact that while the horizontal traction force decreases with the sliding wheel speed, the fluid drag force actually increases as the speed of fluid flow rises. However, the magnitude of the increase of the drag force with speed is rather small compared with the corresponding loss of traction force at any given speed. The

increase in drag force is insufficient to compensate for the loss of traction force. As a result, there is a net loss in the total horizontal resistance force as the locked-wheel sliding speed increases.

6.3 Recommendations for Future Research

This study has investigated the hydroplaning performance of wide-base truck tires and the skid resistance of common rib truck tires on flooded smooth pavement. It will be interesting and worthwhile to explore the skid resistance of wide-base truck tire when validation data are available in the future.

In this thesis, only the sliding condition was considered. However, the rolling wet skid resistance may be more useful for pavement engineers and vehicle operators. Thus it is motivated to study the skid resistance behavior of tires using rolling tire model. The modeling of hydroplaning and skid resistance under different slip and yaw conditions will give a better insight to researchers.

In addition, this study has only considered rib tire with smooth pavement surface for the skid resistance and hydroplaning phenomenon. The effect of transverse grooves and the combination effect of transverse and longitudinal grooves on skid resistance should be given attention, especially in discussing the groove position and groove numbers. Tread patterns of truck tire which has been demonstrated to have effect on hydroplaning on un-flooded pavements should be studied in the future.

The combined effect of tire tread pattern with pavement grooving should also be studied in further research. The hysteresis mechanism, related to the surface microstructures of pavement, can be involved through considering the elastic-plastic properties of rubber and texture profile of pavement surface. Last but not least, the

macrotextures of the pavement surface should be involved to investigate the interlock mechanism between the tread block and pavement surface texture.

REFERENCES

1. AASHTO, (2004). Optimizing the System. American Association of State Highway and Transportation Officials, Washington, D.C., Publication No.: OTS-1.
2. ADINA R&D Inc. (2009). ADINA Theory and Modeling Guide, Watertown, Massachusetts, USA.
3. Al-Qadi, I. L., Elseifi, M. A. and Yoo, P.J. (2004). Pavement Damage due to Different Tires and Vehicle Configurations, Virginia Tech Transportation Institute, VA240602004.
4. Al-Qadi, I. L., Elseifi, M. A. Yoo,, P. J. and Janajreh, I. (2005). Pavement Damage due to Conventional and New Generation of Wide-Base Super Single Tires, Journal of Tire Science and Technology, Vol. 33, No. 4, , pp. 210-226.
5. Allbert, B.J. and Walker, J.C. (1965). Tire to wet road friction. Institute of Mechanical Engineering Proceedings, Vol. 180(2A), No.4.
6. ASTM. (2005a) Standard E 274-97, Standard Test Method for Measuring Surface Frictional Properties Using the British Pendulum Tester, , ASTM Standard Sources, CD-ROM, Philadelphia,.
7. ASTM. (2005b). ASTM Standard: E 965-96. Standard Test Method for Measuring Pavement Macrotexture Depth Using a Volumetric Technique. ASTM Standards Sources, CD-ROM, Philadelphia.
8. ASTM. (2005c). ASTM Standard: E 1859-97. Standard Test Method for Friction Coefficient Measurements between Tire and Pavement using a Variable Slip Technique. ASTM Standards Sources, CD-ROM, Philadelphia.

9. ASTM. (2005 d). ASTM Standard E 2380-05. Standard Test Method for Measuring Pavement Texture Drainage Using an Outflow Meter. ASTM Standards Sources, CD-ROM, Philadelphia.
10. ASTM. (2006). Standard Specification for Standard Smooth Tire for Pavement Skid-Resistance Tests, Philadelphia, E524-88.
11. Balmer G.G. and Gallaway B.M. (1983). Pavement Design and Controls for Minimizing Automotive Hydroplaning and Increasing Traction. Frictional Interaction of Tire and Pavement, ASTM STP 793, 167-190.
12. Bareket, Z. and Fancher, P. (1989). Representation of truck tire properties in braking and handling studies: the influence of pavement and tire conditions on frictional characteristics, UMTRI-89-33.
13. Bathe K.J. and Zhang H. (2002). A Flow-Condition-Based Interpolation Finite Element Procedure for Incompressible Fluid Flows. Computers and Structures, Vol.80, pp. 1267-77.
14. Bathe K.J. and Zhang H. (2004). Finite Element Developments for General Fluid Flows with Structural Interactions. International Journal of Numerical Meth Eng, Vol.60, pp. 21-32.
15. Bergman, W., Clemett, H.R. and Sheth, N.J. (1971). Tire Traction Measurement on the Road and in the Laboratory, SAE Paper No. 710630.
16. Bergman, W. (1976). Skid Resistance Properties of Tires and Their Influence On Vehicle Control, Transportation Research Record, No. 621, TRB, National Research Council, Washington D.C. pp. 8-18.

17. Boer, A., Zuijlen, A.H. and Bijl, H. (2006). Review of coupling methods for non-matching meshes, Computer Methods in Applied Mechanics and Engineering, 196, pp. 1515-1525.
18. Browne, A.L (1971). Dynamic Hydroplaning of Pneumatic Tires. PhD Thesis, North Western University, USA.
19. Carla, A., Gallati, A.U., Mario, Sibilla, A.U. Stefano, (2007). Numerical simulation of fluid-structure interaction by SPH, Computers and Structures, pp. 11-14, doi: DOI: 10.1016/j.compstruc.2007.01.002.
20. Chemical Rubber Company (2003). Handbook of Chemistry and Physics, 83th Edition, CRC Press, Cleveland, Ohio.
21. Chira-Chivala, T. (1986). Problems of Combination Trucks on Wet Pavements: An Accidental Analysis. Transportation Research Record: Journal of the Transportation Research Board, 1068, TRB, National Research Council, Washington D. C., pp. 70-75.
22. Close, W. (1961). Locked Wheel Friction Tests on Wet Pavements, Highway Research Board Bulletin No. 302, Skid Testing, pp18.
23. Comfort, G., (2001), Wet Runway Friction: Literature and Information Review, Fleet Technology Ltd. report TP14002E submitted to the Aerodrome Safety Branch of Transport Canada.
24. COST 334 (2001). Effects of wide single tires and dual tires. Final Report of the Action (Version 29), European Cooperation in the field of Scientific and Technical Research.
25. Dahir, S.H.M., and Gramling, W.L. 1990. Wet pavement safety programs. NCHRP NCHRP National Cooperative Highway Research Program Synthesis of Highway

Practice 158. Transportation Research Board, National Research Council, Washington, D.C.

26. Daughaday, H. and Tung, C. (1969). A mathematical analysis of hydroplaning phenomena, C. A. Lab. Tech. Report No. AG-2495-S-1.
27. David H. and Timm, (2006). Mechanistic Comparison of Wide-Base Single versus Standard Dual Tire Configurations, TRB Annual Meeting CD-ROM.
28. Dijks A. (1974a). A multi-factor examination of wet skid resistance of car tires. SAE International Automobile Tire Conference, Toronto, SAE - 741106.
29. Dijks A. (1974b). Wet skid resistance of car and truck tires. Tire Science and Technology, TSTCA, Vol. 2, 2.
30. Dijks, A. (1976). Influence of Tread Depth on Wet Skid Resistance of Tires. In Transportation Research Record: Journal of the Transportation Research Board, No. 621, TRB, National Research Council, Washington D.C., pp. 136-147.
31. Elseifi, M. A., Al-Qadi, I. L., Yoo, P. J. and Janajreh, I. (2005). Quantification of Pavement Damage Due to Dual and Wide-Base Tires, Journal of the Transportation Research Record, No.1940, Transportation Research Board of the National Academies, Washington, DC, pp. 125-135.
32. Ervin, R. D. and MacAdam, C. C. (1976). Noise and Traction Characteristics of Bias-Ply Truck Tires-Wet Traction Findings, Vol. 2.
33. Ervin, R., et al. (1985). Impact of Specific Geometric Features on Truck Operations and Safety at Interchanges. Final Report, FHWA Contract No. DTFH61-82-C-00054, Rept. No. UMTRI-85-33, Transportation Research Institute, the University of Michigan, USA.

34. Eshel, A.A (1967). Study of Tires on a Wet Runway, Report No. RR67-24, Annex Corporation, Redwood City, California.

35. Fancher, P.S. and Segel, L. (1973). Tire Traction Assessed by Shear Force and Vehicle Performance, Tire Science and Technology, Vol.1, No. 4.

36. Flintsch, G.W., de Leon, E., McGhee, K.K., and Al-Qadi, I.L. (2003). Pavement Surface Macrotexture Measurement and Application. Presented at the TRB 82nd Annual Meeting. Washington, D.C., January 12-16.

37. Fwa, T.F., Kumar, S., Ong, G.P., Huang, C. (2008). Analytical Modeling of Effects of Rib Tires on Hydroplaning. Transportation Research Record: Journal of the Transportation Research Board, No. 2068.

38. Fwa, T.F. and Ong G.P (2006). Transverse Pavement Grooving against Hydroplaning, II-Design. ASCE Journal of Transportation Engineering, Vol. 132, No6, pp 449-457.

39. Fwa, T.F., Kumar, S., Kumar A., Ong, G.P. (2008). Effectiveness of Tire Tread Patterns in Reducing Vehicle Hydroplaning Risk. No. 09-1725, TRB 2009 Annual Meeting CD-ROM, TRB, National Research Council, Washington D.C.

40. Fwa, T.F., and Ong, G.P. (2008). Wet-pavement hydroplaning risk and skid resistance: Analysis. J. Transp. Eng., 134-5, 182–190.

41. Gallaway, B. M., et al. (1979). Pavement and Geometric Design Criteria for Minimizing Hydroplaning. Federal Highway Administration Report No. FHWA-RD-79-31, Texas Transportation Institute, Texas A&M University, USA.

42. Gandhi, P.M., Colucci, B., and Gandhi, S.P. (1991). Polishing of Aggregates and Wet-Weather Accident Rates for Flexible Pavements. Transportation Research Record 1300, Transportation Research Board, National Research Council, Washington, D.C., 71-79.

43. Gargett, T. (1990). The Introduction of a Skidding-Resistance Policy in Great Britain, Surface Characteristics of Roadways: International Research Technologies, ASTM STP 1031, ASTM, Philadelphia, Pennsylvania, pp. 30-38.
44. Gengenback, W. (1968). Experimental Investigation of Tires on Wet Tracks) ,Automobiltechnische Zeitschrift, Vol. 70, pp. 310-316.
45. Giles, C.G. and Lander, F. (1978). The Skid- Resisting Properties of Wet Surfaces at High Speeds: Exploratory measurements with a Small Breaking Force Trailer, Journal of the Royal Aeronautical Society, Vol. 60, 1956, pp.83-94.
46. Gough, V.E. (1959). Discussion of Paper by D. Tabor. Revue Generale Du Caoutchouc, Vol. 36, No. 10, pp.1409.
47. Grime, G. and Giles, C.G. (1976). The Skid- Resisting Properties of Roads and Tires, Proceedin s of t h e Automobile Division, Institute of Mechanical Engineers, 1954-55, No.1, p. 19.
48. Groger, H. and Weis, M. (1996). Calculation of the Three-Dimensional Free Surface Flow Around an Automobile Tire. Tire Science and Technology, Vol. 24, pp. 39-49.
49. Grosch, K.A. and Yaycock, G. (1968). Influence of Test Conditions on Wet Skid Resistance of Tire Tread Compounds, Rubber Chemistry and Technology, Vol. 41, No. 2, pp. 477-493.
50. Haberman, R. (2004). Applied partial differential equations with Fourier series and boundary value problems, Pearson Prentice Hall, New Jersey, fourth Ed.
51. Hankins, K.D., Morgan, R.B., Ashkar, B., and Tutt, P.R. (1971). Influence of vehicle and pavement factors on wet pavement accidents. Highway Research Record,No. 376.

52. Henry, J. J. (1986). Tire Wet-Pavement Traction Measurement: A State-of-the-Art Review. In The Tire Pavement Interface, ASTM STP 929, eds. by M.G. Pottinger and T.J. Yager, Philadelphia: ASTM, pp 3-25.

53. Henry J. J. (2000). Evaluation of Pavement Friction Characteristics, A Synthesis of Highway Practice. NCHRP Synthesis 291.

54. Holmes, K.E., (1970). Braking Force/Braking Slip Measurements Over a Range of Conditions between 0 and 100 Percent Slip, Road Research Laboratory Report LR 292.

55. Horne, W.B and Leland, T.J. (1962). Influence of Tire tread Pattern and Runway Surface Condition on Braking Friction and Rolling Resistance of a Modern Aircraft, NASA TN D-1376.

56. Horne, W.B. and Dreher, R.C. (1963). Phenomena of Pneumatic Tire Hydroplaning. NASA TN D-2056, National Aeronautics and Space Administration, Washington D.C.

57. Horne, W.B. and Joyner, U.T. (1965). Pneumatic Tire Hydroplaning and Some Effect on Vehicle Performance, SAE International Automotive Engineering Congress, Michigan.

58. Horne, W., Yager, T. and Taylor, G. (1968). Review of Causes and Alleviation of Low Tire Traction on Wet Runways, NASA Technical Note TN D-4406.

59. Horne, W., (1974). Elements Affecting Runway Traction, presented at the SAE Transport Committee Meeting, Dallas.

60. Horne, W.B. (1984). Predicting the Minimum Dynamic Hydroplaning Speed for Aircraft, Bus, Truck and Automobile Tires Rolling on Flooded Pavements. ASTM E-17 Committee Meeting, College Station, TX, June4-6.

61. Horne, W.B. (1975). Wet Runways, NASA Technical Memorandum TM X-72650.

62. Horne, W.B., Yager, T.J. and Ivey, D.L. (1986). Recent Studies to Investigate Effects of Tire Footprint Ratio on Dynamic Hydroplaning Speed. The Tire Pavement Interface, ASTM STP 929, ASTM, Philadelphia, pp. 26-46.

63. Hosking, J. R. (1987). Relationship between Skidding Resistance and Accident frequency: Estimates based on seasonal variation. TRRL Report No.RR76, Transport and Road Research Laboratory, UK.

64. Ivey, D.L. (1984). Truck Tire Hydroplaning-Empirical Verification of Home's Thesis. Presentation to the Technical Seminar on Tire Service and Evaluation, ASTh4 Committee F-9, Akron, Ohio, USA.

65. Ivey, D. L., Horne, W.B. and Tonda, R.D. (1986). Strategies for Reducing Truck Accidents on Wet Pavements. Transportation Research Record: Journal of the Transportation Research Board, 1084, TRB, National Research Council, Washington D. C., pp. 1-8.

66. Jayawickrama, P.W., Prasanna, R., and Senadheera, S.P. (1996). Survey of State Practices to Control Skid Resistance on Hot-Mix Asphalt Concrete Pavements. Transportation Research Record 1536, Transportation Research Board, National Research Council, Washington, D.C., 52-58.

67. Kelly, J.D. (1968). Factors Affecting Passenger Tire Traction on the Wet Road, SAE Paper No. 680138.

68. Kennedy, C.K., Young, A.E., and Butler, I.C. (1990). Measurement of Skidding Resistance and Surface Texture and the Use of Results in the United Kingdom. Surface Characteristics of Roadways: International Research and Technologies. ASTM Special Technical Publication 1031. W.E. Meyer and J. Reichert, Eds., American Society of Testing and Materials, Philadelphia, 30-38.

69. Kummer, H.W. and Meyer, W.E. (1966). New Theory Permits Better Frictional Coupling between the Tire and Road. Paper B 11, 11th International FISITA Congress, Munich.

70. Kulakowski, B.T., Harwood, D., Hiltunen, D., Mason, J., Meyer, W., Simoneau, S., and Wambold, J. (1990). Skid Resistance Manual, FHWA report FHWA-IP-90-013.

71. Lander, F.T.W. and Williams, T. (1968). The Skidding Resistance of Wet Runway Surfaces With Reference t o Surface Texture and Tire Conditions, Road Research Laboratory Report LR 184.

72. Lamm, R., B. Psarianos and T. Mailaender. (1999). Highway Design and Traffic Engineering Handbook, McGraw-Hill, New York.

73. Leland, T.J.W. and Taylor, G. R. (1965). An Investigation of the Influence of Aircraft Tire Tread Wear on Wet Runway Braking, NASA Technical Note D-2770.

74. Leland, T. J.W., Yager, T. J. and Joyner, U.T. (1968). Effects of Pavement Texture on Wet Runway Braking Performance, NASA Technical Note D-4323.

75. Liu, Y. R., T. F. Fwa and Y. S. Choo. (2003). Finite Element Modeling of Skid Resistance Test, ASCE Journal of Transportation Engineering, Vol. 129, No. 3. pp. 316-321.

76. Ludema, K.C. (1975). Physical factors in tire traction, Physics in Technology Michigan, USA, pp.11-17.

77. Martin, C.S. (1966). Hydroplaning of Tire Hydroplaning Final Report, Project B-608, Georgia Institute of Technology.

78. Maycock, G. (1967). Experiments on Tire Tread Patterns, Road Research Laboratory Report LR 122.

79. Mayer U.M., Gerstenberger A., Wall W.A. (2009). Interface handling for three-dimensional higher-order XFEM computations in fluid–structure interaction. Int J Numer Methods Eng 79: 846– 869.

80. McLean J., and Foley, G. (1998). Road Surface Characteristics and Condition – Effects on Road Users. Research Report No. 314, ARRB Transport Research Ltd, Vermont South Victoria, Australia.

81. Meades, J.K., (1969). The Effect of Tire Construction on Braking Force Coefficient, Road Research Laboratory Report LR 224.

82. Meyer, W.E. (1991). Pavement Surface Texture and Measurement, ASTM Standardization News, pp. 28-31.

83. Moore, D.F. (1966). Prediction of Skid Resistance Gradient and Drainage Characteristics for Pavements, Highway Research Record 131, pp. 181-203.

84. Moore, D.F. (1967). Prediction A Theory of Viscous Hydroplaning, International Journal of Mechanics Science, Vol. 9, pp. 797-810.

85. Mosher, L.G. (1969). Results from Studies of Highway Grooving and Texturing by Several State Highway Departments. Pavement Traction and Grooving Studies, NASA SP-5073, Washington D.C., USA, pp. 465-504.

86. National Highway Traffic Safety Administration (NHTSA), (2009). Traffic Safety Facts: 2008 Traffic Safety Annual Assessment-Highlights, DOT HS 811 172, Washington, DC.

87. Okano, T. and Koishi, M. (2001). A New Computational Procedure to Predict Transient Hydroplaning of a Tire. Tire Science and Technology, Vol. 29, No. 1, pp. 2-22.

88. Oh, C.W., Kim, T.W., Jeong, H.Y., Park, K.S. and Kim, S.N. (2008). Hydroplaning simulation for a straight-grooved tire by using FDM FEM and an asymptotic method, Journal of Mechanical Science and Technology, Volume 22, No. 1.

89. Ong, G.P., Fwa, T.F. and Guo, J. (2005). Modeling Hydroplaning and the Effects of Pavement Micro-Texture. In Transportation Research Record: Journal of the Transportation Research Board, No. 1905, TRB, National Research Council, Washington D.C., pp. 166-176.

90. Ong G.P and Fwa, T.F. (2006). Transverse Pavement Grooving against Hydroplaning, I-Simulation Model. ASCE Journal of Transportation Engineering, Vol. 132, No.6 pp 441-448.

91. Ong, G.P., Fwa, T.F. (2008). Modeling and Analysis of Truck Hydroplaning on Highways. In Transportation Research Record: Journal of the Transportation Research Board, No. 01084478, TRB, National Research Council, Washington D.C.

92. Ong, G.P. and Fwa, T.F. (2010a). Mechanistic Interpretation of Braking Distance Specifications and Pavement Friction Requirements. No.10-3086, TRB 2010 Annual Meeting CD-ROM, TRB, National Research Council, Washington D.C.

93. Ong, G.P. and Fwa, T.F. (2010b). Modeling Skid Resistance of Commercial Trucks on Highways, Journal of Transportation Engineering 136, 510.

94. Okano, T. and Koishi, M. (2001). A New Computational Procedure to Predict Transient Hydroplaning of a Tire. Tire Science and Technology, Vol. 29, No. 1, pp. 2-22.

95. Permanent International Association of Road Congress (PIARC), (1987). Report of the Committee on Surface Characteristics, Proceeding of 18th World Road Congress, Brussels, Belgium.

96. Quarantay, G., Masaratiy, P. and Mantegazzay, P. (2005). A conservative mesh-free approach for fluid-structure interface problems, Int. Conf. on Computational Methods for Coupled Problems in Science and Engineering, M. Papadrakakis, E. Onate and B. Schreer (Eds), CIMNE, Barcelona, 2005.

97. Robert, D.E., and Luis, B. (1990). Hydroplaning With Lightly-Loaded Truck Tires, Final Report, Transportation Research Institute, The University of Michigan, March 1990.

98. Rose, J.G. and Gallaway, B.M. (1977). Water Depth Influence on Pavement Friction, ASCE Journal of Transportation Engineering, Vol. 103, No. 4, pp. 491-506.

99. Sakai, H., Kanaya, O., and Okayama, T. (1978). The Effect of Hydroplaning on the Dynamic Characteristics of Car, Truck, and Bus Tires. SAE Paper No. 780195.

100. Sabey, B.E., (1966). Road Surface Texture and the Change in Skidding Resistance with Speed, Road Research Laboratory Report No.20.

101. Saito, K., and Henry, J.J., 1983, Mechanistic Model for Predicting Seasonal Variations in Skid Resistance, Transportation Research Record 946.

102. Schulze, K.H. and Beckman, L. (1962). Friction Properties of Pavements at Different Speeds, Skid Resistance, ASTM Special Publication, No. 326, 1962.

103. Seta, E. et al., (2000). Hydroplaning Analysis by FEM and FVM: Effect of Tire Rolling and Tire Pattern on Hydroplaning. Tire Science and Technology, Vol. 28, No. 3, pp. 140-156.

104. Sinnnamon, J.F. and Tielking, J.K. (1974). Hydroplaning and tread pattern hydrodynamics, Report No. UM-HSRI-74-10, Highway Safety Research Institute, University of Michigan

105. Sinnamon, J.F. and Tielking, J.T. (1974). Hydroplaning and Tread Pattern Hydrodynamics, UM-HSRI-PF-74-10, Highway Safety Research Institute, The University of Michigan, October.

106. SIMULIA, Coupled Eulerian-Lagrangian analysis with Abaqus/Explicit. SIMULIA, USA, 2008.

107. Staughton, G.C. (1970). The Effect of Tread Pattern Depth on Skidding Resistance, Road Research Laboratory Report LR323.

108. Staughton, G.C. and Williams, T., (1970). Tire Performance in Wet Surface Conditions, Road Research Laboratory Report LR 355.

109. Tanner, J.A. (1996). Computational Methods for Frictional Contact With Applications to the Space Shuttle Orbiter Nose-Gear Tire, NASA Technical Paper 3573, NASA, Langley Research Center, Hampton, Virginia.

110. Tielking, J.T. (1992). Conventional and Wide Base Radial Truck Tires, Heavy Vehicles and Roads: Technology, Safety and Policy. Thomas Telford, London, pp. 182-190.

111. Tielking J.T. and Pezoldt V.J. (1992). Impact of Wide Base Radial Truck Tires on Highway Safety. AAA Foundation for Traffic Safety, Washington, January.

112. The Tire and Rim Association. (1995). 1995 Year Book. Copley, Ohio.

113. Tsakonas, S., Henry, C.J. and Jacobs, W.R. (1968). Hydrodynamics of Aircraft Tire Hydroplaning. NASA CR-1125, National Aeronautics and Space Administration, Washington D. C.

114. Veldman, A.E.P. (2006). Computational fluid dynamics. University of Groningen, Groningen.

115. Wambold, J.C., Henry, J.J. and Yeh, E.C. (1984). Methodology for Analyzing Pavement Condition Data, report FHWA/RD-83/094 prepared by the Pennsylvania Transportation Institute.

116. Williams, T., (1966). The Relation Between Braking Force Coefficient and Slip for an Aircraft Tire Braked on Four Wet Surfaces, Road Research Laboratory Report No. 50.

117. Williams, J.R. (1969). Aquaplaning: the British Ministry of Technology Program, NASA, Washington Pavement Grooving and Traction Studies, pp. 81-99.

118. Williams, T. and Meades, J.K. (1975). Effects of tread pattern depth and tire grooving on lorry tire skidding resistance. Transport and Road Research Laboratory, Report 687.

119. World Health Organization. (2004) Road safety: a public health issue, 29 Mar 2004, http://www.who.int/features/2004/road_safety/en/ (Accessed 1 March 2009).

120. Wolshon, B. (2004). Geometric Design of Streets and Highway. In Handbook of Transportation Engineering, ed. by M. Kutz, pp. 13.1-13.21, McGraw-Hill, New York.

121. Yager, T.J. (1968). Comparative Braking Performance of Various Aircraft on Grooved and Ungrooved Pavements at the Landing Research Runway, NASA Wallops Station. Pavement grooving and traction studies, Langley Research Center, Hampton, Virginia, USA, Nov. 18-19.

122. Yager, T., Phillips, W.P. and Horne, W. (1970). A Comparison of Aircraft and Ground Vehicle Stopping Performance on Dry, Wet, Flooded, Slush-, Snow-, and Ice-Covered Runways, NASA Technical Note TN D-6098.

123. Yeager R.W. and Tuttle. J.L. (1972). Testing and Analysis of Tire Hydroplaning. In SAE National Automobile Engineering Meeting, Detroit, Michigan.

124. Yeager, R.W. (1974). Tire Hydroplaning: Testing, Analysis and Design, in The Physics of Tire Traction: Theory and Experiment, edited by D. Hays and A. Browne, Plenum Press, pp. 25-58.

125. Yager, T., (1983). Factors Affecting Aircraft Ground Handling Performance, NASA Technical Memorandum 85652.

126. Yoo, J. P., AI-Qadi, I. L. Elseifi, M. A. and Janajreh, I. (2006). Flexible Pavement Responses to Different Loading Amplitudes Considering Layer Interface Conditions and Lateral Shear Forces, International Journal of Pavement Engineering, Vol. 7, No. 1, pp. 73-86.

127. Zmindak, M. and Grajciar, I. (1997). Simulation of the Aquaplane Problem. Computers and Structures, Vol. 64, No. 5/6, pp. 1155-1164.